

EXPANSION POSETS FOR POLYGON CLUSTER ALGEBRAS

By

Andrew Claussen

arXiv:2005.02083v1 [math.CO] 5 May 2020

A DISSERTATION

Submitted to
Michigan State University
in partial fulfillment of the requirements
for the degree of

Mathematics — Doctor of Philosophy

2020

ABSTRACT

EXPANSION POSETS FOR POLYGON CLUSTER ALGEBRAS

By

Andrew Claussen

Define an *expansion poset* to be the poset of monomials of a cluster variable attached to an arc in a polygon, where each monomial is represented by the corresponding combinatorial object from some fixed combinatorial cluster expansion formula. We introduce an involution on several of the interrelated combinatorial objects and constructions associated to type A surface cluster algebras, including certain classes of arcs, triangulations, and distributive lattices. We use these involutions to formulate a dual version of skein relations for arcs, and dual versions of three existing expansion posets. In particular, this leads to two new cluster expansion formulas, and recovers the lattice path expansion of Propp et al. We provide an explicit, structure-preserving poset isomorphism between an expansion poset and its dual version from the dual arc. We also show that an expansion poset and its dual version constructed from the same arc are dual in the sense of distributive lattices.

We show that any expansion poset is isomorphic to a closed interval in one of the lattices $L(m, n)$ of Young diagrams contained in an $m \times n$ grid, and that any $L(m, n)$ has a covering by such intervals. In particular, this implies that any expansion poset is isomorphic to an interval in Young's lattice.

We give two formulas for the rank function of any lattice path expansion poset, and prove that this rank function is unimodal whenever the underlying snake graph is built from at most four maximal straight segments. This gives a partial solution to a recent conjecture by Ovsienko and Morier-Genoud. We also characterize which expansion posets have symmetric rank generating functions, based on the shape of the underlying snake graph.

We show that the support of any type A cluster variable is the orbit of a groupoid. This implies that any such cluster variable can be reconstructed from any one of its monomials.

Finally, in work joint with Nicholas Ovenhouse, we partially generalize T -paths to configurations of affine flags, and prove that a T -path expansion analogous to the type A case holds when the initial seed is from a fan triangulation. We finish by describing the structure of two types of expansion posets in this context.

ACKNOWLEDGMENTS

First and foremost, I would like to thank my advisor Misha Shapiro. Certainly, this thesis would not have been possible without his tireless guidance, endless patience, and unwavering personal and academic support.

I would like to thank the other members of my committee Jonathan Hall, Rajesh Kulkarni, and Bruce Sagan, both for their inspiring courses and lectures, and for their continual support and encouragement throughout the years.

A special thanks goes to my friend and collaborator Nicholas Ovenhouse. In particular, I am grateful for both the innumerable comments and corrections that he offered during the writing of this thesis, and also for his willingness to have our joint work included here.

I would like to thank my fellow graduate students for their friendship and support, especially Nick Ovenhouse, Blake Icabone, Duff Baker-Jarvis, and Sami Merhi.

Likewise, thanks to everyone I met through the advanced track program at MSU, especially Daniel Diroff, Bar Roytman, Christopher Klerkx, Rebecca Sodervick, Jonathan Jonker, and Katrina Suchoski.

I am grateful to Tsvetanka Sendova, Russel Schwab, and Jeanne Wald for their commitment to my professional development, and for all the opportunities they have presented me with during my time at MSU.

Indeed, thanks to all the faculty and staff at MSU with whom I have had the pleasure of working with.

I would like to thank Mark Naber of Monroe County Community College for inspiring me to further my mathematical education.

Finally, I am thankful to all my wonderful family and friends for the love and support they

have given me throughout this endeavor. I'd like to give special thanks to my dad (Rusty), Marshia, Aaron and Autumn, Chris, Jake, Graham, and the Minney family.

To my parents, Kay Marie Claussen and Irvin Boyd Claussen.

TABLE OF CONTENTS

LIST OF TABLES	ix
LIST OF FIGURES	x
Chapter 1 Introduction	1
Chapter 2 Cluster Algebras	7
2.1 Cluster Algebras from Quivers	7
2.2 Cluster Algebras from Surfaces	10
2.3 Cluster Algebras of Finite Type A_n	11
Chapter 3 Combinatorial Constructions	13
3.1 Words	13
3.2 Type A_n Dynkin Quivers	14
3.3 Posets	15
3.4 Triangulations	16
3.5 Arcs, Cluster Variables, and Resolutions	20
3.6 Snake Graphs	24
3.7 Continued Fractions	29
3.8 Distributive Lattices	31
Chapter 4 Expansion Posets	34
4.1 Perfect Matchings of Snake Graphs	34
4.2 Perfect Matchings of Angles	39
4.3 T -Paths	42
Chapter 5 Dual Combinatorial Constructions	50
5.1 Words	50
5.2 Type A_n Dynkin Quivers	50
5.3 Posets	51
5.4 Triangulations	51
5.5 Slides, Arcs, and Cluster Variables	53
5.6 Snake Graphs	55
5.7 Continued Fractions	59
5.8 Distributive Lattices	60
Chapter 6 Dual Expansion Posets	61
6.1 Lattice Paths on Snake Graphs	61
6.2 Lattice Paths of Angles	64
6.3 S -paths	67
6.4 Expansion Duality	73

Chapter 7	Expansion Posets as Intervals in Young’s Lattice	79
7.1	Graded Expansion Posets	80
7.2	Posets of Snake Graphs and the q -binomial Coefficients	82
7.3	The Embeddings $\mathbb{L}_w \hookrightarrow \mathbb{O}_j^n$	85
Chapter 8	A Recursion and Two Rank Formulas	92
8.1	Lattice Path Recursion	92
8.2	Hook Rank Formula	96
8.3	Fibonacci Rank Formula	100
Chapter 9	Unimodality and Symmetry	103
9.1	Rank Unimodality	104
9.2	Rank Symmetry	116
Chapter 10	Expansion Posets as Groupoid Orbits	121
Chapter 11	T-paths for Configurations of Flags	123
11.1	Decorated Teichmüller Spaces	123
11.2	Higher Teichmüller Spaces	125
11.3	Colored SL_3 Diagrams	127
11.4	Crossings in Colored SL_3 Diagrams	128
11.5	Fork-Join Networks	130
11.6	Generalized T -paths	133
11.7	The Recursion Lemmas	135
11.8	Expansion Formulas in Fan Triangulations	142
11.9	Some Expansion Posets	144
REFERENCES		150

LIST OF TABLES

LIST OF FIGURES

Figure 1.1:	A flip inside a triangulated pentagon	3
Figure 1.2:	Expansion duality	4
Figure 2.1:	Quiver mutation	8
Figure 2.2:	Flip inside a quadrilateral	10
Figure 2.3:	One seed for A_3	12
Figure 3.1:	Type A_n Dynkin diagram	14
Figure 3.2:	Orientation of a type A_n Dynkin diagram	14
Figure 3.3:	The Dynkin quiver A_{ab}	15
Figure 3.4:	The poset C_{ab}	15
Figure 3.5:	Four examples of fence posets C_w	16
Figure 3.6:	Clockwise 3-cycles created from edges in A_w	17
Figure 3.7:	Leftmost 3-cycle	17
Figure 3.8:	Rightmost 3-cycle, if $l(w)$ is odd	17
Figure 3.9:	Rightmost 3-cycle, if $l(w)$ is even	18
Figure 3.10:	The quiver Q_{ab}	18
Figure 3.11:	The triangulated polygon Σ_{ab}	19
Figure 3.12:	A fan triangulation	20
Figure 3.13:	The arc γ_{ab} inside Σ_{ab} , and the associated cluster variable x_{ab}	21
Figure 3.14:	Resolution of the intersection point p_i	22
Figure 3.15:	One element of $\text{Tree}(ab)$	23
Figure 3.16:	An arc in a triangulated subpolygon	24

Figure 3.17:	Shorthand to describe the corners and edges of a tile T_i	25
Figure 3.18:	Construction of the snake graph G_{ab}	26
Figure 3.19:	The folding and unfolding maps	27
Figure 3.20:	The sign function s on G_{ab}	28
Figure 3.21:	The sign sequence \mathbf{s}_{ab} on G_{ab}	29
Figure 3.22:	Four Fibonacci cubes	33
Figure 4.1:	The perfect matching P_- on G_{ab}	35
Figure 4.2:	The five perfect matchings on G_{ab}	36
Figure 4.3:	Twist of a perfect matching at tile T_i	37
Figure 4.4:	The poset \mathbb{P}_{ab}	38
Figure 4.5:	The perfect matching of angles A_- on Σ_{ab}	39
Figure 4.6:	Twist of a perfect matching of angles at diagonal δ_i	40
Figure 4.7:	The poset \mathbb{A}_{ab}	42
Figure 4.8:	The T -path T_- with edges from Δ_{ab}	43
Figure 4.9:	Twist of a T -path at diagonal δ_i	44
Figure 4.10:	T -path twists at internal diagonals are always defined	45
Figure 4.11:	The poset \mathbb{T}_{ab}	46
Figure 4.12:	The map $\mathbb{P}_{ab} \rightarrow \mathbb{A}_{ab}$ via angle identification and folding	47
Figure 4.13:	The map $\mathbb{A}_{ab} \rightarrow \mathbb{T}_{ab}$ via diagonal coloring and cancellation	48
Figure 4.14:	The composition $\mathbb{P}_{ab} \rightarrow \mathbb{A}_{ab} \rightarrow \mathbb{T}_{ab} \rightarrow \mathbb{P}_{ab}$ restricted to minimal elements	49
Figure 5.1:	The quiver A_{ab} and its dual A_{bb}	51
Figure 5.2:	The poset C_{ab} and its dual C_{bb}	51
Figure 5.3:	The triangle map applied to Σ_{ab} gives Σ_{bb}	52

Figure 5.4:	Dual resolution of the intersection point p_i	53
Figure 5.5:	One element of $\text{Tree}(bb)^*$	55
Figure 5.6:	Construction of the dual snake graph G_{bb}	57
Figure 5.7:	Transforming G_{ab} into its dual G_{bb}	58
Figure 5.8:	The sign sequence s_{ab} and its dual s_{bb}	59
Figure 5.9:	The Fibonacci cube Γ_3 and its dual	60
Figure 6.1:	The lattice path L_- on G_{bb}	61
Figure 6.2:	Flip of a lattice path at tile T_i	63
Figure 6.3:	The poset \mathbb{L}_{bb}	64
Figure 6.4:	The lattice path of angles B_- on G_{bb}	65
Figure 6.5:	Flip of a lattice path of angles at diagonal δ_i	66
Figure 6.6:	The poset \mathbb{B}_{bb}	67
Figure 6.7:	Flip of an S -path at diagonal δ_i	68
Figure 6.8:	The poset \mathbb{S}_{bb}	70
Figure 6.9:	The map $\mathbb{L}_w \rightarrow \mathbb{B}_{bb}$ via angle identification and folding	72
Figure 6.10:	The map $\mathbb{B}_{bb} \rightarrow \mathbb{S}_{bb}$ via associating edges to angles	72
Figure 6.11:	The arc δ , and the output arc δ^* for both j odd and j even	75
Figure 6.12:	Transforming the minimal element P_- into the minimal element L_-	77
Figure 6.13:	Transforming the minimal element A_- into the minimal element B_-	78
Figure 6.14:	Transforming the minimal element T_- into the minimal element S_-	78
Figure 7.1:	Posets, shapes, and rank functions for three snake graphs	82
Figure 7.2:	Local picture for a morphism between snake graphs	82
Figure 7.3:	The poset \mathbb{O}_2^5	83

Figure 7.4:	The poset $\mathbf{2} \times \mathbf{2}$ (bottom), its lattice of order ideals $\mathcal{I}(\mathbf{2} \times \mathbf{2})$ (top left), and the rank function of $\mathbb{O}_3^7 \cong \mathcal{I}(\mathbf{2} \times \mathbf{2})$ (top right)	85
Figure 7.5:	The Young diagram associated to the partition $(4, 3)$ of 7	86
Figure 7.6:	Snake graphs from lattice paths	86
Figure 7.7:	The posets \mathbb{L}_{ab} and $\mathbb{I}_{ab} \cong \mathbb{L}_{ab}$	87
Figure 7.8:	Three lattice path posets embedded into \mathbb{O}_2^6	89
Figure 7.9:	Snake graphs from perfect matchings	90
Figure 7.10:	The poset dual to \mathbb{O}_2^5	91
Figure 8.1:	The maximal straight segments of G_w	93
Figure 8.2:	Initial step in the recurrence	94
Figure 8.3:	The recurrence for the first maximal straight segment of G_w	95
Figure 8.4:	The recurrence for the second maximal straight segment of G_w	95
Figure 8.5:	Recursive computation of the rank function $\mathbb{L}_{w_3}(q)$	96
Figure 8.6:	The construction of \mathbb{G}_w from G_w	101
Figure 8.7:	The poset \mathbb{G}_{ab} , its node weights, and the rank function $\mathbb{L}_w(q)$	101
Figure 9.1:	The snake graphs G_w and G_0 , and the associated posets \mathbb{L}_{w_0} and \mathbb{L}_w	106
Figure 9.2:	The rank function $\mathbb{L}_{a^2b^5}(q)$ via block stacking	107
Figure 9.3:	The rank function $[m]_q \mathbb{L}_{a^2b^5}(q)$ for $1 \leq m \leq 12$	114
Figure 9.4:	A Markov snake graph	120
Figure 9.5:	The snake graph with continued fraction $[2, 2, 2, 2, 2]$	120
Figure 11.1:	A 3-triangulation	126
Figure 11.2:	Visualization of a Laurent monomial	127
Figure 11.3:	Face resolution	128

Figure 11.4: Edge resolution	128
Figure 11.5: A directed edge and a face which cross	129
Figure 11.6: Two crossing faces	130
Figure 11.7: A fork-join network	131
Figure 11.8: A fork-join network satisfying conditions (A1) and (A2)	131
Figure 11.9: Construction of an alternating fork-join network Ω	132
Figure 11.10: Faces as webs	133
Figure 11.11: Two edge-type T -paths	134
Figure 11.12: Two face-type T -paths	135
Figure 11.13: Set-up for Lemma 11.19	138
Figure 11.14: Set-up for Lemma 11.20	140
Figure 11.15: Covering relations	144
Figure 11.16: The first step in the resolution of the fan face in a hexagon	145
Figure 11.17: Expansion poset of a fan face	146
Figure 11.18: The bijection between a fan face poset and the corresponding SL_2 T -path poset	146
Figure 11.19: The first step in the resolution of the longest edge in a hexagon	147
Figure 11.20: The gluing construction of the expansion poset of the longest edge in a pentagon	149

Chapter 1

Introduction

Cluster algebras are a class of inherently combinatorial commutative algebras that were defined by Fomin and Zelevinsky in [14]. The definition of cluster algebras was motivated by observations in representation theory. Since then, cluster algebra structures have been recognized and studied in various other fields of mathematics, such as decorated Teichmüller theory and Poisson geometry (see [18] and [12], [13]), higher Teichmüller theory [9], rings of invariants (see [10] and [11]), elementary number theory [5] including diophantine equations [33], and knot theory [25], just to name a few.

Each cluster algebra has a distinguished set of generators, called the *cluster variables*. These generators are grouped into overlapping subsets, called *clusters*, all having the same cardinality, called the *rank* of the cluster algebra.

A *seed* of a cluster algebra is a triple consisting of a cluster, a *coefficient tuple*, and a skew-symmetrizable matrix called an *exchange matrix*. In any rank n cluster algebra, each seed can be *mutated* in direction i for any $1 \leq i \leq n$ to produce n more seeds. By construction, seed mutation is an involution. Clusters in adjacent seeds differing by a mutation in direction i are equal, except that the i^{th} variables in each differ from one another by what is called an *exchange relation*. This means that their product is a certain binomial sum whose form is governed by the exchange matrices. Any cluster algebra can be computed by fixing an *initial seed* and iterating seed mutation to produce all the cluster variables.

A *Laurent polynomial* is a polynomial with negative exponents allowed, i.e., any Laurent polynomial can be written as $\sum_{I \in \mathbb{Z}^n} a_I X^I$. One of the first fundamental results of cluster algebra theory is that any cluster variable can be written as a Laurent polynomial with respect to any cluster. This is called the *Laurent phenomenon*.

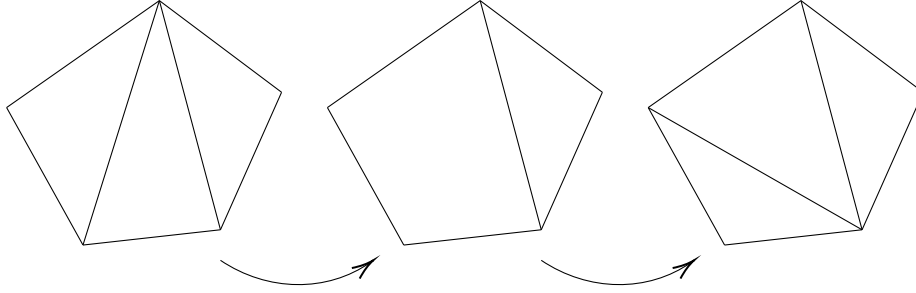
We will work within the subclass of cluster algebras in which exchange matrices and matrix mutation may be replaced by *quivers* and *quiver mutation*, respectively. These cluster algebras are called *cluster algebras from quivers*, or *skew-symmetric cluster algebras of geometric type*

A large subclass of cluster algebras are the *cluster algebras from surfaces* [8]. In such a cluster algebra, the cluster variables are in bijection with certain curves in the surface called *tagged arcs*, seeds are in bijection with *tagged triangulations* of the surface, and mutation corresponds to a *flip* of a tagged arc in a tagged triangulation.

The combinatorics of the subclass of cluster algebras from a disc with $n + 3$ marked points on the boundary (i.e., a polygon) are the main focus of this paper. These cluster algebras are examples of *cluster algebras of finite type A_n* . As the notion of tagged triangulations and tagged arcs is unnecessary in this restricted level of generality, we will henceforth only speak of (*ordinary*) *arcs*. Any seed in a cluster algebra of finite type A_n can be modeled by a triangulated $(n + 3)$ -gon, made up of n triangulating arcs (which we also call *internal diagonals*, or just *diagonals*), and $n + 3$ segments that make up the boundary of the polygon, called *boundary segments*. Mutation corresponds to a flip of one of the n internal diagonals in the triangulation. Figure 1.1 below shows one of the two possible flips inside a triangulated polygon.

Numerous *combinatorial cluster expansion formulas* for surface type and type A_n cluster algebras have been developed in recent years. Each such expansion gives an explicit formula to compute any cluster variable by writing it as a weighted sum over a certain class of combinatorial objects. We recall three such expansion formulas from the literature - *perfect matchings of*

Figure 1.1: A flip inside a triangulated pentagon



snake graphs, *perfect matchings of angles*, and *T-paths*. (see [29] and [30], [41] and [42], and [35], [37], and [36] respectively).

The monomials of any cluster variable can be naturally arranged into a poset [15]. We can equip each such poset with the additional node structure it inherits from some combinatorial expansion formula. We call any such poset an *expansion poset* (in fact, each of these posets is isomorphic to a distributive lattice [30]).

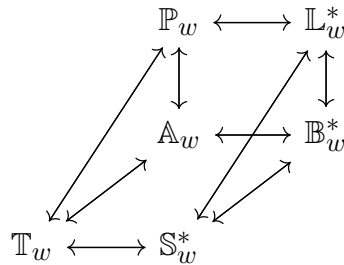
In this paper, inspired by the snake graph involution introduced in [32] and the involution “Jimm” in [40], we define a new notion of *duality*, a certain involution on several of the combinatorial objects found in type A cluster theory, including for instance triangulations of an n -gon, and a certain class of distributive lattices. Each such object is parameterized by a binary word w , so that duality between objects is controlled by duality $w \longleftrightarrow w^*$ on the underlying words. These constructions yield a dual version of skein relations for arcs. Furthermore, we use this duality to produce an equivalent yet combinatorially distinct version (built from the dual arc in the dual triangulation) of each of the three expansion posets mentioned above.

Namely, we observe that there is an explicit poset isomorphism (respecting additional node structure) between the perfect matching expansion poset \mathbb{P}_w , and the *dual lattice path expansion poset* \mathbb{L}_{w^*} associated to the dual word. This duality, minus poset structures, was given in [32] in the context of frieze patterns. We define two more expansion posets, new to the best of our

knowledge, which we call *lattice paths of angles* \mathbb{B}_w and *S-paths* \mathbb{S}_w , respectively. We observe that there is an explicit structure-preserving poset isomorphism between the expansion posets \mathbb{A}_w and \mathbb{B}_{w^*} , and likewise between the *T-path* expansion poset \mathbb{T}_w and \mathbb{S}_{w^*} .

The three isomorphisms just indicated are all written in terms of either snake graph duality, or traingulation duality. Here, we call any such isomorphism an *expansion duality*. The horizontal maps in the figure below represent expansion dualities. The maps comprising the two triangles are written either in terms of the *folding/unfolding maps* from [28], or the *angle projection* maps defined in [42] (or some combination of the two).

Figure 1.2: Expansion duality



Furthermore, we show that the two isomorphism classes of expansion posets attached to any arc are dual in the sense of distributive lattices mentioned above.

A *partition* of a positive number m is a weakly decreasing sequence $(\lambda_1, \lambda_2, \dots, \lambda_l)$ such that $m = \lambda_1 + \lambda_2 + \dots + \lambda_l$. A *Young diagram* is a visualization of a partition of a positive integer by rows of boxes (see [34]). *Young's lattice* is the infinite lattice whose nodes are Young diagrams, which are ordered by inclusion (see [34] and [38]). Young's lattice possesses a collection of finite sublattices, typically called $L(m, n)$, whose nodes are all those Young diagrams that fit within an $m \times n$ rectangular grid, and whose rank function is the q -binomial coefficient $\begin{bmatrix} n+m \\ m \end{bmatrix}_q$. We give a groupoid structure on the set of all snake graphs which reconstructs the posets $L(m, n)$. That is, each orbit of this groupoid can be given the structure of a poset, which is isomorphic to one of

the lattices $L(m, n)$, and furthermore (the isomorphism class of) every $L(m, n)$ can be obtained in this way. We show that each expansion poset considered above is isomorphically embedded as a closed interval in some $L(m, n)$, and moreover that each $L(m, n)$ has a covering by such embeddings.

We provide two closed formulas for the rank function $\mathbb{L}_w(q)$ of any lattice path expansion poset \mathbb{L}_w of lattice paths on the snake graph G_w . The first is written as sums of products of *hook snake graphs*, and its terms are parameterized by the nodes in a Boolean lattice. The second formula we introduce is a refinement of the first, and is written in terms of q -numbers corresponding to lengths of the maximal straight segments that G_w is built from. The latter formula is obtained by considering the snake graph G_w itself as a lattice path on another snake graph. In fact, this construction makes G_w into the central node in a *Fibonacci cube*, an interconnection topology defined in [22].

Recently, a conjecture was made in [26] that is equivalent to asking if the coefficients of the rank generating function of any expansion poset are *unimodal*, meaning that they weakly increase, and then weakly decrease. By again studying lattice path expansions, we show this conjecture to be true for snake graphs built from at most four maximal straight segments. We also characterize, based on the shape of the underlying snake graph, which expansion posets have palindromic, or *symmetric*, coefficients.

Next, we interpret the support of any cluster variable x_w in a type A surface cluster algebra as an orbit of a certain groupoid. It follows that any two cluster variables, written with respect to the same initial seed, have disjoint supports. Thus, any cluster variable x_w is completely determined by any one of its Laurent monomials.

Lastly, in work joint with Nicholas Ovenhouse, we partially generalize the T -path expansion mentioned above to configurations of affine flags (see [9]). We describe in two special cases the

poset structure on the Laurent monomials from an expansion in this context.

Chapter 2

Cluster Algebras

We begin this chapter by defining the subclass of cluster algebras called *cluster algebras from quivers*, or *skew-symmetric cluster algebras of geometric type*. Next, we introduce *cluster algebras from surfaces*. Finally, we describe *surface cluster algebras of type A*, which is the class of cluster algebras we study in the rest of the paper.

2.1 Cluster Algebras from Quivers

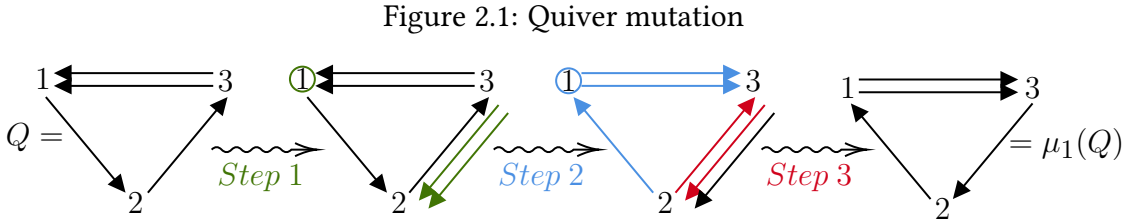
Definition 2.1. A *quiver* is a 4-tuple $Q = (Q_0, Q_1, s, t)$, where Q_0 is a set of *nodes* or *vertices*, Q_1 is a multiset of *arrows* whose elements are from $Q_0 \times Q_0$, and the *source* and *target* functions $s, t : Q_1 \rightarrow Q_0$ are the first and second projection, respectively. A quiver Q contains a *loop* if there exists a node $v \in Q_0$ and an arrow $e \in Q_1$ such that $v = s(e) = t(e)$. We say Q contains a *2-cycle* if there exists two distinct nodes $v_1, v_2 \in Q_0$ and two arrows $e_1, e_2 \in Q_1$ such that $v_1 = s(e_1) = t(e_2)$ and $v_2 = s(e_2) = t(e_1)$. A quiver Q contains a *3-cycle* if there exist three distinct nodes $v_1, v_2, v_3 \in Q_0$ and three arrows $e_1, e_2, e_3 \in Q_1$ such that $v_1 = s(e_1) = t(e_3)$, $v_2 = s(e_2) = t(e_1)$, and $v_3 = s(e_3) = t(e_2)$. We say Q is *finite* if both Q_0 and Q_1 are finite sets. In this case, we label the vertices of Q by $1, 2, \dots, \#\{\text{nodes in } Q\}$.

From now on, we only consider finite quivers (unless stated otherwise) that do not contain any loops or 2-cycles.

Definition 2.2. Let $Q = (Q_0, Q_1)$ be a quiver with vertices $Q_0 = \{1, 2, \dots, n\}$. We define *quiver mutation at vertex k* to be the map on quivers μ_k whose image $\mu_k(Q)$ is defined by the following procedure:

1. For each pair of arrows $i \rightarrow k \rightarrow j$, create a new directed edge $i \rightarrow j$ (note that prohibiting 2-cycles implies that $i \neq j$).
2. Reverse the orientation of each arrow incident to k
3. Delete any and all 2-cycles created in step 1.

Example 2.3. In Figure 2.1, we illustrate the three-step process in Definition 2.2 by mutating the left-most quiver at vertex 1 to produce the right-most quiver.



One can check that quiver mutation at vertex k is an involution, so that mutation equivalence is indeed an equivalence relation.

Definition 2.4. Fix $n \leq m$ and let $Q = (Q_0, Q_1)$ be a quiver with vertices $Q_0 = \{1, 2, \dots, n, n + 1, \dots, m\}$. Partition Q_0 into the two sets $Q_0^{mutable} = \{1, 2, \dots, n\}$ and $Q_0^{frozen} = \{n + 1, n + 2, \dots, m\}$, which we call the *mutable vertices* and the *frozen vertices*, respectively. Fix an *ambient field* $F \cong \mathbb{Q}(f_1, f_2, \dots, f_n, f_{n+1}, \dots, f_m)$. By associating to each vertex i in Q_0 the indeterminate f_i , we obtain a *seed* in F , denoted $((f_1, f_2, \dots, f_m), Q)$. The variables f_1, f_2, \dots, f_n are called *cluster variables* (or *mutable variables*), and f_{n+1}, \dots, f_m are called *frozen variables*.

The n -tuple (f_1, f_2, \dots, f_n) is called the *cluster* of the seed $((f_1, f_2, \dots, f_m), Q)$, and the m -tuple (f_1, f_2, \dots, f_m) is the *extended cluster* of the seed $((f_1, f_2, \dots, f_m), Q)$.

Definition 2.5. Consider the seed $((f_1, f_2, \dots, f_m), Q)$. For $1 \leq k \leq n$, we define *seed mutation at variable k* to be the map on seeds μ_k whose image $\mu_k((f_1, f_2, \dots, f_m), Q) = ((\tilde{f}_1, \tilde{f}_2, \dots, \tilde{f}_m), \mu_k(Q))$ is defined as follows:

- If $j \neq k$, then $\tilde{f}_j = f_j$.
- If $j = k$, then f_k and \tilde{f}_k are related by the following *exchange relation*:

$$f_k \tilde{f}_k = \prod_{s \rightarrow k} f_s + \prod_{k \rightarrow t} f_t.$$

Definition 2.6. Consider the *initial seed* $((x_1, x_2, \dots, x_m), Q)$ with *initial cluster* (x_1, x_2, \dots, x_n) and *initial cluster variables* x_1, x_2, \dots, x_n . Let \mathcal{S} be the set of all seeds mutation equivalent to $((x_1, x_2, \dots, x_m), Q)$, and let \mathcal{X} be the union of all cluster variables in all seeds in \mathcal{S} . Let $R = \mathbb{Z}[x_{n+1}, \dots, x_m]$. The *cluster algebra* $\mathcal{A} = \mathcal{A}((x_1, x_2, \dots, x_m), Q)$ from the quiver Q is the R -algebra generated by \mathcal{X} . The *rank* of the cluster algebra \mathcal{A} is the cardinality n of any of its clusters.

Below we state the Laurent Phenomenon in the restricted generality of cluster algebras from quivers.

Theorem 2.7. (Theorem 3.1 in [14]) *Let \mathcal{A} be the cluster algebra from the quiver Q with arbitrary initial seed $((x_1, x_2, \dots, x_m), Q)$. Then any cluster variable in \mathcal{A} can be expressed as a Laurent polynomial in the variables x_1, x_2, \dots, x_n , with coefficients in \mathbb{Z} .*

2.2 Cluster Algebras from Surfaces

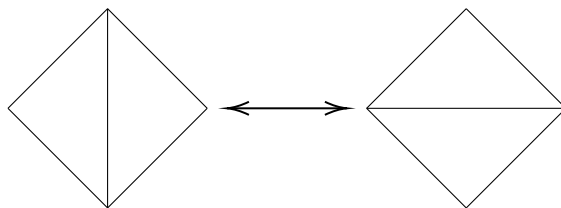
See [12], [9] for details on the topics presented in this section. In particular, we remind the reader that tagged arcs are required for the general discussion but will not be mentioned here.

Definition 2.8. An oriented surface Σ with nonempty boundary is called a *marked surface* if Σ comes equipped with a collection of finitely many marked points on its boundary.

Definition 2.9. An *arc* is any curve inside Σ with endpoints at marked points, considered up to isotopy relative the set of marked points on the boundary of Σ , and such that the relative interior of this curve is disjoint from the boundary of Σ . Any curve beginning and ending at distinct marked points which lies entirely within the boundary of Σ and does not contain any marked points in its interior is called a *boundary segment*.

Definition 2.10. Two arcs in Σ are called *compatible* if they have isotopy representatives that do not intersect, except possibly at endpoints. An *ideal triangulation* Δ is a maximal collection of distinct pairwise compatible arcs, along with all boundary segments. The arcs of a triangulation cut the surface into *ideal triangles*. A *flip* (or *Whitehead move*) of an ideal triangulation at an arc γ is the process of removing γ from Δ and replacing it with the unique arc $\tilde{\gamma}$ that gives another ideal triangulation of Σ (see Figure 6.2).

Figure 2.2: Flip inside a quadrilateral



It is known that any two ideal triangulations of Σ are connected by a sequence of flips.

Definition 2.11. Let Σ be a marked surface. We now construct a cluster algebra $\mathcal{A}(\Sigma)$, called the *cluster algebra from the surface Σ* , that depends only on Σ . To do this, we construct a quiver whose nodes are in one-to-one correspondence with the collection of arcs and boundary segments of some ideal triangulation Δ of Σ , and whose arrows form clockwise 3-cycles inside each ideal triangle. This construction does not depend on the choice of ideal triangulation.

The correspondences below follow from the construction given in the previous definition.

initial cluster variables of $\mathcal{A}(\Sigma) \longleftrightarrow$ arcs in Δ

non-initial cluster variables of $\mathcal{A}(\Sigma) \longleftrightarrow$ arcs in Σ that are not in Δ

frozen variables of $\mathcal{A}(\Sigma) \longleftrightarrow$ boundary segments of Σ

seeds of $\mathcal{A}(\Sigma) \longleftrightarrow$ triangulations Δ of Σ

seed mutations in $\mathcal{A}(\Sigma) \longleftrightarrow$ flips of arcs in Δ

2.3 Cluster Algebras of Finite Type A_n

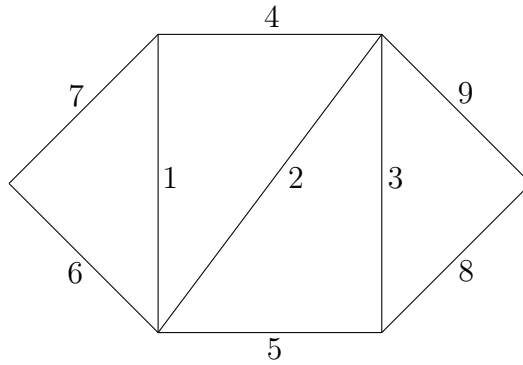
Definition 2.12. A *cluster algebra of (finite) type A_n* is any cluster algebra from a quiver $Q = (Q_0, Q_1, s, t)$ such that the induced subquiver on the mutable vertices $Q_0^{mutable}$ is mutation equivalent to some orientation of a type A_n Dynkin diagram.

Any cluster algebra from a surface $\mathcal{A}(\Sigma)$ such that Σ is an $(n + 3)$ -gon, i.e. Σ is a closed disc with $n + 3$ marked points on its boundary, is a rank n cluster algebra of type A_n . As is the case for general surfaces, cluster variables correspond to arcs in the $(n + 3)$ -gon, frozen variables correspond to the boundary segments, seeds correspond to triangulations, and seed mutations

correspond to flips of arcs.

Example 2.13. Figure 2.3 below shows one seed of a surface cluster algebra of type A_3 .

Figure 2.3: One seed for A_3 .



We will use this seed as the basis for a running example to be followed throughout the rest of this text.

Chapter 3

Combinatorial Constructions

In this chapter, we recall several interrelated objects and constructions naturally occurring in type A cluster combinatorics. The objects found in this chapter are parameterized by binary words.

3.1 Words

Definition 3.1. A (binary) word of length $n - 1$ is a finite string formed from $n - 1$ choices of elements from the set $\{a, b\}$. A word of length $n - 1$ will be denoted $w = w_1w_2\dots w_{n-1}$ and its length is $l(w) = n - 1$.

The word

$$w = \underbrace{aa\dots a}_{k_1 \text{ times}} \underbrace{bb\dots b}_{k_2 \text{ times}} \dots$$

will be abbreviated $w = a^{k_1}b^{k_2} \dots$.

As mentioned above, the constructions that follow are parameterized by the words w .

Definition 3.2. A word w is *straight* if the only letter occurring in w is a , or the only letter occurring in w is b . Conversely, a word is *zigzag* if neither of the substrings aa nor bb occur in w .

Example 3.3. We fix the word $w = ab$ for our concrete running example to be followed throughout this section. Note that the word $w = ab$ is zigzag.

3.2 Type A_n Dynkin Quivers

A *type A_n Dynkin diagram* is an undirected graph with n nodes $1, 2, \dots, n$ and one edge between each pair of consecutive nodes i and $i + 1$ for $1 \leq i \leq n - 1$. We picture any type A_n Dynkin diagram as shown in Figure 3.1.

Figure 3.1: Type A_n Dynkin diagram

$$1 \text{ --- } 2 \text{ --- } \dots \text{ --- } n$$

Order the nodes $1, 2, \dots, n$ and edges $\overline{i, i + 1}$ of any type A_n Dynkin diagram by $1 < 2 < \dots < n$ and $\overline{1, 2} < \overline{2, 3} < \dots < \overline{n - 1, n}$, respectively. An *orientation* of a type A_n Dynkin diagram is a choice of orientation for each of the $n - 1$ edges of A_n .

Definition 3.4. A *type A_n Dynkin quiver* is a quiver that is mutation equivalent to an orientation of a type A_n Dynkin diagram.

Figure 3.2 shows one of the 2^{n-1} possible orientations of a Dynkin diagram of type A_n , each of which is an example of a type A_n Dynkin quiver (since it is mutation equivalent to itself).

Figure 3.2: Orientation of a type A_n Dynkin diagram

$$1 \longrightarrow 2 \longrightarrow \dots \longrightarrow n$$

Definition 3.5. Let $w = w_1 w_2 \dots w_{n-1}$ be a word of length $l(w) = n - 1$, and A_n the Dynkin diagram of type A_n with nodes labeled $1, 2, \dots, n$. The *type A_n Dynkin quiver A_w associated to w* is defined by mapping each w_i to the i^{th} edge $\overline{i, i + 1}$ of the Dynkin diagram A_n and declaring that any edge labeled by a becomes oriented $i \longleftarrow i + 1$, and that any edge labeled by b becomes oriented $i \longrightarrow i + 1$.

Example 3.6. The word $w = ab$ gives the Dynkin quiver A_w shown in Figure 3.3.

Figure 3.3: The Dynkin quiver A_{ab}

$$1 \xleftarrow{a} 2 \xrightarrow{b} 3$$

Remark 3.7. If the word w is straight then the edges in the Dynkin quiver A_w are all oriented in the same direction. Conversely, if the word w is zigzag then the edges in A_w alternate in orientation.

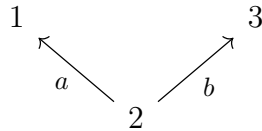
3.3 Posets

The posets we define here are called *piecewise-linear posets* in [1], and *zig-zag chains* in [24].

Definition 3.8. Define the *poset* C_w associated to w to be the Hasse diagram of a poset whose underlying graph is the Dynkin diagram A_n and covering relations are $i < j$ in C_w iff $i \rightarrow j$ in A_w . We visualize the edges of C_w as taking unit diagonal steps upwards.

Example 3.9. Figure 3.4 shows the poset C_{ab} .

Figure 3.4: The poset C_{ab}



Remark 3.10. If the word w of length $l(w) = n - 1$ is straight then the poset C_w is a linear chain with n elements and $n - 1$ edges. In this case, the covering relations are

$$1 > 2 > 3 > \cdots > n$$

if $w = a^{n-1}$, or

$$1 < 2 < 3 < \cdots < n$$

if $w = b^{n-1}$. Conversely, if the word w is zigzag, then the poset C_w is a *fence* or *zigzag poset* (see [27]) with n elements and $n - 1$ edges, with covering relations

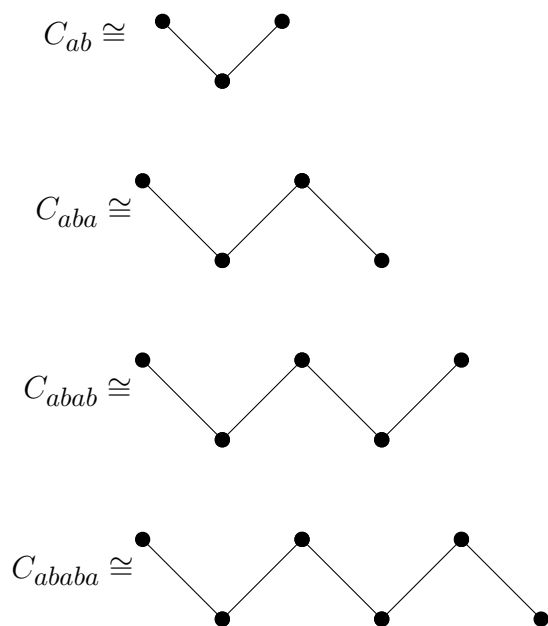
$$1 > 2 < 3 > \dots$$

if $w = ababa \dots$, or

$$1 < 2 > 3 < \dots$$

if $w = babab \dots$. See Figure 3.5 for four examples of a fence poset from a word w .

Figure 3.5: Four examples of fence posets C_w

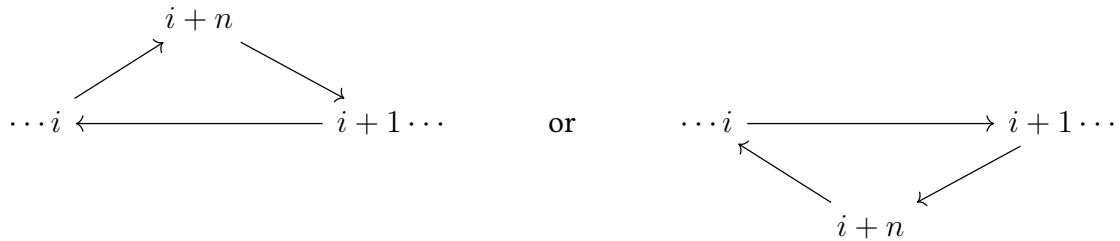


3.4 Triangulations

Form a new quiver Q_w , containing A_w as a complete subquiver, by adding $n + 3$ frozen nodes and $2n + 4$ directed edges to and from A_w as follows:

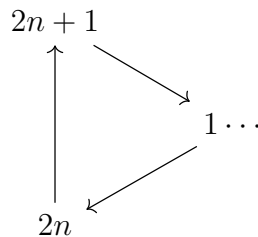
- For each edge $\overline{i, i+1}$ in A_w , introduce a node $n+i$ and two directed edges between $n+i$ and the endpoints i and $i+1$ of $\overline{i, i+1}$ such that a clockwise 3-cycle is formed. See Figure 3.6.

Figure 3.6: Clockwise 3-cycles created from edges in A_w



- Add two nodes $2n$ and $2n+1$ that form a clockwise 3-cycle with the first node 1 of A_w .

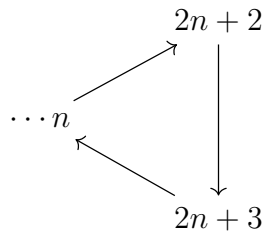
Figure 3.7: Leftmost 3-cycle



- Add two nodes $2n+2$ and $2n+3$ that form a clockwise 3-cycle with the last node n of A_w .

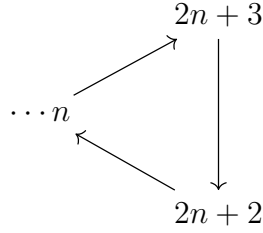
If $l(w)$ is odd, or $l(w)$ is even and w ends in a^2 or b^2 , form the following 3-cycle:

Figure 3.8: Rightmost 3-cycle, if $l(w)$ is odd



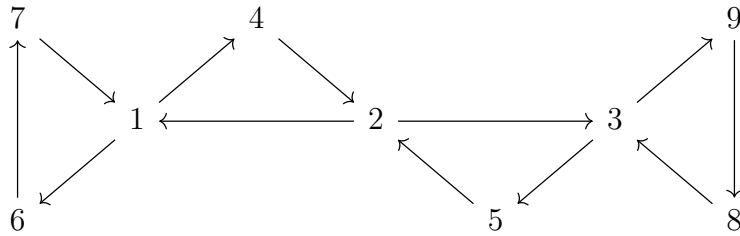
If $l(w)$ is even and w ends in ba or ab , form the following 3-cycle instead:

Figure 3.9: Rightmost 3-cycle, if $l(w)$ is even



Example 3.11. Figure 3.10 shows the quiver Q_{ab} .

Figure 3.10: The quiver Q_{ab}



Definition 3.12. The quiver Q_w induces the *triangulation* Δ_w associated to w of the $(n+3)$ -gon Σ whose elements are the internal diagonals labeled by $1, 2, \dots, n$ and boundary edges labeled by $n+1, n+2, \dots, 2n+3$.

The ordering of nodes in $A_w \leftrightarrow Q_w$ induces an ordering of the internal diagonals

$$\delta_1 < \delta_2 < \dots < \delta_n$$

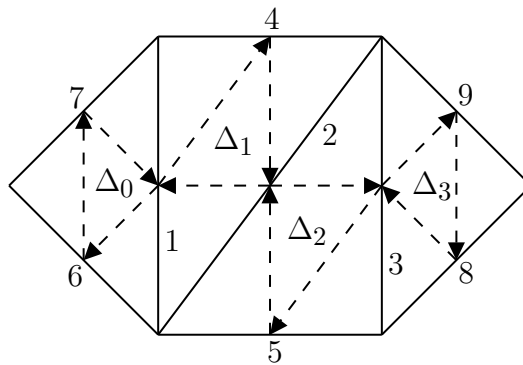
of Δ_w .

For $1 \leq i \leq n-1$, let Δ_i be the unique triangle cut out by Δ_w such that the two internal diagonals δ_i and δ_{i+1} are sides of Δ_i . Let Δ_0 be the unique triangle with sides consisting of two boundary segments and the internal diagonal δ_1 , and Δ_n the unique triangle with sides consisting of two boundary segments and the internal diagonal δ_n . The ordering of the internal diagonals induces an ordering $\Delta_0 < \Delta_1 < \dots < \Delta_n$ on the triangles Δ_i .

By construction, the pair of consecutive triangles Δ_{i-1} and Δ_i each has precisely one edge labeled i , and there are no other common labels among their edges. We use the notation $\Sigma_w = [\Delta_0, \Delta_1, \dots, \Delta_n]$ to indicate that the surface Σ with the triangulation Δ_w can be built by successively gluing Δ_{i+1} to Δ_i along the edge labeled $i + 1$ for each i .

Example 3.13. Figure 3.11 shows the triangulated polygon Σ_{ab} , with both edge labels i and triangles Δ_i indicated (along with the quiver Q_{ab} , its edges pictured here with dashed arrows).

Figure 3.11: The triangulated polygon Σ_{ab}



The quiver Q_w induces a type A_n cluster algebra $\mathcal{A}(\Sigma)_w$ with initial extended cluster equal to $(x_1, x_2, \dots, x_n, x_{n+1}, \dots, x_{2n+3})$. In the next section we assign to any word w a cluster variable in the associated cluster algebra.

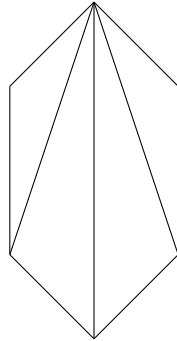
Definition 3.14. We say that Δ_w is a *fan triangulation* if there exists some vertex v of Σ such that each internal diagonal $\delta_1, \delta_2, \dots, \delta_n$ has v as one of its endpoints. We say that Δ_w is a *zigzag triangulation* if no three internal diagonals share a common endpoint.

Remark 3.15. If w is straight, then Δ_w is a fan triangulation. Conversely, if w is zigzag, then Δ_w is zigzag triangulation.

Example 3.16. The triangulation Δ_{ab} shown in Example 3.13 is a zigzag triangulation. Figure

3.12 below shows one example of a fan triangulation. This particular triangulation will be encountered again later, starting in Chapter 5.

Figure 3.12: A fan triangulation



3.5 Arcs, Cluster Variables, and Resolutions

Definition 3.17. Let a be the vertex of Δ_0 that is not an endpoint of edge δ_1 , and let b be the vertex of Δ_n that is not an endpoint of edge δ_n . Consider the oriented arc $\gamma_w = \gamma_{a \rightarrow b}$ in Σ_w with initial vertex a and terminal vertex b . We call the arc γ_w the *arc in Σ_w associated to w* , and the resulting cluster variable x_w the *cluster variable associated to w* .

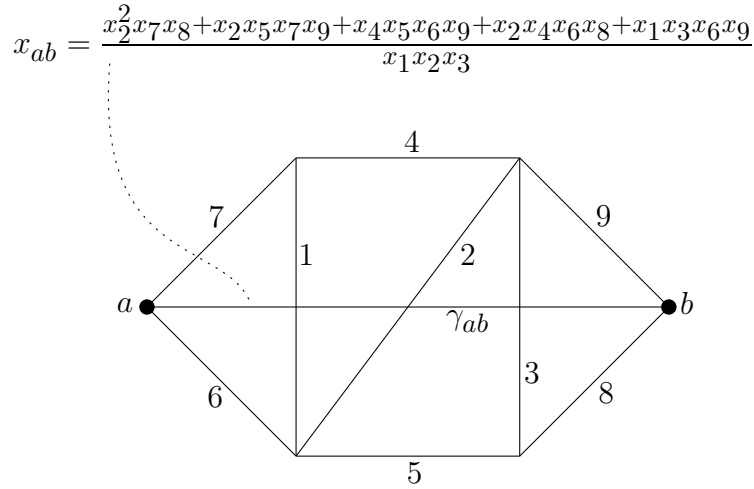
Example 3.18. Figure 3.13 below shows the arc γ_{ab} and the associated cluster variable x_{ab} , parameterized by the word $w = ab$.

Any cluster variable x_w can be written as

$$x_w = \frac{f(x_1, x_2, \dots, x_n)}{x_1 x_2 \dots x_n},$$

where f is a polynomial with coefficients from $\mathbb{Z}[x_{n+1}, x_{n+2}, \dots, x_{2n+3}]$. The first goal of the remainder of this section is to explain the resolution process given in [19] used to compute the

Figure 3.13: The arc γ_{ab} inside Σ_{ab} , and the associated cluster variable x_{ab}



monomials in f , and hence the cluster variable x_w . The second goal is to define the set $\text{Res}(w)$ of resolutions associated to w , and the set $\text{Tree}(w)$ of resolution trees associated to w .

Fix w and consider the arc γ_w inside the triangulated polygon Σ_w . Recall the diagonals of Δ_w are $\delta_1, \delta_2, \dots, \delta_n$ and that by construction γ_w crosses each of these n internal diagonals, creating n intersection points in Σ_w . Call these intersection points $p_i = \gamma_w \cap \delta_i$.

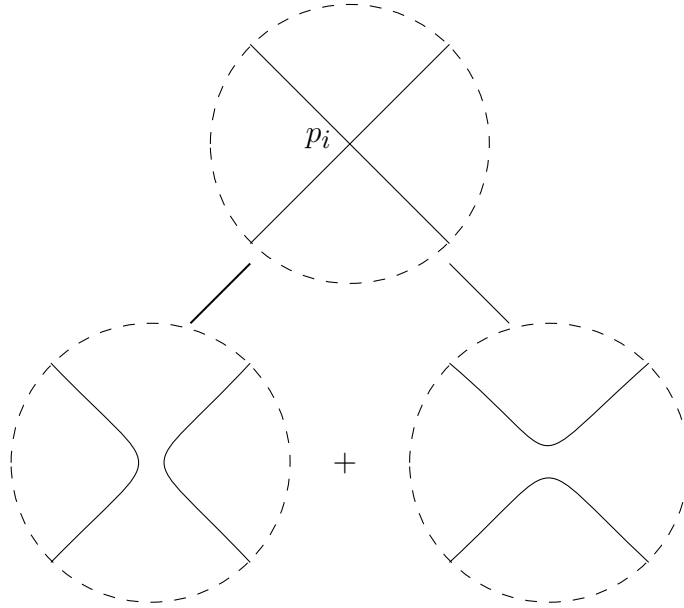
To resolve the intersection point p_i , we choose a small neighborhood of p_i and replace it with a pair of nonintersecting smooth curves in one of two different ways, shown below in Figure 3.14.

Choose one resolution out of the two above for each intersection point p_i ; this results in a collection of $n + 1$ nonintersecting curves in Σ . Note that closed curves based at some $v \in \Sigma$ can occur, but that this process never leads to a closed curve that is not attached to some vertex of Σ .

Definition 3.19. The set of resolutions $\text{Res}(w)$ associated to w consists of those diagrams that can be obtained from resolving each p_i in one of the two possible ways, in some chosen order.

Each element in $\text{Res}(w)$ is weighted as follows. First, replace each arc in $r \in \text{Res}(w)$ with distinct endpoints with the arc or boundary segment from Δ_w that it is isotopic to. Let $E(r)$ be the collection of arcs and boundary segments from Δ_w produced from the resolution r , along with

Figure 3.14: Resolution of the intersection point p_i



\emptyset if any closed loops are present. Define the *weight* of any resolution r to be $x_r = \prod_{j \in E(r)} x_j$, where $x_\emptyset = 0$.

Proposition 3.20. (Proposition 2.1 in [19]) Fix the word w . Consider the arc γ_w in the triangulated polygon Σ_w triangulated by Δ_w . Then any internal diagonals obtained by a resolution belong to Δ_w . The cluster variable x_w is equal to

$$x_w = \frac{1}{x_1 x_2 \dots x_n} \sum_{r \in \text{Res}(w)} x_r.$$

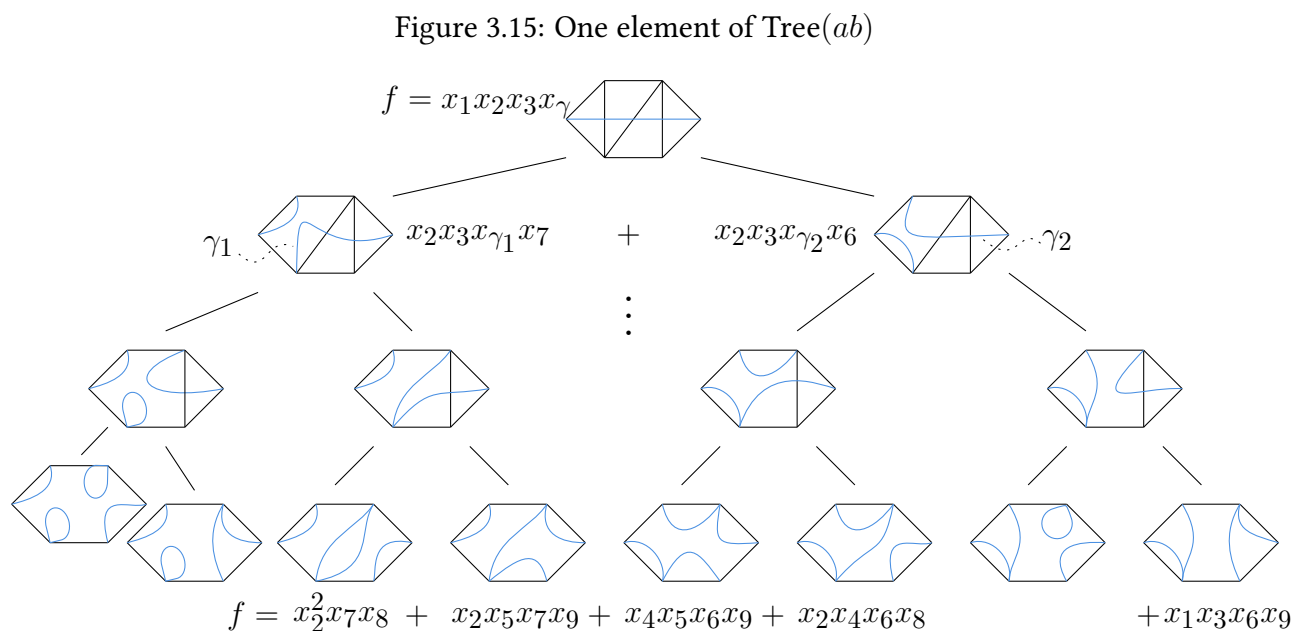
We now describe how to produce a *resolution tree from w* . Each node of such a tree is a diagram of arcs inside the $(n+3)$ -gon Σ , and is weighted by the product of cluster variables associated to those arcs (or zero if there is a closed loop in the diagram). The root of any resolution tree from w is the diagram consisting of the arc γ_w inside Σ_w . Choosing an intersection point p_i to resolve at creates two children of this root (see Figure 3.14). If we continue along in this way (choosing an intersection point to resolve at in each child, etc.), and halt whenever we have resolved every

intersection point, a binary tree (with additional node structure) is produced.

Definition 3.21. The set of *resolution trees* $\text{Tree}(w)$ associated to w is the set whose elements are the binary resolution trees from w as described above.

Note that $\text{Res}(w)$ is equal to the union of the leaves of the trees in $\text{Tree}(w)$.

Example 3.22. The figure below shows one element of $\text{Tree}(w)$ for the word $w = ab$.



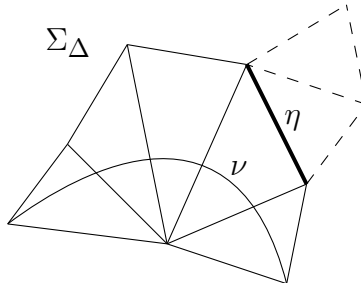
Although our construction of arcs seems restrictive, the next lemma shows that there is in fact no loss of generality.

Lemma 3.23. Any cluster variable associated to an arc in a polygon can be computed as x_w for some word w .

Proof. Let ν be an arc in the triangulated polygon Σ_Δ , triangulated by Δ . If ν crosses every internal diagonal in Δ , then we are done. Otherwise, we work inside the triangulated subpolygon Σ'_Δ in Σ_Δ obtained by deleting from Δ any edge that is not an edge of some triangle crossed by

ν . Furthermore, we “freeze” any edge η bordering a deleted triangle, meaning we disallow this arc to be flipped, so that also x_η cannot be mutated.

Figure 3.16: An arc in a triangulated subpolygon



The result now follows by noting that any arc obtained by resolving ν will be contained entirely within the triangulated subpolygon just mentioned.

□

3.6 Snake Graphs

Definition 3.24. The *snake graph* G_w associated to w is the labeled planar graph recursively defined by the procedure given below.

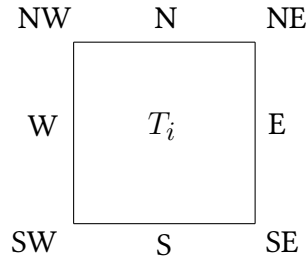
1. Choose an orientation-preserving embedding of the triangulated square $[\Delta_0, \Delta_1]$ into the discrete plane \mathbb{Z}^2 such that its image \tilde{T}_1 is a triangulated unit square with vertices $(0, 0)$, $(1, 0)$, $(0, 1)$, and $(1, 1)$ in \mathbb{Z}^2 , and such that the point $a \in \Delta_0$ maps to the point $(0, 0)$. Note that the (line spanned by the) image of the triangulating edge will have slope -1 .
2. Choose an orientation-reversing map of $[\Delta_1, \Delta_2]$ into \mathbb{Z}^2 such that its image \tilde{T}_2 is a triangulated unit square (again, with triangulating edge having slope -1) glued to \tilde{T}_1 along the unique edge in each \tilde{T}_i labeled $j \in \{n + 1, \dots, 2n + 3\}$. Note that if the intersection point

of the diagonals δ_1 and δ_2 is to the left (resp. right) of γ , then \widetilde{T}_2 is the triangulated square directly to the right of (resp. above) \widetilde{T}_1 .

3. Continue this process, using orientation-preserving maps for i odd and orientation-reversing maps for i even, to get the graph \widetilde{G}_w , built from triangulated unit squares in \mathbb{Z}^2 (with all triangulating edges having slope -1) glued either above or to the right of the previous square. Each \widetilde{T}_i will be called a *tile* of \widetilde{G}_w . The triangulating edge of each \widetilde{T}_i is called the *diagonal* of \widetilde{T}_i .
4. The *snake graph* G_w is the graph in \mathbb{Z}^2 gotten by deleting each diagonal from each tile in \widetilde{G}_w .

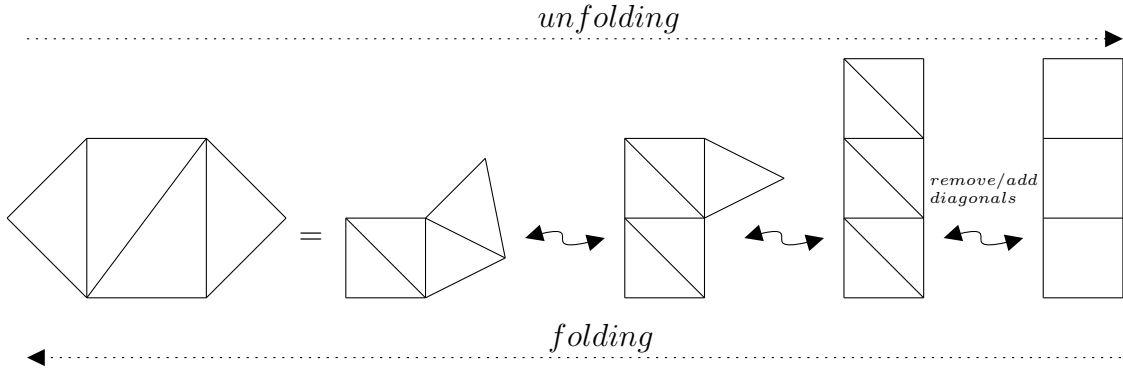
Let T_i be the tile \widetilde{T}_i after its diagonal has been removed. We will call T_i a *tile* of G_w . We will often refer to the corners (SW, SE, NE, NW) and edges (S,E,N,W) of a tile T_i as indicated in the next figure.

Figure 3.17: Shorthand to describe the corners and edges of a tile T_i



Order the tiles of G_w by $T_1 < T_2 < \dots < T_n$. A *boundary edge* of G_w is any edge of G_w not occurring as a shared edge between any two of its consecutive tiles. Any edge that is not a boundary edge (i.e., each gluing edge) will be called an *internal edge* of G_w . Let the internal edges of G_w be labeled e_1, e_2, \dots, e_{n-1} , where e_i is the gluing edge between tiles T_i and T_{i+1} .

Figure 3.19: The folding and unfolding maps



Definition 3.29. Fix a word w and the snake graph G_w . Form a word $\text{sh}(G_w)$ of length $n - 1$, called the *shape of the snake graph* G_w , by letting i run through $1, 2, \dots, n$ in the following rule: If tile T_{i+1} is glued to the right of tile T_i , write the letter a , and if tile T_{i+1} is glued to the top of tile T_i , write the letter b

Example 3.30. The shape of the snake graph for the word $w = ab$ is $\text{sh}(G_w) = bb$.

Remark 3.31. If w is straight then G_w is zigzag (see Remark 3.27) and so $\text{sh}(G_w)$ is zigzag. Conversely, if w is zigzag then G_w is straight and hence $\text{sh}(G_w)$ is straight.

Definition 3.32 and Definition 3.34 below will be used in the next section to define the continued fraction associated to a word.

Recall that G_w has an embedding into \mathbb{Z}^2 such that the first tile T_1 of G_w has vertices $(0, 0)$, $(1, 0)$, $(0, 1)$, and $(1, 1)$. Additionally, recall that each tile T_i of G_w is glued either above or to the right of the previous tile T_{i-1} . Informally, the snake graph G_w “goes up and to the right”.

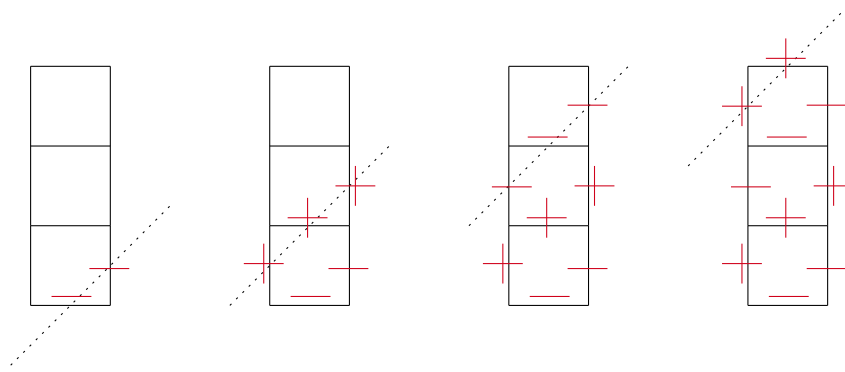
Definition 3.32. (see [5]) Fix the word w and the associated snake graph G_w . Let x and y be the names of the coordinate functions on \mathbb{Z}^2 . Note that the midpoint m_e of each edge e in G_w lies on precisely one of the diagonal lines $y = x + (j + \frac{1}{2})$ for $j \in \mathbb{Z}$. The *sign function* s on G_w is

the function on the edges e of G_w to the set $\{-, +\}$ defined by

$$s(e) = \begin{cases} -, & \text{if } m_e \text{ lies on } y = x + (j + \frac{1}{2}) \text{ for } j \text{ even} \\ +, & \text{if } m_e \text{ lies on } y = x + (j + \frac{1}{2}) \text{ for } j \text{ odd.} \end{cases}$$

Example 3.33. The construction of the sign function s on G_{ab} is shown below in Figure 3.20.

Figure 3.20: The sign function s on G_{ab}



For $\epsilon \in \{-, +\}$, define

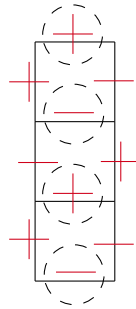
$$-\epsilon = \begin{cases} + & \text{if } \epsilon = - \\ - & \text{if } \epsilon = +. \end{cases}$$

Recall the internal edges of G_w are labeled e_1, \dots, e_{n-1} . Let e_0 be the S edge of the first tile T_1 of G_w . Define e_n to be either the N or E edge of tile T_n according to whether the last three tiles of G_w form a straight or zigzag snake graph; if the last three tiles are straight, the edge e_n is across from e_{n-1} (so that $s(e_n) = -s(e_{n-1})$), and if the last three tiles of G_w instead form a zigzag snake graph then the edge e_n is adjacent to e_{n-1} (thus, $s(e_n) = s(e_{n-1})$). If $\text{sh}(G_w) = bb$, then we choose e_2 to be across from e_1 . If $\text{sh}(G_w) = aa$, then we choose e_2 to be adjacent to e_1 . If G_w has only one tile, then say e_1 is across from e_0 .

Definition 3.34. (see [5]) Fix the word w , the associated snake graph G_w , and the sign function s on the edges of G_w . The *sign sequence* \mathbf{s}_w associated to the word w is the sequence $\mathbf{s}_w = (s(e_0), s(e_1), \dots, s(e_n))$.

Example 3.35. For $w = ab$ the associated sign sequence is $\mathbf{s}_{ab} = (-, +, -, +)$.

Figure 3.21: The sign sequence \mathbf{s}_{ab} on G_{ab}



3.7 Continued Fractions

In [5] (see also [6], [25]), connections between cluster algebras, continued fractions, and snake graphs were established. We review some of the basic definitions found there, and use them to define the continued fraction associated to a word w .

Definition 3.36. Fix $a_1 \in \mathbb{Z}$ and for $2 \leq i \leq k$ fix the positive integers $a_i \in \mathbb{Z}$. A *finite continued fraction*, denoted by $[a_1, a_2, \dots, a_k]$ is an expression of the form

$$a_1 + \frac{1}{a_2 + \frac{1}{a_3 + \frac{1}{\ddots + \frac{1}{a_k}}}}$$

Say that the continued fraction $[a_1, a_2, \dots, a_k]$ is *positive* if $a_i > 0$ for every i . From now on we will only consider positive continued fractions.

Definition 3.37. Fix a word w of length $n - 1$, along with the snake graph G_w . Recall the sign sequence $\mathbf{s}_w = (s(e_0), \dots, s(e_n))$ of G_w , and our convention that $s(e_0) = -$. Let $\epsilon = -$. Define positive integers a_1, \dots, a_k as indicated below.

$$\mathbf{s}_w = (s(e_0), \dots, s(e_n)) = \underbrace{(\epsilon, \epsilon, \dots, \epsilon)}_{a_1 \text{ times}}, \underbrace{(-\epsilon, -\epsilon, \dots, -\epsilon)}_{a_2 \text{ times}}, \dots, \underbrace{((-1)^k \epsilon, (-1)^k \epsilon, \dots, (-1)^k \epsilon)}_{a_k \text{ times}}.$$

Define the (*finite, positive*) *continued fraction* $CF(w)$ associated to w to be $CF(w) = [a_1, a_2, \dots, a_k]$.

Remark 3.38. By Theorem A in [5] (which we recall as Theorem 4.5 below), simplifying the continued fraction $CF(w)$ gives a rational number in lowest terms that is greater than 1.

Example 3.39. The continued fraction $CF(ab)$ is equal to $\frac{5}{3}$. Indeed, the associated sign sequence is $\mathbf{s}_{ab} = (-, +, -, +)$, so that

$$CF(ab) = [1, 1, 1, 1] = 1 + \frac{1}{1 + \frac{1}{1 + \frac{1}{1}}}$$

Remark 3.40. Suppose the word w is either straight or zigzag, and that its length is $l(w) = n - 1$. Let the Fibonacci numbers be denoted by $F_1 = 1, F_2 = 1, F_3 = 2$, etc. Consider the continued fraction $CF(w)$.

(a) If w is the straight word $w = a^{n-1}$ then

$$\text{CF}(w) = [2, \underbrace{1, \dots, 1}_{n-1 \text{ times}}] = \frac{F_{n+2}}{F_n},$$

(b) If w is the straight word $w = b^{n-1}$ then

$$\text{CF}(w) = [\underbrace{1, 1, 1, \dots, 1}_{n+1 \text{ times}}] = \frac{F_{n+2}}{F_{n+1}}.$$

(c) If w is the zigzag word $w = bab \dots$ then $\text{CF}(w) = [1, n] = \frac{n+1}{n}$.

(d) If w is the zigzag word $w = aba \dots$ then $\text{CF}(w) = [n] = \frac{n}{1} = n$.

3.8 Distributive Lattices

Definition 3.41. Let D be a finite poset. The *meet* of the elements $p \in D$ and $q \in D$ is the unique element denoted $p \wedge q \in D$ (if it exists) that satisfies:

- (a) $p \wedge q < p$ and $p \wedge q < q$, and
- (b) if there exists some $r \in D$ such that $r < p$ and $r < q$, then $r < p \wedge q$.

The *join* of p and q is the unique element $p \vee q \in D$ (if it exists) that satisfies:

- (a) $p \vee q > p$ and $p \vee q > q$, and
- (b) if there exists some $r \in D$ such that $r > p$ and $r > q$, then $r > p \vee q$.

We say D is a *lattice* if for any two elements $p, q \in D$, both $p \wedge q$ and $p \vee q$ exist.

Remark 3.42. It is easy to see that every finite lattice has a unique minimum element and a unique maximum element.

Definition 3.43. Suppose that the finite poset D is a lattice. We say D is a *distributive lattice* if for all $p, q, r \in D$ the following two distributive laws hold:

$$(a) \quad p \wedge (q \vee r) = (p \wedge q) \vee (p \wedge r)$$

$$(b) \quad p \vee (q \wedge r) = (p \vee q) \wedge (p \vee r).$$

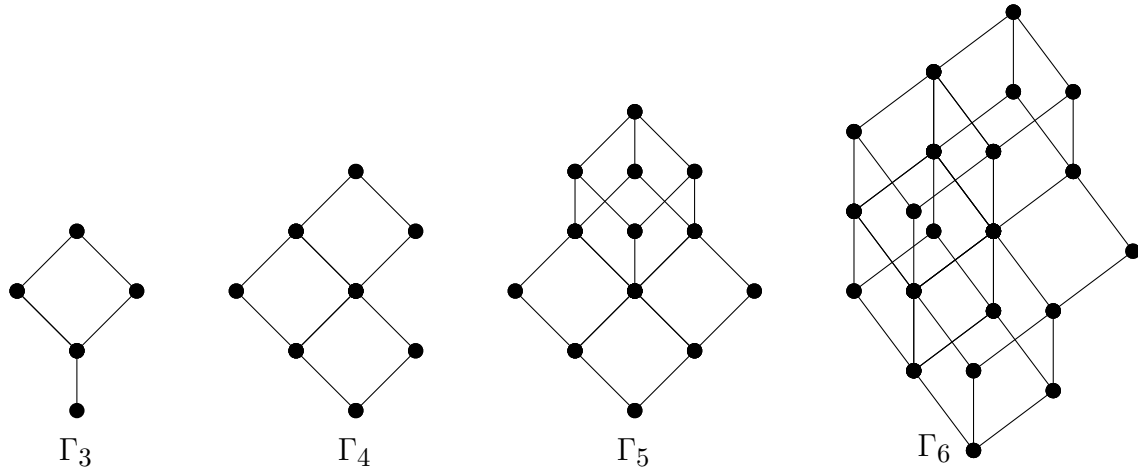
Definition 3.44. Let C be a finite poset. An *order ideal* I of C is a subset of C such that if $p \in I$ and $q \in C$ with $q < p$, then $q \in I$. We denote by $\mathcal{I}(C)$ the poset (ordered by inclusion) of order ideals of C .

Example 3.45. The poset of order ideals of a fence on n vertices is called a *Fibonacci cube of order n* , which we denote Γ_n . Alternatively, the Fibonacci cube of order n may be defined as a graph, with vertices those binary words from $\{0, 1\}$ with n bits that do not contain two consecutive instances of the bit 1. There is an edge between two vertices if they differ by precisely one bit in the same position. For original references, see [21] and [22]. For a somewhat recent survey on Fibonacci cubes, see [23]. Figure 3.22 below shows the Fibonacci cubes which result from computing the poset of order ideals on each of the four zigzag posets shown in Figure 3.5.

Definition 3.46. Let D be a finite lattice. An element $r \in D$ is said to be *join-irreducible* if r is not the unique minimum element of D (see Remark 3.42) and there do not exist two elements $p, q \in D$ with $p < r, q < r$, and $r = p \vee q$. We denote by $\mathcal{J}(D)$ the poset (with the induced order) of join-irreducible elements of D .

Theorem 3.47. (see [2]) *Let D be a finite lattice. Let $C = \mathcal{J}(D)$ be the poset of join-irreducibles of D . Then D is a distributive lattice if and only if D is isomorphic to $\mathcal{I}(C)$.*

Figure 3.22: Four Fibonacci cubes



By Theorem 3.47, $\mathcal{I}(C_w)$ is a distributive lattice for any word w .

Definition 3.48. The *distributive lattice* D_w associated to w is defined by $D_w = \mathcal{I}(C_w)$

Example 3.49. The distributive lattice D_{ab} is isomorphic to the Fibonacci cube Γ_3 , shown as the leftmost poset in Figure 3.22.

Chapter 4

Expansion Posets

Fix a word w of length $l(w) = n - 1$ and the associated objects defined in the previous chapter.

The goals of this chapter are as follows:

- (1) Recall three known combinatorial interpretations of the terms in the Laurent expansion of any cluster variable x_w parameterized by the arc γ_w .
- (2) Equip each such representation with a poset structure.

4.1 Perfect Matchings of Snake Graphs

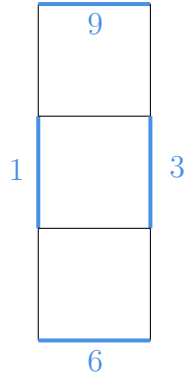
It is easy to see that any snake graph with n tiles has an even number $2(n + 1)$ of vertices.

Definition 4.1. A *perfect matching* P of the snake graph G_w is a choice of $n + 1$ edges in G_w such that each vertex of G_w is the endpoint of exactly one edge e in P .

The *weight* of the edge e is the initial cluster variable x_e . The *weight* of a perfect matching P is defined to be the product of initial cluster variables $x_P = \prod_{e \in P} x_e$. Let \mathbb{P}_w be the set of all perfect matchings of the snake graph G_w .

Example 4.2. Figure 4.1 shows one perfect matching P_- (see Definition 4.6 and Figure 4.4 below for the notation P_-) of the snake graph G_{ab} . The weight of this perfect matching is $x_1 x_3 x_6 x_9$.

Figure 4.1: The perfect matching P_- on G_{ab}



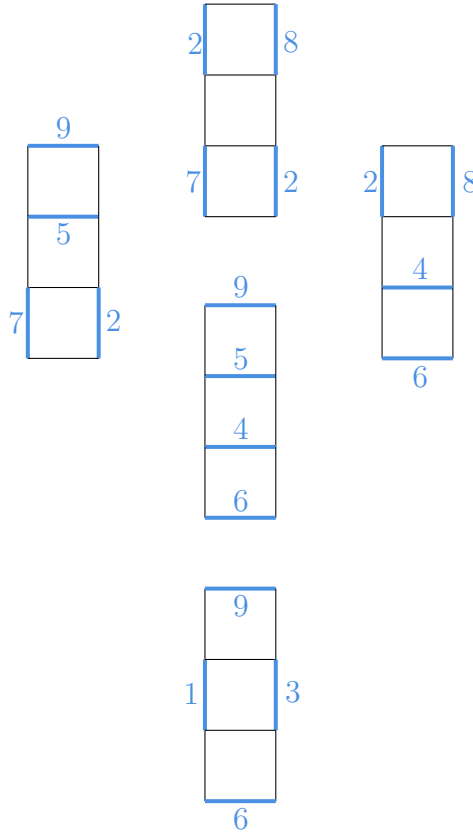
Theorem 4.3. (Theorem 3.1 in [28]) Let w be any word, and consider the set \mathbb{P}_w of perfect matchings on the snake graph G_w . Then the cluster variable x_γ can be written as the sum

$$x_\gamma = \frac{1}{x_1 x_2 \dots x_n} \sum_{P \in \mathbb{P}_w} x_P.$$

Example 4.4. Figure 4.2 below shows the five perfect matchings on the snake graph G_{ab} . Note that summing over the weights of these perfect matchings gives the cluster variable x_{ab} displayed in Figure 3.13.

Consider the word w , the snake graph G_w , and the associated continued fraction $\text{CF}(w) = [a_1, a_2 \dots a_k]$. Let $G_w^{a_1}$ be the subsnake graph of G_w obtained from G_w by deleting its first a_1 tiles. Denote the cardinality of the set \mathbb{P}_w by $|\mathbb{P}_w|$. Let $\mathbb{P}_w^{a_1}$ be the perfect matchings on $G_w^{a_1}$, and $|\mathbb{P}_w^{a_1}|$ the cardinality of the set $\mathbb{P}_w^{a_1}$.

Figure 4.2: The five perfect matchings on G_{ab}



Theorem 4.5. (Theorem 3.4 in [5]) For any word w , its associated continued fraction $CF(w)$ is equal to the quotient of cardinalities

$$CF(w) = \frac{|\mathbb{P}_w|}{|\mathbb{P}_w^{a_1}|},$$

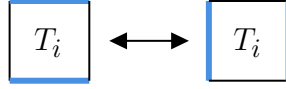
and the fraction on the right hand side is reduced.

We now give the set \mathbb{P}_w a poset structure.

Let $P \in \mathbb{P}_w$. A *twist* of P at tile i is the local move that takes two edges in P that are located opposite one another on tile T_i of G_w and replaces them with the remaining two edges of T_i .

Directly below is the local picture for the twist at a generic tile T_i .

Figure 4.3: Twist of a perfect matching at tile T_i



An *up-twist* at tile T_i is a twist that meets the *twist-parity condition* (see Theorem 5.4 in [30]):

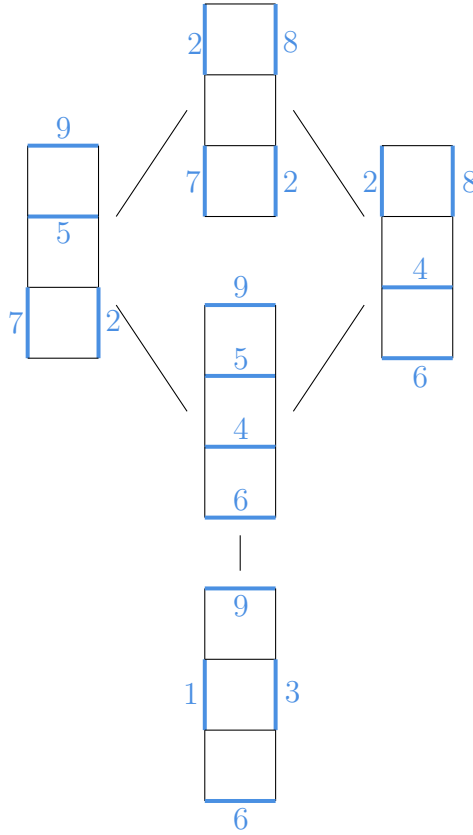
- (1) If i is odd, the horizontal edges of T_i are replaced with the vertical edges of T_i , or
- (2) If i is even, the vertical edges of T_i are replaced with the horizontal edges of T_i .

Definition 4.6. The *minimal matching* P_- of \mathbb{P}_w is the unique perfect matching of G_w such that every edge in P_- is a boundary edge of G_w and the S edge of tile T_1 is in P_- . The *maximal matching* P_+ of \mathbb{P}_w is the unique perfect matching of G_w such that every edge in P_+ is a boundary edge of G_w and the S edge of tile T_1 is not in P_+ .

Definition 4.7. Define a *poset structure* on \mathbb{P}_w as follows. The unique minimal element of \mathbb{P}_w is the minimal matching P_- , and the unique maximal element is P_+ . A perfect matching P_2 covers a perfect matching P_1 if there exists a tile T_i such that P_2 can be obtained from P_1 by performing a single up-twist of P_1 at T_i .

Example 4.8. The poset \mathbb{P}_{ab} of perfect matchings on the snake graph G_{ab} is shown below in Figure 4.4. Note that \mathbb{P}_{ab} is isomorphic to the Fibonacci cube Γ_3 . The sum of the weights attached to each perfect matching gives the cluster variable x_{ab} shown in Example 3.13.

Figure 4.4: The poset \mathbb{P}_{ab}



Remark 4.9. Let the length of w be $l(w) = n - 1$.

- (a) The poset of perfect matchings \mathbb{P}_w on a zigzag snake graph G_w is isomorphic to a linear chain with $n + 1$ elements and n edges.
- (b) The poset of perfect matchings \mathbb{P}_w on a straight snake graph G_w with n tiles is isomorphic to the Fibonacci cube Γ_n .

Remark 4.10. The two posets \mathbb{A}_w and \mathbb{T}_w defined below are each isomorphic to a linear chain when w is straight, and are each isomorphic to a Fibonacci cube when w is zigzag. In general, the three posets defined in this chapter are isomorphic to one another when they are parameterized by the same word. In Proposition 4.24, we recall explicit isomorphisms between these posets which respects the additional node structure present in each.

4.2 Perfect Matchings of Angles

Fix a word w of length $l(w) = n - 1$. By the constructions above, this choice determines the arc $\gamma_w = \gamma_{a \rightarrow b}$ in the triangulated $(n + 3)$ -gon Σ_w . Recall the notation $\Sigma_w = [\Delta_0, \Delta_1, \dots, \Delta_n]$.

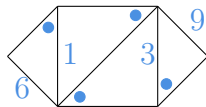
Definition 4.11. Any angle o of the triangle Δ_i is *incident* to its vertex. A *perfect matching of angles in Σ_w* is a selection of $n + 1$ angles from the triangles $\Delta_0, \Delta_1, \dots, \Delta_n$ of Σ_w , one per triangle, such that

- (1) Each angle is incident to an endpoint of one of the internal diagonals $\delta_1, \delta_2, \dots, \delta_n$.
- (2) No two angles are incident to the same vertex of the polygon Σ .

The *weight* of each angle o in Δ_i is the cluster variable x_o associated to the edge of Δ_i opposite of o . The *weight of α* is defined to be the product of initial cluster variables $x_\alpha = \prod_{o \in \alpha} x_o$. Let \mathbb{A}_w be the set of all perfect matchings of angles in Σ_w .

Example 4.12. Shown in Figure 4.5 is one perfect matching of angles in Σ_{ab} (in fact, it is the *minimal matching A_-* , explained below). Selecting an angle to be included in a particular matching is visualized by placing a ball “close” to that angle inside the appropriate triangle.

Figure 4.5: The perfect matching of angles A_- on Σ_{ab} .



Note that the weight $x_1 x_3 x_6 x_9$ of this element is the same as the weight of the snake graph perfect matching shown in Example 4.1.

Theorem 4.13. (Theorem 1.2 in [42]) Let w be any word, and consider the set \mathbb{A}_w of perfect matchings of angles on the triangulated surface Σ_w . Then the cluster variable x_w can be written as

$$x_w = \frac{1}{x_1 x_2 \dots x_n} \sum_{\alpha \in \mathbb{A}_w} x_\alpha.$$

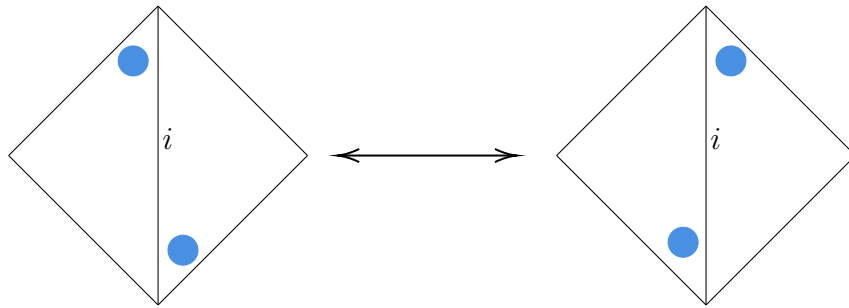
Definition 4.14. An angle is *incident* to the two arcs in Δ_w which are sides of that angle. By a *boundary angle* of Σ_w , we mean any angle of Σ_w that is incident to exactly one boundary edge of Δ_w . Any angle that is neither incident to a or b nor to a boundary angle will be called an *internal angle*.

We now give the set \mathbb{A}_w a poset structure.

Let $A \in \mathbb{A}_w$. A *twist* of A at diagonal δ_i is the local move that takes two angles in A incident to opposite vertices of the same internal diagonal i and replaces them with the remaining two angles incident to δ_i .

Directly below is the local picture for the twist at diagonal δ_i .

Figure 4.6: Twist of a perfect matching of angles at diagonal δ_i



The arc $\gamma_{a \rightarrow b}$ naturally partitions the set $\{\text{vertices of } \Sigma\} - \{a, b\}$ into two sets; those vertices which are to the left of $\gamma_{a \rightarrow b}$, and those vertices of Σ to the right of $\gamma_{a \rightarrow b}$. Let l_i be the endpoint of i to the left of $\gamma_{a \rightarrow b}$, and r_i the endpoint to the right. A twist at δ_i is an *up-twist* if the angle from Δ_i matched to r_i is replaced with the angle matched to l_i , and the angle from Δ_{i-1} matched

to l_i is replaced with the angle matched to r_i .

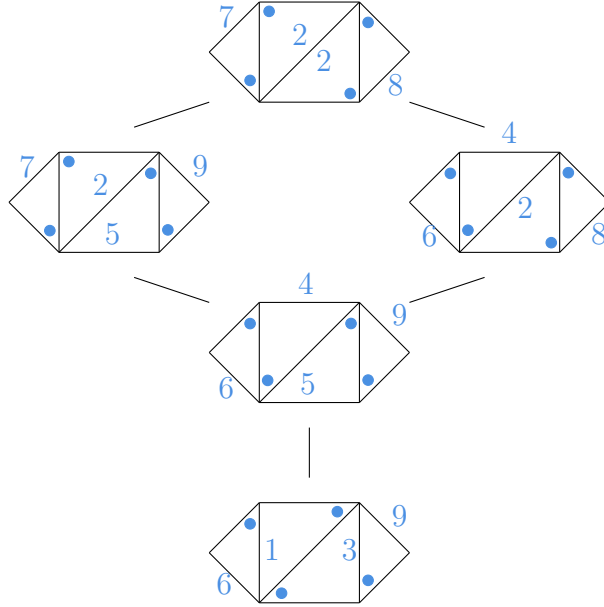
Definition 4.15. The *minimal matching* A_- of \mathbb{A}_w is the unique perfect matching of angles in Σ_w such that the boundary angle in Δ_0 with boundary edge δ_{2n+1} is matched, and only boundary angles are used in A_- . The *maximal matching* A_+ is the unique perfect matching of angles in Σ_w such that the boundary angle in Δ_0 with boundary edge δ_{2n} is matched, and only boundary angles are used in A_+ .

Definition 4.16. The *poset structure on \mathbb{A}_w* is defined as follows. The unique minimal element of \mathbb{A}_w is the minimal matching A_- , and the unique maximal element is A_+ . A perfect matching of angles A_2 covers a perfect matching of angles A_1 if there exists a diagonal δ_i such that A_2 can be obtained from A_1 by performing a single up-twist of A_1 at δ_i .

Remark 4.17. Alternatively, A_- can be defined by the following *min-condition*, found in [41]. At each vertex v of Σ_w , order the angles incident to v in counterclockwise order around v . For each vertex v of the triangulated polygon Σ_w that is incident to at least one internal diagonal of Δ_w , the angle $o \in A_-$ at v is the first angle at v . Similarly, a *max-condition* (replace “counterclockwise” with “clockwise” in the above) can be used to define A_+ .

Figure 4.7 shows the poset of perfect matchings of angles in Σ_{ab} . This poset is isomorphic to the one given in Example 4.4, and one can check that the respective weights coincide as well.

Figure 4.7: The poset \mathbb{A}_{ab}



4.3 T -Paths

Recall that the internal diagonals of Δ_w are labeled $1, 2, \dots, n$ and are ordered $\delta_1 < \delta_2 < \dots < \delta_n$, and the notation for the intersection points $p_i = \gamma_w \cap \delta_i$.

Definition 4.18. A T -path from a to b , denoted $T = (T_1, T_2, \dots, T_{l(T)})$, is an ordered selection of bicolored (either blue or red) edges from the triangulation Δ_w subject to the following conditions:

1. The edges in T form a path from a to b .
2. The number of edges $l(T)$ in T is odd (we call $l(T)$ the *length* of the T -path).
3. The odd-indexed edges in T are all colored blue, and the even-indexed edges in T are all colored red.
4. All edges in T are distinct.
5. Every red edge in T crosses $\gamma_{a \rightarrow b}$.

6. If δ_i and δ_j are two internal diagonals of the triangulation that $\gamma_{a \rightarrow b}$ crosses and $i < j$ then the crossing point of δ_i and $\gamma_{a \rightarrow b}$ is closer to a than the crossing point of δ_j and $\gamma_{a \rightarrow b}$.

For any $T \in \mathbb{T}_w$ let B_T be the set of blue edges from T , and let R_T be the red edges from T .

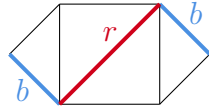
Define the *weight* x_T of T by

$$x_T = \prod_{b \in B_T} x_b \prod_{r \in R_T} x_r^{-1}.$$

Let \mathbb{T}_w be the set of all T -paths from a to b .

Example 4.19. Figure 4.8 shows one T -path on the triangulation Σ_{ab} (in fact, it is the *minimal T -path* T_- , explained below). The weight of this T -path is $\frac{x_6 x_9}{x_2}$. Note that multiplying this weight by $x_1 x_2 x_3$ gives $x_1 x_3 x_6 x_9$, the weight of the elements in Example 4.1 and Example 4.5.

Figure 4.8: The T -path T_- with edges from Δ_{ab}



Theorem 4.20. (Theorem 1.2 in [35]) Let w be any word, and consider the set \mathbb{T}_w of T -paths on the triangulated surface Σ_w . Then the cluster variable x_w can be written as

$$x_w = \sum_{T \in \mathbb{T}_w} x_T.$$

We now give the set \mathbb{T}_w a poset structure.

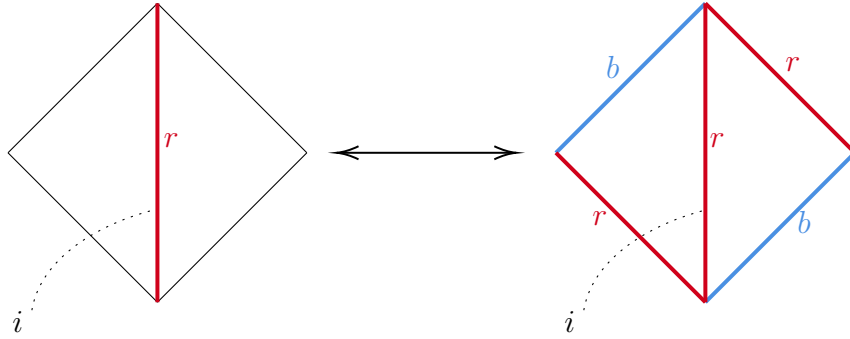
Let $T \in \mathbb{T}_w$ and let $T = (T_1, T_2, \dots, T_{l(T)})$ be a T -path. Pick a red edge T_r from T , which necessarily has as its underlying edge an internal diagonal of Δ_w . The two triangles Δ_i and Δ_{i+1}

from Σ_w that are glued along the underlying edge of T_r determine a triangulated quadrilateral $[\Delta_i, \Delta_{i+1}]$ with diagonal T_r .

Define a *twist* of T to be the local move that colors the four (non-triangulating) sides of the quadrilateral $[\Delta_i, \Delta_{i+1}]$ as follows: two edges of $[\Delta_i, \Delta_{i+1}]$ that are opposite one another are colored blue, the other two edges are colored red, and uncolored boundary edges in Δ_w are not allowed to be colored red. Here, if a red edge is colored blue then the colors cancel one another and that edge is not used in the resulting T -path, and similarly for if a blue edge is colored red [20].

Directly below is the local picture for the T -path twist at diagonal δ_i .

Figure 4.9: Twist of a T -path at diagonal δ_i



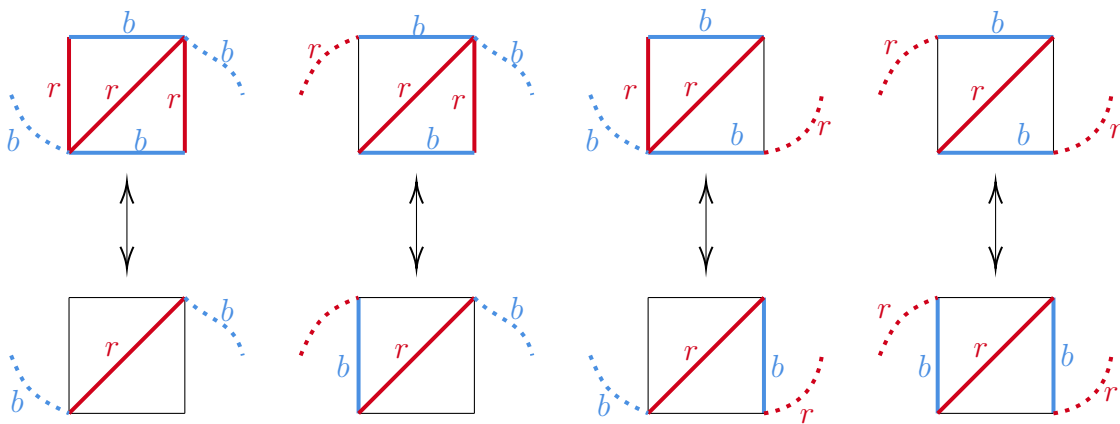
The arc $\gamma_{a \rightarrow b}$ naturally partitions the set $\{\text{vertices of } \Sigma\} - \{a, b\}$ into two sets; those vertices which are to the left of $\gamma_{a \rightarrow b}$, and those vertices of Σ to the right of $\gamma_{a \rightarrow b}$. Let l_i be the endpoint of δ_i to the left of $\gamma_{a \rightarrow b}$, and r_i the endpoint to the right of $\gamma_{a \rightarrow b}$. Let u_{i-1} and d_{i-1} be the two edges of Δ_{i-1} that are not equal to δ_i , such that u_{i-1} is adjacent to l_i , and d_{i-1} is adjacent to r_i . Let the two edges u_i and d_i of Δ_i be defined similarly. A twist at δ_i is an *up-twist* if it colors d_{i-1} and u_i red, and colors d_i and u_{i-1} blue.

Recall that the sides of the first triangle Δ_0 of Σ_w are labeled $1 \rightarrow 2n \rightarrow 2n + 1 \rightarrow 1$ in clockwise order. The *minimal element* T_- of \mathbb{T}_w is the unique T -path that starts with the blue edge δ_{2n} and uses only internal diagonals for its edges, except for the first and last boundary

edges. The *maximal element* T_+ of \mathbb{T}_w is the unique T -path from a to b that starts with the blue edge δ_{2n+1} and uses only internal diagonals for its edges, except for the first and last boundary edges.

Remark 4.21. It is not obvious that a twist of a T -path is always defined. Figure 4.10 shows the eight possibilities for how any T -path looks locally at an internal diagonal which is not the first or last. In each quadrilateral shown, the top two edges are boundary edges, the other three are internal diagonals, and the dotted lines can be either, as long as a red edge is not on the boundary. Each of the four arrows indicate when two T -paths are related by a twist.

Figure 4.10: T -path twists at internal diagonals are always defined

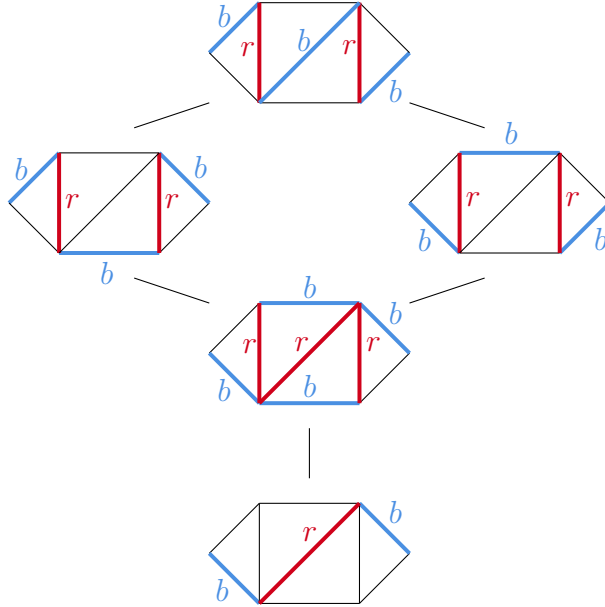


Thus, twists are well-defined for any diagonal that isn't the first or last. A similar analysis shows twists are always defined for the first and last diagonals, as well.

Definition 4.22. The *poset structure* on \mathbb{T}_w is defined as follows. The unique minimal element of \mathbb{T}_w is T_- , and the unique maximal element is T_+ . A T -path T_2 covers a T -path T_1 if there exists a diagonal δ_i such that T_2 can be obtained from T_1 by performing a single up-twist of T_1 at diagonal δ_i .

Example 4.23. Figure 4.11 shows the poset \mathbb{T}_{ab} of T -paths from a to b associated to the word $w = ab$.

Figure 4.11: The poset T_{ab}



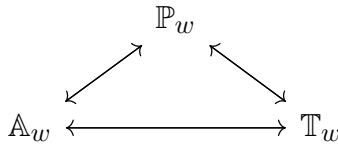
If we sum over the weights of this poset, we obtain

$$x_{ab} = \frac{x_6 x_9}{x_2} + \frac{x_4 x_5 x_6 x_9}{x_1 x_2 x_3} + \frac{x_5 x_7 x_9}{x_1 x_3} + \frac{x_4 x_6 x_8}{x_1 x_3} + \frac{x_2 x_7 x_8}{x_1 x_3}.$$

If we find a common denominator for the five terms in this sum, we see that this expression for x_{ab} is equivalent to the one given in Example 3.13.

It is known that perfect matchings on G_w are equivalent to both perfect matchings of angles on Σ_w (see [42]) and T -paths on Σ_w (see [28]).

Proposition 4.24. *Fix the word w . Then there are poset isomorphisms*



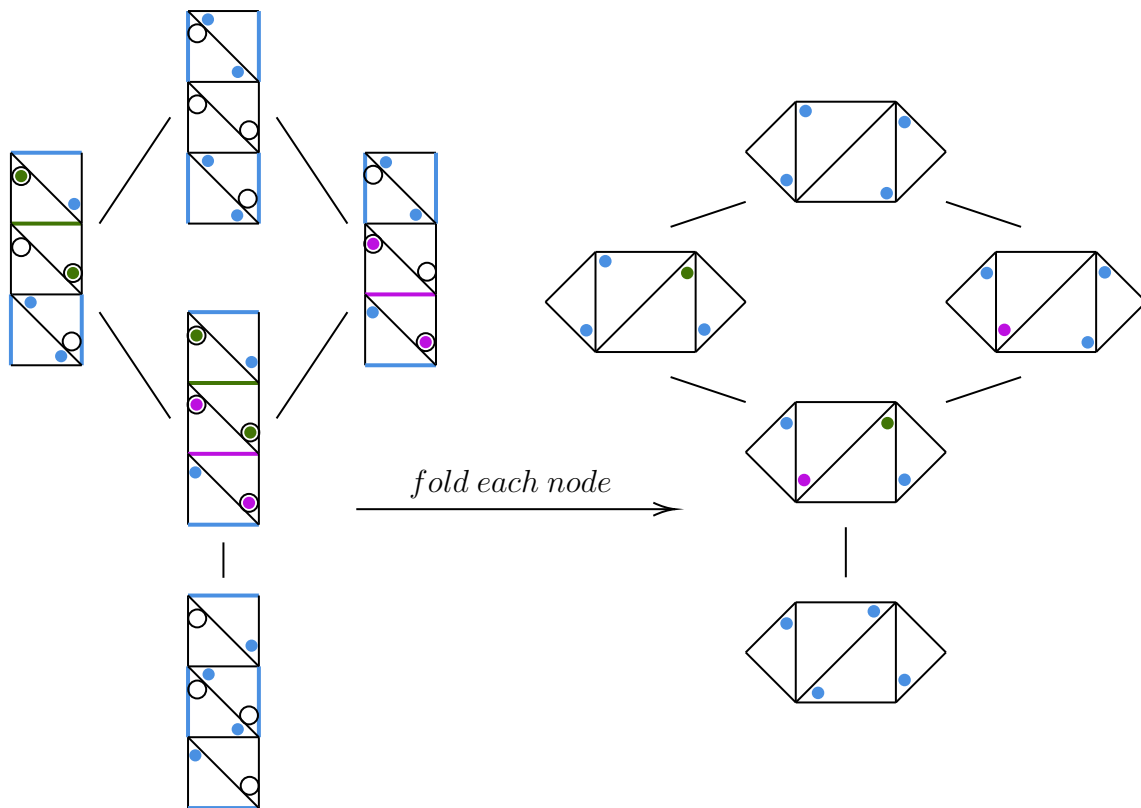
which respect the additional node structure of each poset.

We illustrate Proposition 4.24 with the three posets associated to the word $w = ab$ from our running example. By Lemma 3.2 in [42] there is a bijection between the edges in G_w and

the angles in Σ_w , induced by identifying certain pairs of angles in \widetilde{G}_w . The pairs of angles that are identified are those that are opposite one another in the quadrilateral determined by two consecutive tiles of \widetilde{G}_w . Any pair of angles in \widetilde{G}_w which have been identified correspond to a single internal angle in Σ_w .

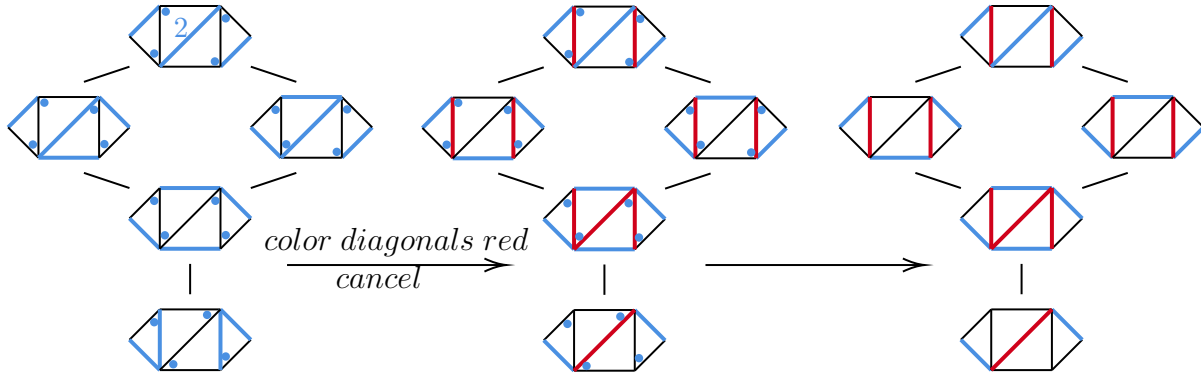
Thus, given a perfect matching $P \in \mathbb{P}_w$, we can associate to it a collection of angles in \widetilde{G}_w and fold the result to obtain the corresponding perfect matching of angles A in Σ_w . This assignment extends to a map of posets, since \mathbb{A}_w can be obtained by starting with the poset \mathbb{P}_w and folding every node. See Figure 4.12 for an illustration using the objects from our running example.

Figure 4.12: The map $\mathbb{P}_{ab} \rightarrow \mathbb{A}_{ab}$ via angle identification and folding



The second map $\mathbb{A}_w \rightarrow \mathbb{T}_w$ is defined by sending each angle in a matching A to the edge in Δ_w it is opposite of, and then coloring each internal diagonal red.

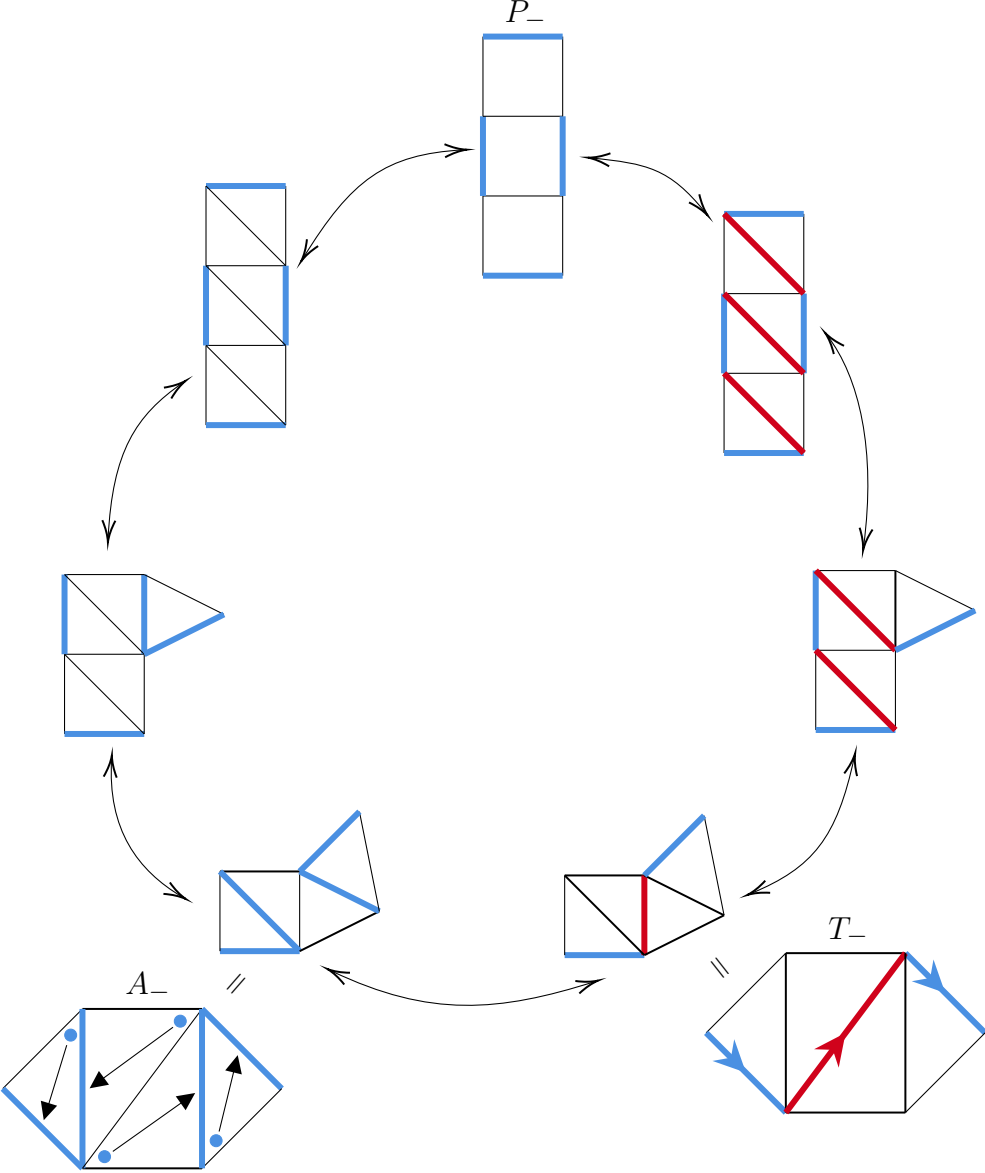
Figure 4.13: The map $\mathbb{A}_{ab} \rightarrow \mathbb{T}_{ab}$ via diagonal coloring and cancellation



Example 4.25. Figure 4.14 shows explicitly the application of the composition of bijections

$$\mathbb{P}_{ab} \rightarrow \mathbb{A}_{ab} \rightarrow \mathbb{T}_{ab} \rightarrow \mathbb{P}_{ab} \text{ to the input } P_- \in \mathbb{P}_{ab}.$$

Figure 4.14: The composition $\mathbb{P}_{ab} \rightarrow \mathbb{A}_{ab} \rightarrow \mathbb{T}_{ab} \rightarrow \mathbb{P}_{ab}$ restricted to minimal elements



Chapter 5

Dual Combinatorial Constructions

5.1 Words

For any $w_i \in \{a, b\}$, let $w_i^* \in \{a, b\}$ be the image of w_i under the involution $a \longleftrightarrow b$.

Definition 5.1. Let $w = w_1 w_2 \dots w_{n-1}$ be a word of length $n - 1$. The *dual word* w^* is the word of length $n - 1$ defined by $w^* = w_1^* w_2 w_3^* w_4 w_5^* \dots$

Example 5.2. The dual of the word $w = ab$ is $w^* = a^* b = bb$.

Remark 5.3. The dual of a straight word w is a zigzag word w^* and vice versa.

5.2 Type A_n Dynkin Quivers

Definition 5.4. Let A_w be the Dynkin quiver associated to the word w . The *dual Dynkin quiver* A_w^* is obtained by reversing the orientation of every other edge of A_w , starting with the first.

The next result is clear from the definitions.

Proposition 5.5. For any word w , we have $A_w^* = A_{w^*}$.

Example 5.6. In Figure 5.1, the Dynkin quiver A_{ab} is shown on the left, and the dual Dynkin quiver $A_w^* = A_{w^*} = A_{bb}$ is shown on the right.

Figure 5.1: The quiver A_{ab} and its dual A_{bb}



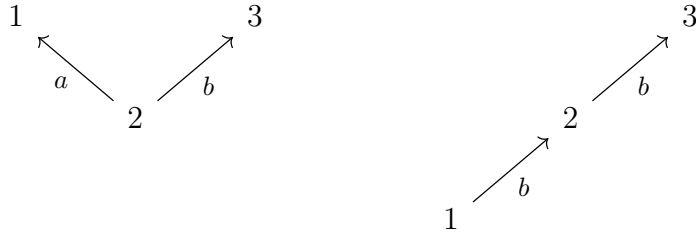
5.3 Posets

Definition 5.7. Recall the poset C_w associated to the word w . Define the *orientation* of an edge in C_w to be either NW or NE, according to whether it is labeled by a or b , respectively. The *dual poset* C_w^* is defined by changing the orientation of every other edge of C_w , starting with the first.

Proposition 5.8. For any word w , we have $C_w^* = C_{w^*}$.

Example 5.9. The leftmost poset in Figure 5.2 is the poset C_{ab} (see Figure 3.4), and on the right is the dual poset $C_w^* = C_{w^*} = C_{bb}$.

Figure 5.2: The poset C_{ab} and its dual C_{bb}



Remark 5.10. If w is straight then C_w is isomorphic to a linear chain, and the dual poset C_w^* is isomorphic to a fence.

5.4 Triangulations

Recall the notation $\Sigma_w = [\Delta_0, \Delta_1, \dots, \Delta_n]$, where Δ_i are the ideal triangles (with edge labels from Definition 3.12) cut out by the triangulation Δ_w of Σ . Let ∇_i be the edge-labeled triangle with the same positive integer labels as Δ_i but with opposite orientation. Define the *triangle map*

by the assignment

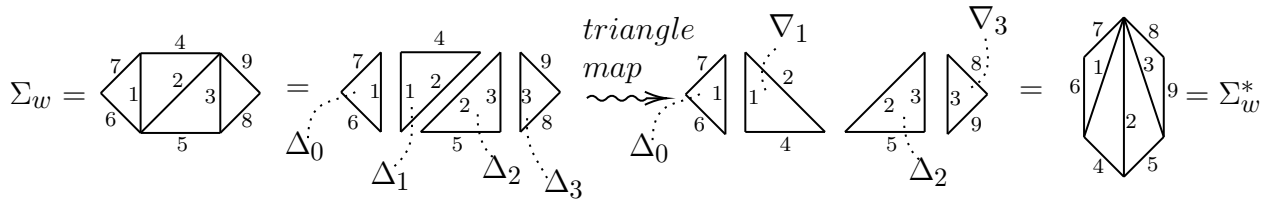
$$\Sigma_w = [\Delta_0, \Delta_1, \dots, \Delta_n] \mapsto [\Delta_0, \nabla_1, \Delta_2, \nabla_3, \Delta_4, \dots].$$

Define the image of this map to be Σ_w^* .

Definition 5.11. Consider the triangulation Δ_w of Σ associated to w . The *dual triangulation* Δ_w^* of Σ is the triangulation of Σ obtained by application of the triangle map $\Sigma_w \mapsto \Sigma_w^*$.

Example 5.12. Fix $w = ab$. Figure 5.3 shows how the dual triangulation $\Delta_w^* = \Delta_{ab}^* = \Delta_{bb}$ is built by applying the triangle map to Σ_{ab} .

Figure 5.3: The triangle map applied to Σ_{ab} gives Σ_{bb}



The next result again follows from the constructions given thus far.

Proposition 5.13. For any word w , we have $\Sigma_w^* = \Sigma_{w^*}$ and $\Delta_w^* = \Delta_{w^*}$.

Remark 5.14. If w is straight then Δ_w is a fan triangulation and the dual Δ_w^* is a zigzag triangulation. Conversely, if w is zigzag then Δ_w is a zigzag triangulation and the dual Δ_w^* is a fan triangulation.

Application of the triangle map to Σ_w gives a new seed for a cluster algebra $\mathcal{A}(\Sigma)_{w^*}$ isomorphic to $\mathcal{A}(\Sigma)_w$. If the new initial variable y_i is attached to the arc labeled i in Σ_w^* , we relabel this arc with the variable x_i . This combinatorial relabeling is introduced so that when we compute cluster variables attached to arcs in the dual triangulation, the result is a Laurent monomial in the initial cluster variables from the original seed.

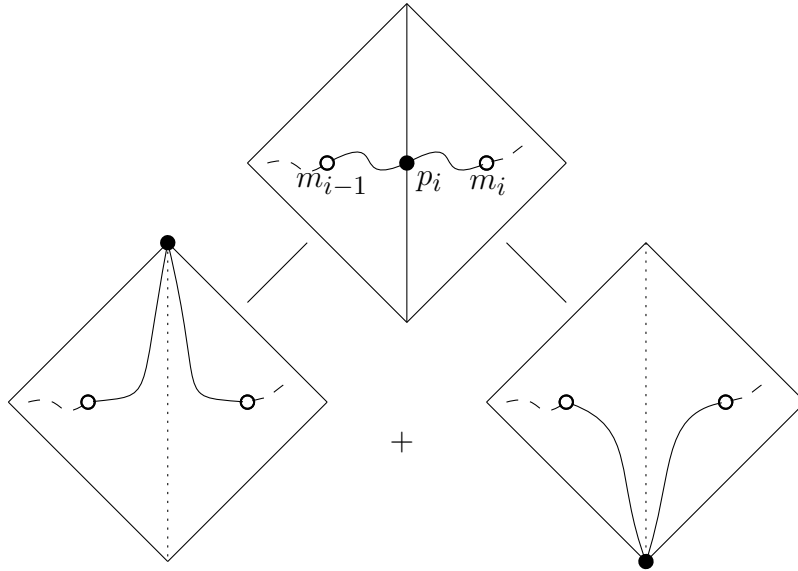
5.5 Slides, Arcs, and Cluster Variables

Fix a word w and the associated arc $\gamma = \gamma_{a \rightarrow b}$ in Σ_w . Recall the internal diagonals of Δ_w are $\delta_1, \delta_2, \dots, \delta_n$. For $1 \leq i \leq n$, let $p_i = \gamma_w \cap \delta_i$ be the intersection point of γ_w with the i^{th} internal diagonal δ_i of Δ_w . Set $p_0 = a$ and $p_{n+1} = b$. Choose a point $m_i \in \text{Int}(\Delta_i) \cap \gamma$ for each $0 \leq i \leq n$. Let γ_i be the portion of the arc γ_w strictly between m_{i-1} and m_i . Let γ_i^{left} be the portion of γ_i strictly between m_{i-1} and p_i , and γ_i^{right} the portion of γ_i strictly between p_i and m_i .

Definition 5.15. For $1 \leq i \leq n$, define a *slide* of γ_w at p_i by the following two-step process.

- (1) Perform the smooth isotopy that fixes $\gamma_w - \gamma_i$ and sends p_i to one of the endpoints of δ_i such that the images of γ_i^{left} and γ_i^{right} do not intersect any arc, and have no self-intersections.
- (2) Delete the diagonal δ_i .

Figure 5.4: Dual resolution of the intersection point p_i



Choosing one of the two possible slides at each p_i results in a collection of nonintersecting curves in Σ . Note that closed curves based at some $v \in \Sigma$ are the only loops that can occur.

Replace each curve with distinct endpoints by the arc or boundary segment from Δ_w with the same endpoints, and replace each closed curve with \emptyset . See Figure 5.4 below.

Definition 5.16. The set of *dual resolutions* $\text{Res}(w)^*$ associated to w has as its elements those diagrams that can be obtained from sliding each p_i in one of the two possible ways, in some order. For $r^* \in \text{Res}(w)^*$, let $E(r^*)$ be the collection of arcs and boundary segments from Δ_w produced from the resolution r^* , along with \emptyset if any closed loops are present. Define the *weight* of any dual resolution r^* to be $x_{r^*} = \prod_{j \in E(r^*)} x_j$, where $x_\emptyset = 0$.

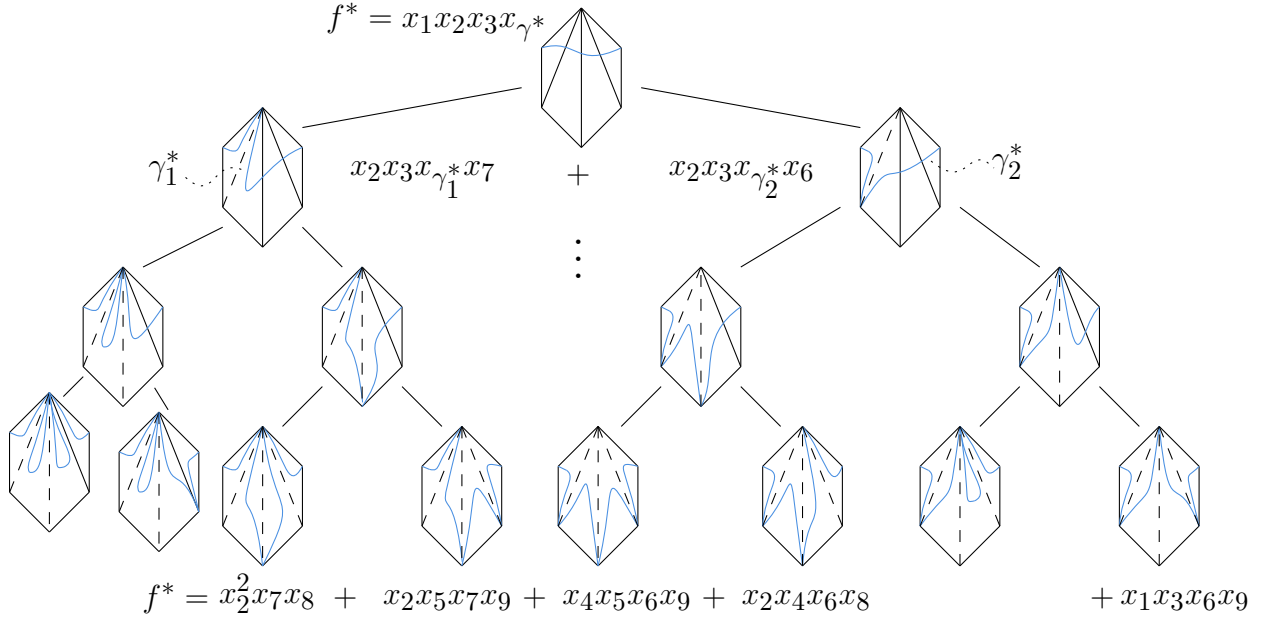
We now describe how to produce a *dual resolution tree* from w . Each node of such a tree is a diagram of arcs inside the $(n+3)$ -gon Σ , and is weighted by the product of cluster variables associated to those arcs, or zero if there is a closed loop in the diagram. The root of a dual resolution tree from w is the diagram consisting of the arc γ_w inside Σ_w . Choosing an intersection point p_i to slide at creates two children of this root (see Figure 5.4). Continuing in this way (choosing an intersection point to slide at in each child, etc.) and halting whenever either we create a loop or we have performed a slide at every intersection point, a binary tree (with additional node structure) is produced.

Definition 5.17. The set of *dual resolution trees* $\text{Tree}(w)^*$ associated to w is the set whose elements are dual slide trees from w as described above.

Remark 5.18. The set $\text{Res}(w)^*$ is equal to the union of the leaves of the trees in $\text{Tree}(w)^*$.

Example 5.19. Fix $w = ab$. Figure 5.5 shows one element of $\text{Tree}(w^*)^* = \text{Tree}(bb)^*$. Note that this tree is isomorphic to the element of $\text{Tree}(w) = \text{Tree}(ab)$ from Example 3.15, and that the weights of the leaves here coincide with the weights of the leaves there.

Figure 5.5: One element of $\text{Tree}(bb)^*$



Definition 5.20. Let a^* and b^* be the images of a and b under the triangle map $\Sigma_w \mapsto \Sigma_w^*$. The dual of the arc γ is the oriented arc $\gamma_{w^*} = \gamma_{a^* \rightarrow b^*}^*$ from a^* to b^* inside the polygon Σ_w^* . The cluster variable x_w^* dual to x_w is defined by

$$x_w^* = \frac{1}{x_1 x_2 \dots x_n} \sum_{r^* \in \text{Res}(w)^*} x_{r^*}.$$

Remark 5.21. We caution that in general the arc γ_w^* is not equal to the arc γ_w . Furthermore, we do not yet know that x_w^* is in fact a cluster variable in a cluster algebra; this is part (c) in Theorem 6.22 below.

5.6 Snake Graphs

The notion of a dual snake graph was introduced in [32].

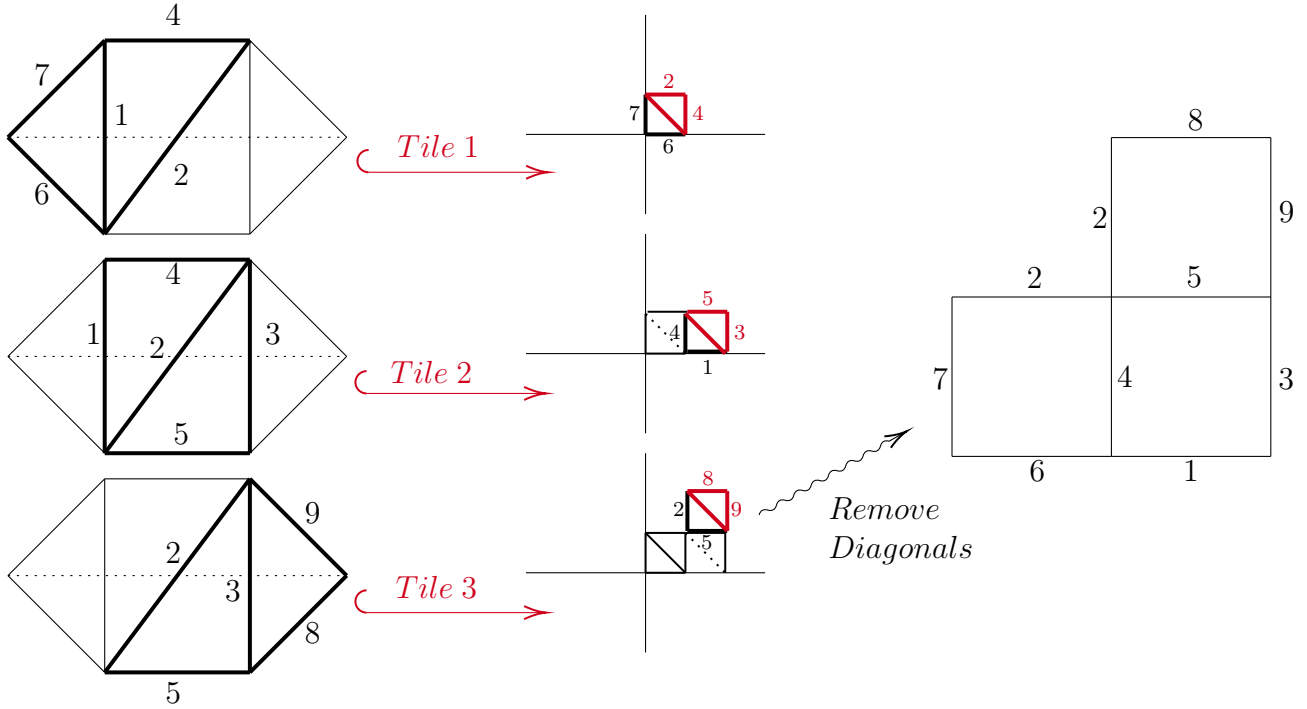
Definition 5.22. Fix the arc γ in the triangulated polygon Σ_w triangulated by Δ_w . The dual

snake graph G_w^* associated to w is the labeled planar graph recursively defined as follows:

1. Choose an orientation-preserving embedding of the triangulated square $[\Delta_0, \nabla_1]$ into the discrete plane \mathbb{Z}^2 such that its image \widetilde{T}_1^* is a triangulated unit square with vertices $(0, 0)$, $(1, 0)$, $(0, 1)$, and $(1, 1)$ in \mathbb{Z}^2 , and such that the point $a \in \Delta_0$ maps to the point $(0, 0)$. Note that the (line spanned by the) image of the triangulating edge will have slope -1 .
2. Choose an orientation-preserving map of $[\Delta_1, \nabla_2]$ into \mathbb{Z}^2 such that its image \widetilde{T}_2^* is a triangulated unit square (again, with triangulating edge having slope -1) glued to \widetilde{T}_1^* along the unique edge in each \widetilde{T}_i^* labeled $j \in \{n + 1, \dots, 2n + 3\}$. Note that if the intersection point of the diagonals δ_1 and δ_2 is to the left (resp. right) of γ_w , then \widetilde{T}_2^* is the triangulated square directly above (resp. to the right of) \widetilde{T}_1^* .
3. Continue this process, using orientation-preserving maps for both i odd and even, to get the graph \widetilde{G}_w^* , built from triangulated unit squares in \mathbb{Z}^2 (with all triangulating edges having slope -1) glued either above or to the right of the previous square. Each \widetilde{T}_i^* will be called a *tile* of \widetilde{G}_w^* . The triangulating edge of each \widetilde{T}_i^* is called the *diagonal* of \widetilde{T}_i^* .
4. The *dual snake graph* G_w^* is the graph in \mathbb{Z}^2 gotten by deleting each diagonal from each tile in \widetilde{G}_w^* .

Example 5.23. Fix $w = ab$. Figure 5.6 illustrates the construction of the dual snake graph $G_w^* = G_{bb}$ from the triangulation Δ_{ab} .

Figure 5.6: Construction of the dual snake graph G_{bb}



We give now an explicit procedure $G_w \mapsto G_w^*$ for computing the dual snake graph, starting from G_w .

Definition 5.24. Consider the snake graph G_w with tiles T_1, T_2, \dots, T_n . Let the diagonal of T_i be called d_i . The *antidiagonal* of tile T_i , denoted a_i , is the line segment inside T_i formed by joining the SW and NE corners of T_i .

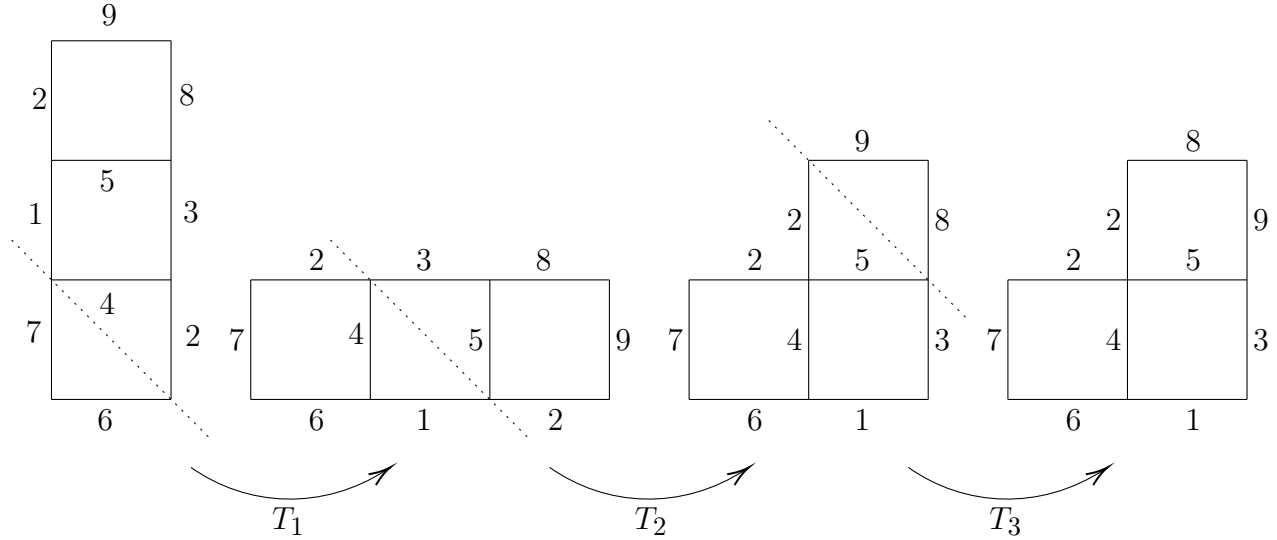
For any snake graph H with n tiles, the diagonal d_i of T_i gives two subgraphs H_{i-1} and H_i of H that respectively consist of all vertices and edges of H weakly below or weakly above the line spanned by d_i . Define H^{T_i} to be the snake graph produced by reflecting H_i about the line spanned by a_i and regluing the image of H_i to H_{i-1} . It is clear that the result of this operation is another snake graph. Write $(H^{T_i})^{T_j} = H^{T_i \circ T_j}$.

One can see from the constructions that we have $G_w \mapsto G_w^{T_1 \circ T_2 \circ \dots \circ T_n} = G_w^*$. Namely, performing this composition of maps gives each tile of G_w a half-twist (as in Definition 5.22),

and furthermore the shape of $G_w^{T_1 \circ T_2 \circ \dots \circ T_n}$ coincides with the shape of G_w^* .

Example 5.25. We demonstrate in Figure 5.7 the factorization $G_{ab} \mapsto G_{ab}^{T_1 \circ T_2 \circ \dots \circ T_n} = G_{bb}$.

Figure 5.7: Transforming G_{ab} into its dual G_{bb}



The next result follows from the factorization just given.

Proposition 5.26. For any word w , we have

- (a) $sh(G_w) = w^*$ and $sh(G_w^*) = w$.
- (b) $sh(G_w)^* = sh(G_w^*)$.
- (c) $G_w^* = G_{w^*}$.

Definition 5.27. Fix the word w , and consider the sign sequence $\mathbf{s}_w = (s(e_0), s(e_1), \dots, s(e_n))$

on the snake graph G_w . The *dual sign sequence* \mathbf{s}_w^* is defined by

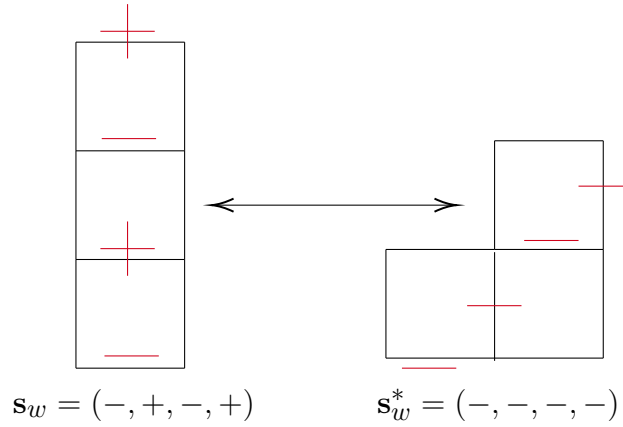
$$\mathbf{s}_w^* = (s(e_0), -s(e_1), s(e_2), -s(e_3), \dots).$$

Proposition 5.28. For any word w , we have $\mathbf{s}_w^* = \mathbf{s}_{w^*}$.

Proof. This follows immediately from Proposition 5.26. □

Example 5.29. Below is the sign sequence s_{ab} and its dual $s_{ab}^* = s_{bb}$.

Figure 5.8: The sign sequence s_{ab} and its dual s_{bb}



5.7 Continued Fractions

For more on the involution on continued fractions given in the next definition, see [40].

Definition 5.30. Consider the finite positive continued fraction $[a_1, a_2, \dots, a_d]$. The *dual continued fraction* $[a_1, a_2, \dots, a_d]^*$ is gotten from $[a_1, a_2, \dots, a_d]$ by first writing each a_i as $1+1+\dots+1$, substituting these expressions into their respective entries in the continued fraction, and applying the involution that exchanges the symbol “ $-$ ” with the symbol “ $+$ ”.

Example 5.31. The continued fraction associated to the word $w = ab$ is $\text{CF}(ab) = [1, 1, 1, 1]$ (see Example 3.39). The dual continued fraction is computed as

$$\text{CF}(w)^* = \text{CF}(ab)^* = [1, 1, 1, 1]^* = [1 + 1 + 1 + 1] = [4] = \text{CF}(bb) = \text{CF}(w^*)$$

Remark 5.32. The continued fractions in (a) from Remark 3.40 are dual to those in (c), and the same for (b) and (d).

Proposition 5.33. For any word w we have

$$CF(w)^* = CF(w^*).$$

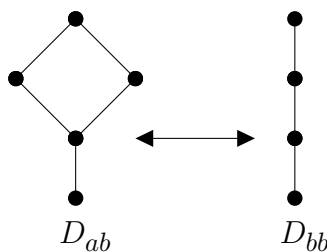
Proof. This follows immediately from Proposition 5.28. □

5.8 Distributive Lattices

Definition 5.34. The distributive lattice dual to D_w is simply $D_{w^*} = \mathcal{I}(C_w^*)$.

Example 5.35. The three expansion posets pictured in Examples 4.4, 4.7, and 4.11 are all isomorphic to the same distributive lattice $D_{ab} \cong \Gamma_3$. The dual lattice D_{bb} is a chain poset on 4 vertices. See Figure 5.9.

Figure 5.9: The Fibonacci cube Γ_3 and its dual



Remark 5.36. In general, a chain poset with $n + 1$ vertices is dual to the Fibonacci cube Γ_n .

Chapter 6

Dual Expansion Posets

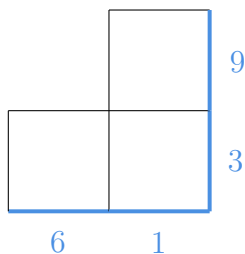
6.1 Lattice Paths on Snake Graphs

We recall here the *lattice path expansion posets* from [32].

Definition 6.1. A *lattice path* in a snake graph G_w with n tiles is a choice of $n + 1$ edges L from G_w which when concatenated form a path, taking only unit steps right or up, from the SW vertex of tile T_1 to the NE vertex of tile T_n . The *weight* x_L of L is defined to be the product of initial cluster variables $x_L = \prod_{l \in L} x_l$. Let \mathbb{L}_w be the set of all lattice paths of the snake graph G_w .

Example 6.2. Figure 6.1 shows one of the five lattice paths on the snake graph G_{bb} dual to G_{ab} . Note that the weight of this lattice path coincides with the weight of the the perfect matching shown in Figure 4.1.

Figure 6.1: The lattice path L_- on G_{bb}



The next expansion formula is from [32].

Theorem 6.3. *Let w be any word, and consider the set \mathbb{L}_{w^*} of lattice paths on the dual snake graph G_{w^*} . Then the cluster variable x_w can be written as*

$$x_w = \frac{1}{x_1 x_2 \dots x_n} \sum_{L \in \mathbb{L}_{w^*}} x_L.$$

Corollary 6.4. *For any word w , we have $|\mathbb{P}_w| = |\mathbb{L}_{w^*}|$ and $|\mathbb{L}_w| = |\mathbb{P}_{w^*}|$.*

Let $\text{CF}(w) = [a_1, a_2, \dots, a_k]$ and $\text{CF}(w^*) = [b_1, b_2, \dots, b_l]$. Let $G_w^{a_1}$ be the subsnake graph of G_w obtained by deleting the first a_1 tiles of G_w (see the discussion directly before Theorem 4.5). Let $G_w^{b_1}$ be the subsnake graph of G_w obtained by deleting the first b_1 tiles of G_w . Combining Corollary 6.4 with Theorem 4.5 gives the next result.

Corollary 6.5. *For any word w , we have*

$$\text{CF}(w) = \frac{|\mathbb{P}_w|}{|\mathbb{P}_w^{a_1}|} = \frac{|\mathbb{L}_{w^*}|}{|\mathbb{L}_{w^*}^{a_1}|}$$

and

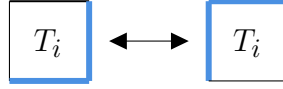
$$\text{CF}(w)^* = \frac{|\mathbb{P}_{w^*}|}{|\mathbb{P}_{w^*}^{b_1}|} = \frac{|\mathbb{L}_w|}{|\mathbb{L}_w^{b_1}|}.$$

We now give the set \mathbb{L}_w a poset structure.

A *flip* of L at tile T_i is the local move that takes two edges of L located on the same tile T_i of G_w that are incident to a common vertex of T_i (so, necessarily the two edges in question are the S and E edges of T_i , or the W and N edges of tile T_i) and replaces them with the other two edges of T_i .

Directly below is the local picture for the flip at a generic tile T_i .

Figure 6.2: Flip of a lattice path at tile T_i



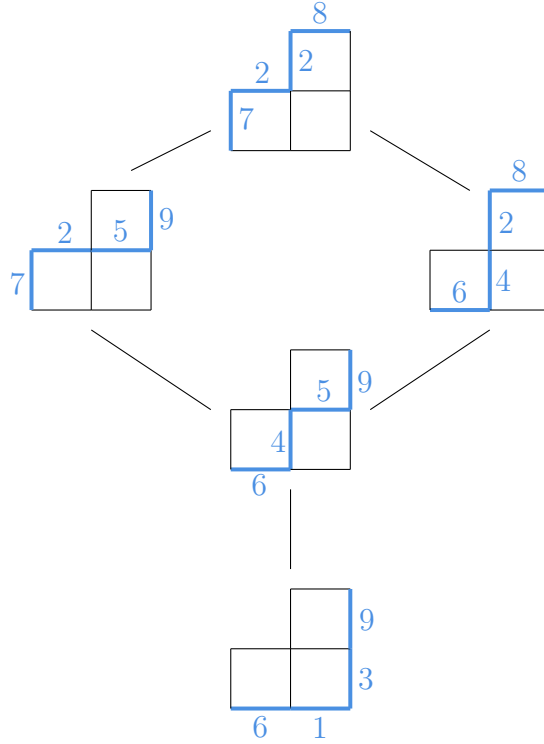
An *up-flip* at tile T_i is a flip that replaces the S and E edges of T_i with the N and W edges of T_i .

Definition 6.6. The *minimal element* L_- of \mathbb{L}_w is the unique lattice path of G_w such that every edge in L_- is a boundary edge of G_w and the S edge of tile T_1 is in L_- . The *maximal element* L_+ of \mathbb{L}_w is the unique lattice path of G_w such that every edge in L_+ is a boundary edge of G_w and the S edge of tile T_1 is not in L_- .

Definition 6.7. The *poset structure* on \mathbb{L}_w is defined as follows. The unique minimal element of \mathbb{L}_w is the minimal lattice path L_- , and the unique maximal element is L_+ . A lattice path L_2 covers a lattice path L_1 if there exists a tile T_i such that L_2 can be obtained from L_1 by performing a single up-flip of L_1 at T_i .

Example 6.8. Fix $w = ab$. In Figure 6.3, we illustrate the poset $\mathbb{L}_{w^*} = \mathbb{L}_{bb}$ of lattice paths on the dual snake graph G_{bb} . Compare with Figures 4.4, 4.7, and 4.11 from Chapter 4.

Figure 6.3: The poset \mathbb{L}_{bb}



Remark 6.9. If the word w is straight, the poset \mathbb{P}_w is isomorphic to a Fibonacci cube (see (b) in 4.9), and likewise \mathbb{L}_{w^*} is isomorphic to the same Fibonacci cube. Conversely, if the word w is zigzag, then both the posets \mathbb{P}_w and \mathbb{L}_{w^*} are isomorphic to the same linear chain. Similar remarks hold for the other expansion formulas. See Theorem 6.22 below for details.

6.2 Lattice Paths of Angles

Say that a vertex v of Σ is *incident* to any triangle that it is a vertex of.

Definition 6.10. A *lattice path of angles* β of Σ_w is a selection of $n + 1$ angles from the triangles $\Delta_0, \Delta_1, \dots, \Delta_n$ of Δ , one per triangle, such that

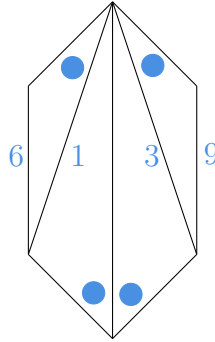
- (1) Each angle is incident to an endpoint of one of the internal diagonals $\delta_1, \delta_2, \dots, \delta_n$.

- (2) An even number of angles from β are incident to each vertex of the polygon Σ_w which is incident to an even number of triangles from Σ_w , and an odd number of angles from β are incident to each vertex of the polygon Σ_w which is incident to an odd number of triangles of Σ_w .

Each angle b in Δ_i can be assigned the cluster variable x_b associated to the edge of Δ_i opposite of b . The *weight of β* is defined to be the product of initial cluster variables $x_\beta = \prod_{b \in \beta} x_b$. Let \mathbb{B}_w be the set of all lattice paths of angles in Σ_w .

Example 6.11. Below we show one of the five lattice paths of angles on the dual triangulated surface $\Sigma_{ab}^* = \Sigma_{bb}$.

Figure 6.4: The lattice path of angles B_- on G_{bb}



The next result is included as part of the statement of Theorem 6.22 (e), and is proved there.

Theorem 6.12. *Let w be any word. Consider the set \mathbb{B}_{w^*} of lattice paths of angles on the dual triangulated surface Σ_w^* . Then the cluster variable x_w can be written as*

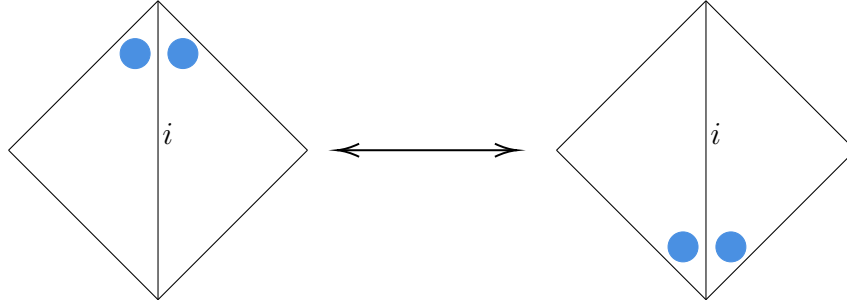
$$x_w = \frac{1}{x_1 x_2 \dots x_n} \sum_{\beta \in \mathbb{B}^*} x_\beta.$$

We now give the set \mathbb{B}_w a poset structure.

A *flip* of B at diagonal δ_i is the local move that takes two angles in B that are each incident to the same endpoint of the internal diagonal δ_i and replaces them with the remaining two angles incident to δ_i .

Directly below is the flip at a generic internal diagonal δ_i .

Figure 6.5: Flip of a lattice path of angles at diagonal δ_i



Let l_i be the endpoint of δ_i to the left of $\gamma_{a \rightarrow b}$, and r_i the endpoint to the right. An *up-flip* of β at diagonal δ_i is a flip that meets either of the following two conditions:

- (1) i is odd, and the two angles matched to l_i are replaced with the two angles matched to r_i ,
- or
- (2) i is even, and the two angles matched to r_i are replaced with the two angles matched to l_i .

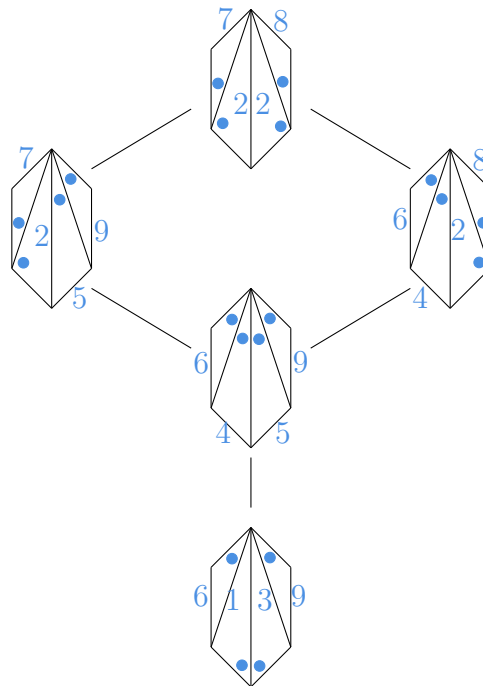
Definition 6.13. The *minimal element* B_- of \mathbb{B}_w is the unique lattice path of angles such that the boundary angle in Δ_0 with boundary edge δ_{2n+1} is matched, and only boundary angles are used in B_- . The *maximal element* B_+ of \mathbb{B}_w is the unique lattice path of angles such that the angle the boundary angle in Δ_0 with boundary edge δ_{2n} is matched, and only boundary angles are used in B_+ .

Definition 6.14. The *poset structure* on \mathbb{B}_w is defined as follows. The unique minimal element of \mathbb{B}_w is the minimal lattice path of angles B_- , and the unique maximal element is B_+ . A lattice

path of angles B_2 covers another lattice path of angles B_1 if there exists a diagonal δ_i such that B_2 can be obtained from B_1 by performing a single up-twist of B_1 at δ_i .

Example 6.15. Fix $w = ab$. The poset of lattice paths of angles on the dual triangulated surface Σ_{bb} is shown in Figure 6.6 below.

Figure 6.6: The poset \mathbb{B}_{bb}



6.3 S -paths

Definition 6.16. An S -path from a to b is an ordered (uncolored) selection S of edges from the triangulation Δ_w subject to the following conditions:

- (1) The edges in S form a path from a to b
- (2) The number of edges in S is $n + 1$

(3) At least one edge from each triangle Δ_i in Σ_w occurs in S .

Define the *weight* x_S of S by $x_S = \prod_{s \in S} x_s$. Let \mathbb{S}_w be the set of all S -paths from a to b .

Again, the proof of the next result is given in Theorem 6.22 below.

Theorem 6.17. *Let w be any word. Consider the set \mathbb{S}_{w^*} of S -paths from a^* to b^* with edges taken from the dual triangulation Δ_w^* . Then the cluster variable x_w can be written as*

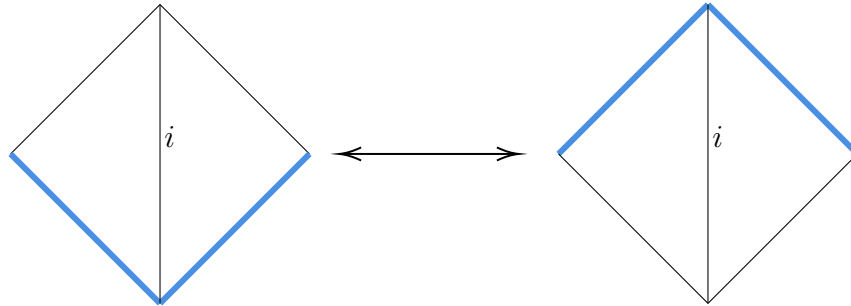
$$x_w = \frac{1}{x_1 x_2 \dots x_n} \prod_{S \in \mathbb{S}_{w^*}} x_S.$$

We now give the set \mathbb{S}_w a poset structure.

A *flip* of S at diagonal δ_i is the local move that takes two edges in S which are both incident to the same endpoint of the minimal quadrilateral Q_i defined by the diagonal δ_i , and replaces them with the other two edges of Q_i .

Directly below is the local picture of an S -path flip at a generic internal diagonal δ_i .

Figure 6.7: Flip of an S -path at diagonal δ_i



Let l_i be the endpoint of δ_i to the left of $\gamma_{a \rightarrow b}$, and r_i the endpoint to the right. An *up-flip* of S at diagonal δ_i is a flip that meets either of the following two conditions:

- (1) i is odd, and the two edges in S incident to r_i are replaced with the two edges in Q_i incident to l_i , or

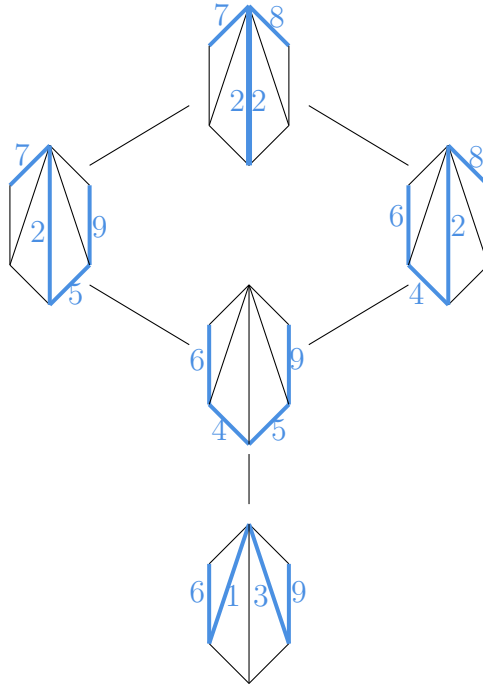
- (2) i is even, and the two edges in S incident to l_i are replaced with the two edges in Q_i incident to r_i .

Definition 6.18. The *minimal element* S_- of \mathbb{S}_w is the unique S -path that starts with the boundary edge δ_{2n+1} , and only uses internal diagonals as edges, except for the first and last (boundary) edges. The *maximal element* S_+ of \mathbb{S}_w is the unique S -path that starts with the edge δ_{2n} , and only uses internal diagonals as edges, except for the first and last (boundary) edges.

Definition 6.19. The *poset structure* on \mathbb{S}_w is defined as follows. The unique minimal element of \mathbb{S}_w is the minimal S -path S_- , and the unique maximal element is S_+ . An S -path S_2 covers another S -path S_1 if there exists a diagonal δ_i such that S_2 can be obtained from S_1 by performing a single up-flip of S_1 at δ_i .

Example 6.20. Fix $w = ab$. The poset of S -paths on the dual triangulated surface $\Sigma_{ab}^* = \Sigma_{bb}$ is displayed in Figure 6.8. Note that the “middle” internal diagonal in S_+ is used twice.

Figure 6.8: The poset \mathbb{S}_{bb}



We now give the analogue of Proposition 4.24.

Proposition 6.21. *Fix the word w . There are poset isomorphisms*

$$\begin{array}{ccc}
 & \mathbb{L}_w & \\
 \swarrow & & \searrow \\
 \mathbb{B}_w & \longleftrightarrow & \mathbb{S}_w
 \end{array}$$

which respect the additional node structure of each poset.

Proof. Let $A(\widetilde{G}_w)$ be the set of angles in \widetilde{G}_w that are incident to a diagonal and a side of \widetilde{G}_w . Let $E(G_w)$ be the edges of $G_w \subset \widetilde{G}_w$. Let $A(\Sigma_w)$ be the set of angles in Σ_w which are neither incident to a nor b . Recall from [42] the canonical surjection $A(\widetilde{G}_w) \rightarrow E(G_w)$, which induces the bijection $E(G_w) \rightarrow A(\Sigma_w)$. The map $\mathbb{L}_w \rightarrow \mathbb{B}_w$ is defined by taking the preimage of the lattice path L under the map $A(\widetilde{G}_w) \rightarrow E(G_w)$, and then folding the result to obtain an element in $A(\Sigma_w)$. That this map is well-defined can be seen by induction on the number of tiles n . That covering relations are preserved is straightforward to check. The inverse map is defined

by unfolding and then applying the map $A(\widetilde{G}_w) \rightarrow E(G_w)$. It follows that $\mathbb{L}_w \rightarrow \mathbb{B}_w$ is a poset isomorphism respecting the additional node structure.

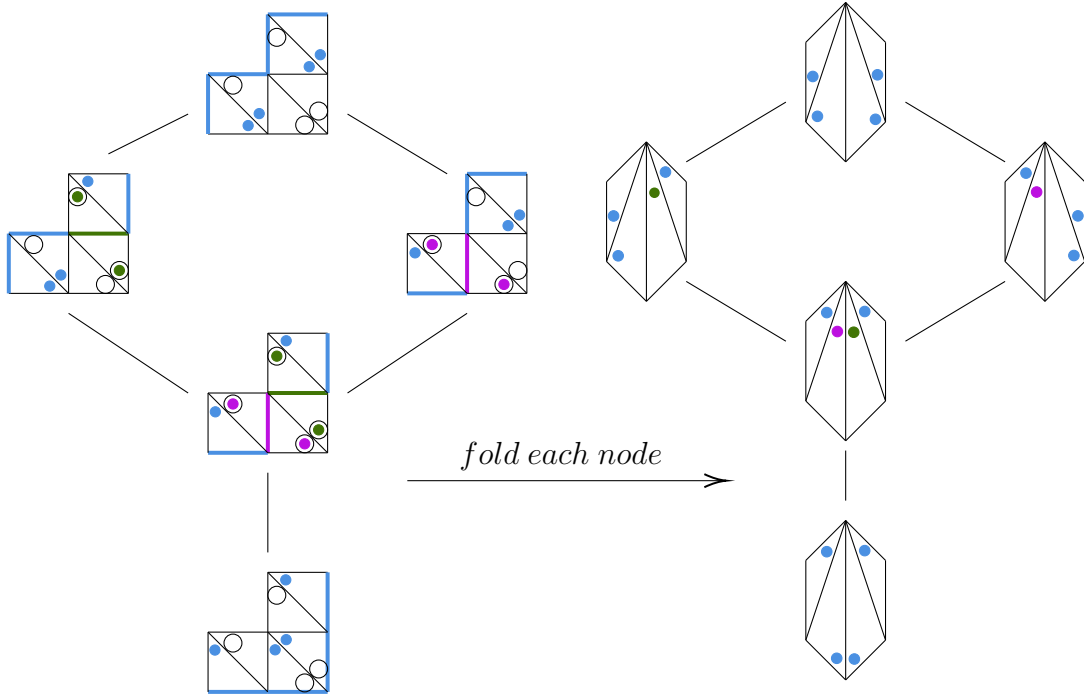
The map $\mathbb{L}_w \rightarrow \mathbb{S}_w$ is the folding map, additionally keeping track of the images of the edges selected by $L \in \mathbb{L}_w$ after each fold. One can check using induction that this map is well-defined. Again, it is straightforward to see that covering relations are preserved. The inverse map is induced by the unfolding map. It follows that $\mathbb{L}_w \rightarrow \mathbb{S}_w$ is a poset isomorphism respecting the additional node structure.

Finally, one can check that the map $\mathbb{B}_w \rightarrow \mathbb{S}_w$ is the composition of the two poset isomorphisms above. □

We illustrate Proposition 6.21 with the three dual posets \mathbb{L}_{bb} , \mathbb{B}_{bb} , and \mathbb{S}_{bb} from the running example. By Lemma 3.2 in [42] there is a bijection between the angles in Σ_w and the edges in G_w induced by identifying certain pairs of angles in \widetilde{G}_w . The pairs of angles that are identified are those that are opposite one another in the quadrilateral determined by two consecutive tiles of \widetilde{G}_w . Any pair of angles in \widetilde{G}_w which have been identified correspond to a single internal angle in Σ_w .

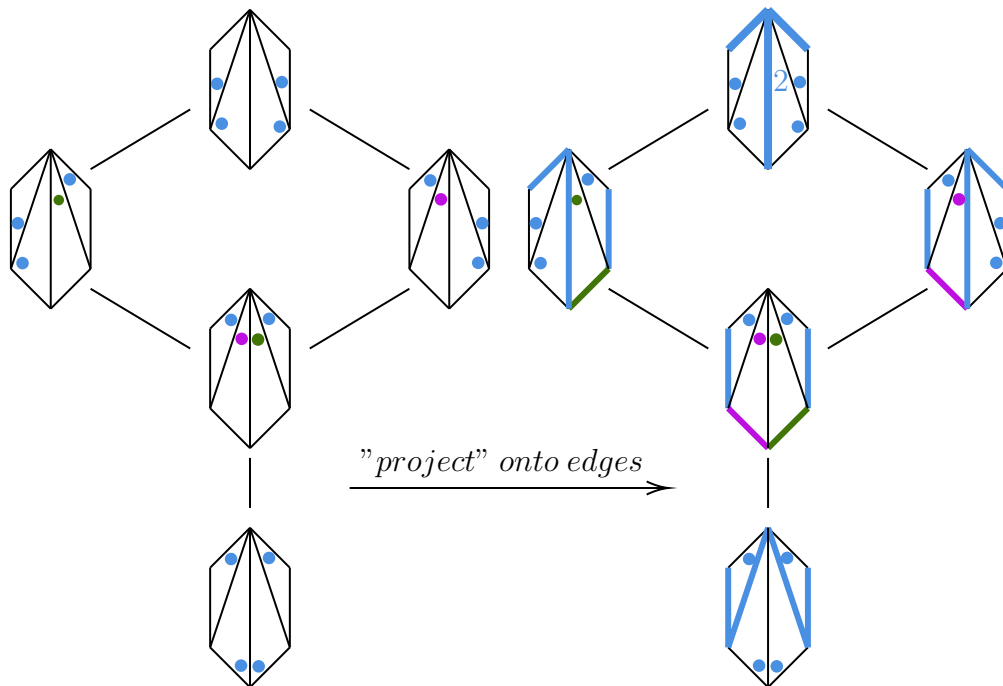
Thus, given a lattice path $L \in \mathbb{L}_w$, we can associate to it a collection of angles in \widetilde{G} and fold the result to obtain a lattice path of angles B in Σ_w .

Figure 6.9: The map $\mathbb{L}_w \rightarrow \mathbb{B}_{bb}$ via angle identification and folding



The map $\mathbb{B}_w \rightarrow \mathbb{S}_w$ is defined by taking the collection of edges which are opposite some vertex in $S \in \mathbb{S}_w$. See Figure 6.10 below.

Figure 6.10: The map $\mathbb{B}_{bb} \rightarrow \mathbb{S}_{bb}$ via associating edges to angles



The map $\mathbb{L}_w \longrightarrow \mathbb{S}_w$ is defined by folding and is the composition of the previous two.

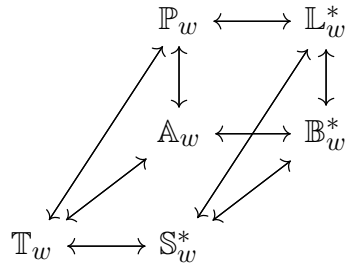
6.4 Expansion Duality

Theorem 6.22. *Fix the word w .*

- (a) *There is an explicit bijection $\text{Tree}(w)^* \longrightarrow \text{Tree}(w^*)$ that preserves additional node structure, and weights of leaves.*
- (b) *There is a weight-preserving bijection $\text{Res}(w)^* \longrightarrow \text{Res}(w^*)$ respecting additional node structure.*
- (c) *The Laurent polynomial x_w^* is a cluster variable in $\mathcal{A}(\Sigma)_{w^*}$, and is equal to $x_w^* = x_{w^*}$.*
- (d) *There are explicit isomorphisms of distributive lattices*

$$\mathbb{P}_w \xrightarrow{\sim} \mathbb{L}_{w^*}, \mathbb{A}_w \xrightarrow{\sim} \mathbb{B}_{w^*}, \text{ and } \mathbb{T}_w \xrightarrow{\sim} \mathbb{S}_{w^*}$$

respecting the additional structure of each lattice, and making the following diagram commute.



Namely, corresponding nodes in the six posets have the same weight, except for the nodes of the T -path expansion poset. In this case, node weights have an additional factor of $\frac{1}{x_1 x_2 \dots x_n}$ that is not preset in any of the node weights for the other five expansion posets.

(e) The cluster variable x_w can be written as

$$x_w = \frac{1}{x_1 x_2 \dots x_n} \sum_{L \in \mathbb{L}_w} x_L = \frac{1}{x_1 x_2 \dots x_n} \sum_{B \in \mathbb{B}_w} x_B = \frac{1}{x_1 x_2 \dots x_n} \sum_{S \in \mathbb{S}_w} x_S.$$

(f) There are isomorphisms of distributive lattices $D_w \cong \mathcal{I}(C_w) \cong \mathbb{P}_w$ and $D_{w^*} \cong \mathcal{I}(C_w^*) \cong \mathbb{L}_w$. Thus, \mathbb{P}_w and \mathbb{L}_w are dual to one another in the sense of distributive lattices (see Definition 5.34).

Proof. (a) Let $t \in \text{Tree}(w)^*$. The map $\text{Tree}(w)^* \rightarrow \text{Tree}(w^*)$ is defined by the application of the triangle map to each node of the input tree t , except that we must additionally specify how to transform arcs $\delta \in \Sigma_w$ which are not contained in the triangulation Δ_w into arcs $\delta^* \in \Sigma_w^*$.

Suppose $\delta \notin \Delta_w$ is an arc in a diagram which is a node in t , and that δ crosses the triangles $\Delta_i, \dots, \Delta_j$. The obvious one-to-one correspondence induced by the triangle map between angles in Σ_w and angles in Σ_w^* gives a natural candidate for the image of the arc δ .

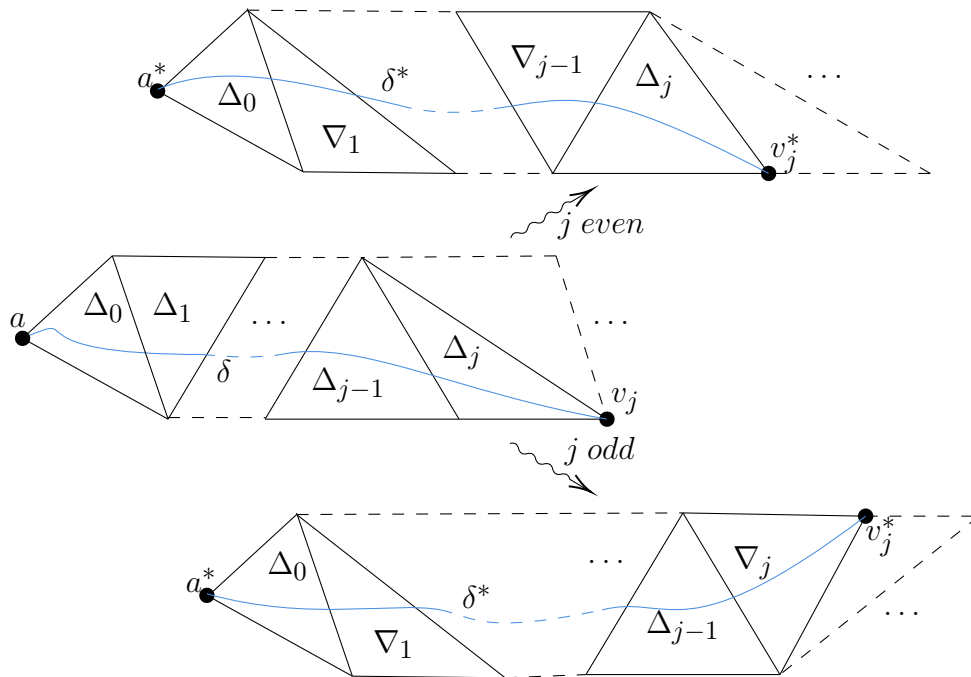
Namely, suppose the endpoints of δ are v_i and v_j , corresponding to the angles α_i and α_j in Δ_i and Δ_j , respectively. Let α_i^* and α_j^* be the angles which are the respective images of α_i and α_j under the triangle map. Let v_i^* be the vertex that α_i^* is matched to, and let v_j^* be the vertex that α_j^* is matched to. Then δ^* is the arc that

- (1) starts at the vertex v_i^* ,
- (2) ends at the vertex v_j^* ,
- (3) passes through the center of precisely those triangles in Σ_w^* which are the images of the triangles $\Delta_i, \dots, \Delta_j$ under the triangle map, and

(4) has as its only intersections (besides endpoints) the midpoint of each internal diagonal it crosses.

For instance, suppose the arc δ starts at a , is contained in the triangulated subpolygon $[\Delta_0, \Delta_1, \dots, \Delta_j]$, and ends at vertex v_j of Δ_j . The output δ^* for the two subcases j even and j odd are shown in Figure 6.11.

Figure 6.11: The arc δ , and the output arc δ^* for both j odd and j even



This map is well-defined by induction on n , and that edge weights of leaves are preserved is obvious. The inverse map $\text{Tree}(w)^* \rightarrow \text{Tree}(w^*)$ is defined similarly, and the composition is the identity. Hence the map in question is an invertible bijection respecting additional node structure as claimed.

(b) This follows directly from (a), since $\text{Res}(w)$ is equal to the union of the leaves in the trees in $\text{Tree}(w)$, and $\text{Res}(w)^*$ is equal to the union of the leaves in the trees in $\text{Tree}(w)^*$.

(c) From (b) we have

$$x_w^* = \frac{1}{x_1 x_2 \cdots x_n} \sum_{r^* \in \text{Res}(w)^*} x_{r^*} = \frac{1}{x_1 x_2 \cdots x_n} \sum_{r \in \text{Res}(w^*)} x_r = x_{w^*}.$$

(d) The first poset isomorphism $\mathbb{P}_w \longrightarrow \mathbb{L}_{w^*}$ is defined by applying the map $G_w \mapsto G_w^{T_1 \circ T_2 \circ \dots \circ T_n}$

to each node P of \mathbb{P}_w , keeping track of the images under the maps T_i of all the edges in P .

That this map is well-defined is a straightforward induction on the number of tiles n of G_w .

That weights are preserved is obvious. If the perfect matching P_2 covers P_1 , then P_2 can

be obtained from P_1 by performing an up-twist at some tile T_i . Suppose L_1 is the image of

P_1 , and L_2 is the image of P_2 . Then one can check that L_2 covers L_1 by using the twist-

parity condition given directly after Figure 4.3 and cases on the parity of i . The inverse

$\mathbb{L}_{w^*} \longrightarrow \mathbb{P}_w$ of this map is again application of the snake graph factorization $T_1 \circ \dots \circ T_n$

(the map $\mathbb{L}_{w^*} \longrightarrow \mathbb{P}_w$ is equal to the composition $T_n \circ \dots \circ T_1$, and these factors commute).

Thus $\mathbb{P}_w \longrightarrow \mathbb{L}_{w^*}$ is indeed a poset isomorphism that respects additional node structure.

The second map $\mathbb{A}_w \longrightarrow \mathbb{B}_{w^*}$ takes any perfect matching of angles $A \in \mathbb{A}_w$ to a lattice path

of angles in \mathbb{B}_{w^*} via the triangle map. That this map is a well-defined poset isomorphism

that preserves node structure now follows from the bijection $\mathbb{P}_w \longrightarrow \mathbb{L}_{w^*}$ and Propositions

4.24 and 6.21.

The third map $\mathbb{T}_w \longrightarrow \mathbb{S}_{w^*}$ takes any $T \in \mathbb{T}_w$ to an S -path on Σ_w^* by first superimposing

a blue edge onto each internal diagonal of Δ_w (this accounts for multiplying each T -path

weight by $x_1 x_2 \dots x_n$), canceling any blue/red pairs that result, and then applying the tri-

angle map. Again, that this gives a well-defined poset isomorphism preserving additional

node structure follows from Propositions 4.24 and 6.21 and the map $\mathbb{P}_w \longrightarrow \mathbb{L}_{w^*}$.

That \mathbb{P}_w is a distributive lattice given in Theorem 5.2 in [30]. Thus, the rest are distributive lattices as well.

(e) Follows directly from (d).

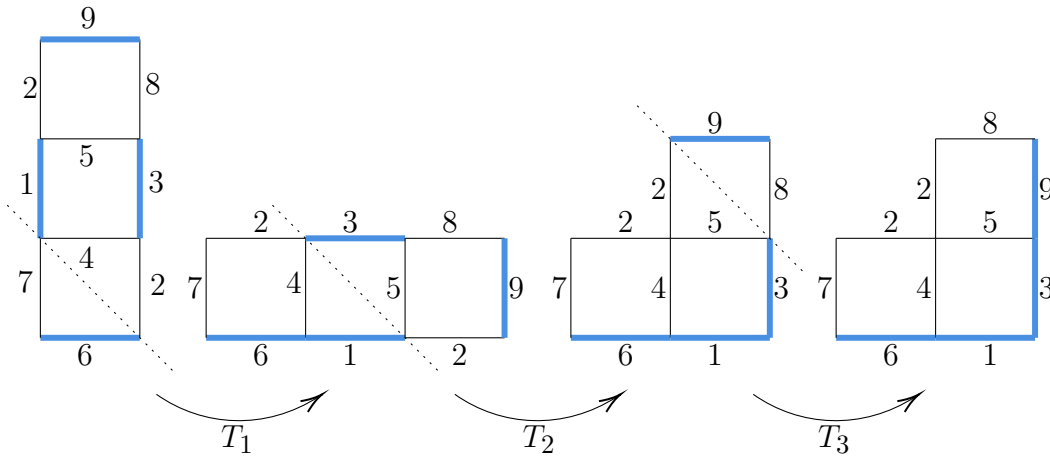
(f) That $\mathcal{I}(C_w) \cong \mathbb{P}_w$ follows from Definition 5.3 and Theorem 5.4 in [30]. That $\mathcal{I}(C_w^*) \cong \mathbb{L}_w$ follows from the construction on page 18 of [24]. Namely, the poset C_w^* can be built from the minimal path L_- in G_w by deleting the first and last steps in L_- , and rotating the result 45° clockwise. That \mathbb{P}_w and \mathbb{L}_w are dual as distributive lattices follows from the definition.

□

Example 6.23. We illustrate how applying the isomorphisms from Theorem 6.22 (d) to the three minimal elements in the running example from the previous chapter gives the three respective minimal elements from the running example in this chapter.

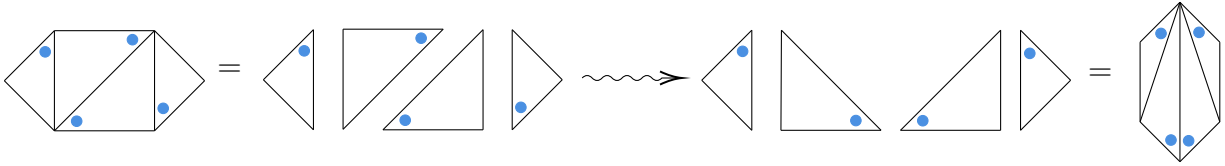
Figure 6.12 shows the minimal matching P_- in \mathbb{P}_{ab} being sent to L_- in \mathbb{L}_{bb} .

Figure 6.12: Transforming the minimal element P_- into the minimal element L_-



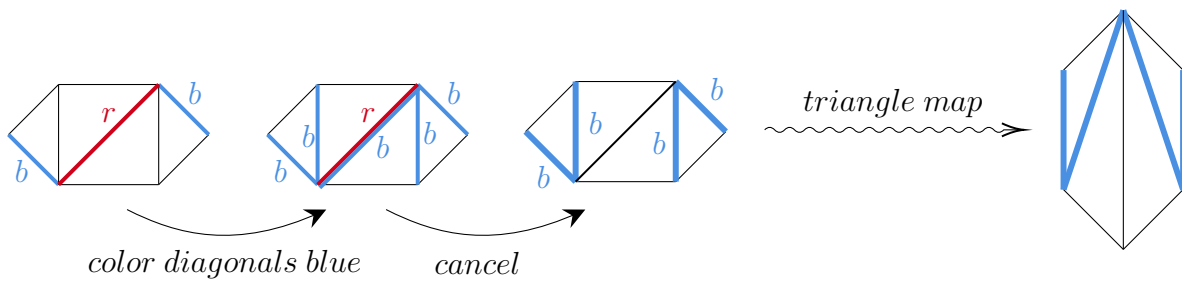
To compute the image of $A_- \in \mathbb{A}_{ab}$ under $\mathbb{A}_{ab} \rightarrow \mathbb{B}_{bb}$, we apply the triangle map. This is shown in Figure 6.13.

Figure 6.13: Transforming the minimal element A_- into the minimal element B_-



The isomorphism $\mathbb{T}_{ab} \rightarrow \mathbb{S}_{bb}$ is obtained by coloring all internal diagonals blue, canceling blue-red pairs if necessary, and then applying the triangle map. See Figure 6.14.

Figure 6.14: Transforming the minimal element T_- into the minimal element S_-



Chapter 7

Expansion Posets as Intervals in Young's Lattice

Loosely speaking, a graded poset is one whose elements can be arranged into “horizontal ranks”. Each graded poset has an associated rank-generating function, which is a polynomial in one variable whose j^{th} nonnegative integer coefficient records the number of elements sitting at rank j . The first objective of this chapter is to give some preliminaries on graded posets and their rank functions, and to note that each expansion poset we have studied thus far is graded.

Our second objective is to put a groupoid structure on the set of all snake graphs, and refine each orbit of this groupoid to a graded poset. The covering relation in each such poset resembles a flip of a lattice path inside a snake graph. We observe that each poset of snake graphs from our construction is isomorphic to one of the well-known lattices $L(m, n)$ whose rank generating functions are the classical q -binomial coefficients. For more on the posets $L(m, n)$ and their (symmetric and unimodal) rank generating functions (and much more on unimodality in general, and related concepts), see [39], [4], and [3].

Our final objective in this chapter is to show how each poset $L(m, n)$ has a covering by intervals, each of which is isomorphic to one of the lattice path expansion posets considered above. This covering is such that two lattice path expansions embed into the same lattice $L(m, n)$ if and only if their underlying snake graphs are related by a morphism as mentioned above.

Finally, since each $L(m, n)$ is itself an interval in Young's lattice, this shows that each expansion poset is isomorphic to an interval in the latter.

7.1 Graded Expansion Posets

Definition 7.1. Let D be a finite poset. A *chain in D* is a totally ordered subset of D . A *maximal chain in D* is a chain that is not a proper subset of any other chain in D . The *length* of a chain with k elements is $k - 1$. We say that D is a *graded poset* if all maximal chains in D have the same finite length. If D is graded then there exists a *rank function* $\rho : D \rightarrow \mathbb{N} = \{0, 1, 2, \dots\}$ that satisfies the following.

- (1) The minimal elements of D map to 0.
- (2) For every $x, y \in D$, $x < y$ implies $\rho(x) < \rho(y)$.
- (3) If $x < y$ and there does not exist $z \in D$ such that $x < z < y$ (i.e., if y strictly covers x), then $\rho(y) = \rho(x) + 1$.

We say the element $x \in D$ has *rank i* if $\rho(x) = i$. The *rank* of the finite graded poset D is equal to the length of any maximal chain.

It is an easy consequence of Birkhoff's Theorem 3.47 above that every finite distributive lattice D is graded. Indeed, for input the order ideal $I \in \mathcal{I}(C) \cong D$ the rank is $\rho(I) = |I|$, the cardinality of I . Thus, $D_w \cong \mathcal{I}(C_w)$ is graded for each word w .

Proposition 7.2. *The rank of any lattice path $L \in \mathbb{L}_w$ is the number of tiles enclosed by the symmetric difference $L \ominus L_-$ of L with the minimal lattice path L_- from Definition 6.6.*

Proof. Follows from Theorem 5.1 in [28] and Proposition 5.26. □

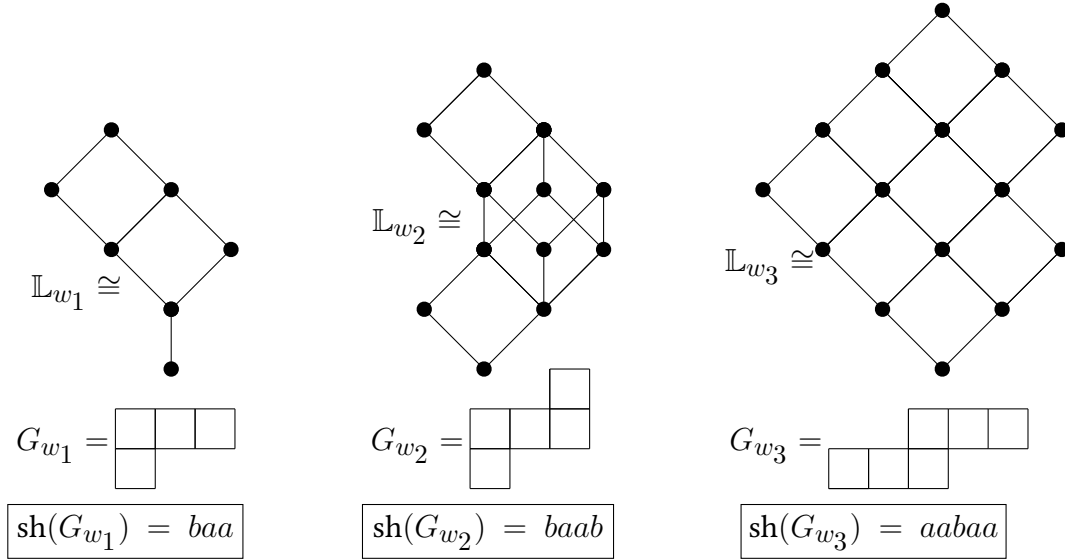
Definition 7.3. Suppose w has length $n - 1$ and consider the graded distributive lattice \mathbb{L}_w . The *rank-generating function* $\mathbb{L}_w(q)$ of the lattice \mathbb{L}_w is the polynomial in q of degree n defined by $\mathbb{L}_w(q) = \sum_{i=0}^n r_i q^i$, where r_i equals the number of lattice paths of rank i in \mathbb{L}_w .

Definition 7.4. Let ρ be the rank-generating function of a graded poset D of rank n . The rank-generating function $\rho(q) = \sum_{i=0}^n r_i q^i$ is *unimodal* if there exists some m such that $r_0 \leq r_1 \leq \dots \leq r_{m-1} \leq r_m \geq r_{m+1} \geq \dots \geq r_n$. We say $\rho(q)$ is *symmetric* if $r_{n-i} = r_i$ for each i . We call D a *rank-unimodal poset* (or just *unimodal*) if its rank function is unimodal, and call D a *rank-symmetric poset* (or just *symmetric*) if its rank function is symmetric.

For instance, Fibonacci cubes are unimodal, and those of even order are symmetric. [27].

Example 7.5. Figure 7.1 shows three snake graphs G_{w_1} , G_{w_2} , and G_{w_3} , along with their respective shapes and lattices. Below these figures, we indicate the respective rank generating functions. Note the rank-generating functions $\mathbb{L}_{w_i}(q)$ are unimodal for $i = 1, 2, 3$ and symmetric for $i = 2$ or 3 .

Figure 7.1: Posets, shapes, and rank functions for three snake graphs



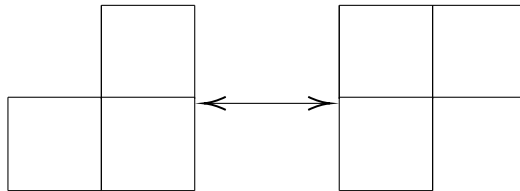
$$\begin{aligned} \mathbb{L}_{w_1}(q) &= 1 + q + 2q^2 + 2q^3 + q^4 \\ \mathbb{L}_{w_2}(q) &= 1 + 2q + 3q^2 + 3q^3 + 2q^4 + q^5 \\ \mathbb{L}_{w_3}(q) &= 1 + 2q + 3q^2 + 3q^3 + 3q^4 + 2q^5 + q^6 \end{aligned}$$

7.2 Posets of Snake Graphs and the q -binomial Coefficients

Definition 7.6. A *groupoid* is a category such that every morphism is invertible.

Let \mathcal{L}^n be the set of snake graphs with $n \geq 1$ tiles. Let $\mathcal{L} = \cup \mathcal{L}^n$. Consider \mathcal{L} a groupoid by saying its elements are the objects, and declaring that there is a morphism between two snake graphs if they have the same number of tiles, and are related by the following local move:

Figure 7.2: Local picture for a morphism between snake graphs



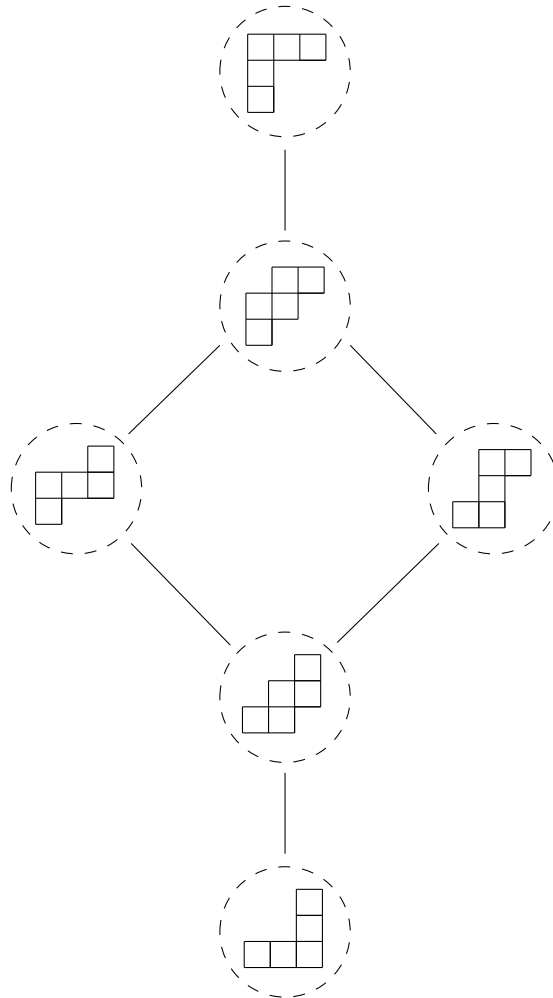
In particular, each straight snake graph (and each snake graph with less than three tiles) is the sole member of its orbit.

Each \mathcal{L}^n is an induced subgroupoid of \mathcal{L} . For $n \geq 3$, we parameterize any orbit of \mathcal{L}^n by the snake graph $G_-^{n,j}$ it contains which is of shape $a^{k_1-1}b^{k_2-1} = a^{k_1-1}b^j$, where $n = k_1 + k_2 - 1$. Use the notation O_j^n for the $n - 2$ orbits of the subgroupoid \mathcal{L}^n .

Refine each orbit O_j^n of $\mathcal{L}^n \hookrightarrow \mathcal{L}$ to a poset \mathbb{O}_j^n by declaring that the snake graph $G_-^{n,j}$ is the minimal element, and by saying that performing the swap $ab \mapsto ba$ corresponds to going up in the poset.

Example 7.7. Figure 7.3 show the poset \mathbb{O}_2^5 from the subgroupoid $\mathcal{L}^5 \hookrightarrow \mathcal{L}$.

Figure 7.3: The poset \mathbb{O}_2^5



The rank functions of the posets \mathbb{O}_j^n are well known.

Definition 7.8. The q -binomial coefficients are defined by

$$\begin{bmatrix} n \\ k \end{bmatrix}_q = \frac{[n]_q!}{[k]_q! [n-k]_q!},$$

where $[k]_q! = (1+q)(1+q+q^2) \dots (1+q+\dots+q^{k-1})$. Each q -binomial coefficient is a rational function in the indeterminate q , and is in fact a polynomial function with positive coefficients.

Note that taking the limit $q \rightarrow 1$ recovers the standard binomial coefficients.

Definition 7.9. The *product* of two posets $(\mathcal{P}, \leq_{\mathcal{P}})$ and $(\mathcal{Q}, \leq_{\mathcal{Q}})$ is the poset whose underlying set is equal to the Cartesian product $\mathcal{P} \times \mathcal{Q}$ with covering relations given by

$$(p_1, q_1) \leq_{\mathcal{P} \times \mathcal{Q}} (p_2, q_2) \iff p_1 \leq_{\mathcal{P}} p_2 \text{ and } q_1 \leq_{\mathcal{Q}} q_2.$$

Let \mathbf{k} and \mathbf{l} be the chain posets with k and l vertices, respectively. Consider the product poset $\mathbf{k} \times \mathbf{l}$. Then the rank generating function of the poset of order ideals of $\mathbf{l} \times \mathbf{k}$ is equal to the q -binomial coefficient $\begin{bmatrix} k+l \\ l \end{bmatrix}$ (see [39]). The q -binomial coefficients are also the rank generating functions for lattice paths in \mathbb{Z}^2 from the origin to the point (k, l) with positive coordinates, or equivalently the Young diagrams that fit inside a k by l rectangular grid.

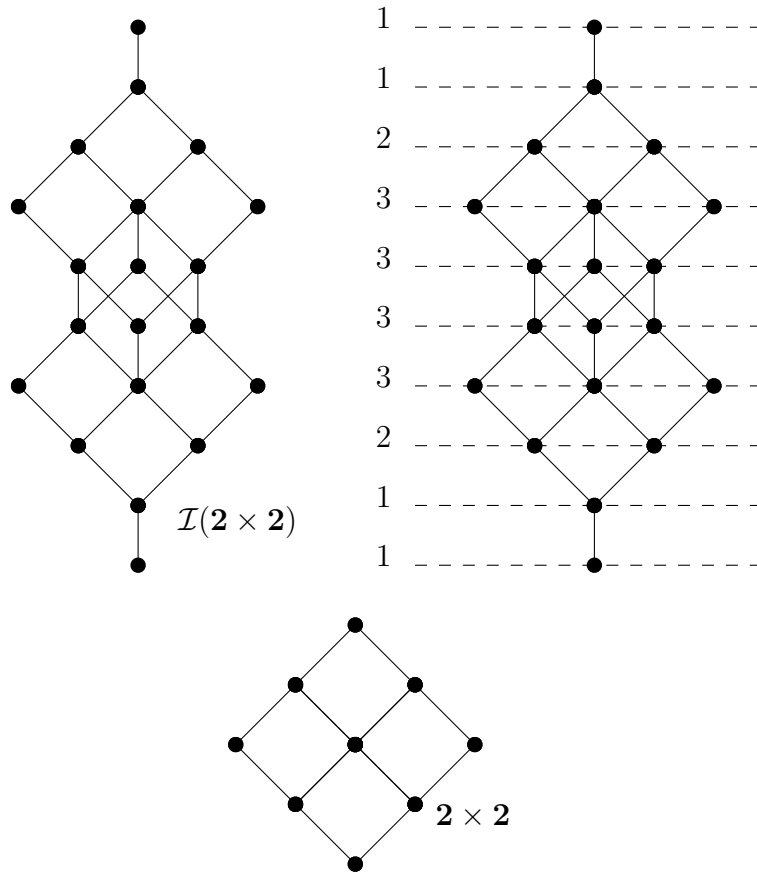
It is not hard to see that any q -binomial coefficient is symmetric (for instance see [39]). However, it is a nontrivial fact that these coefficients are unimodal. This was first proved by Sylvester in 1878 (see [39] and [3]). The first combinatorial proof of unimodality was given over one hundred years later by O'Hara in [31].

Example 7.10. For instance, the rank generating function of $\mathbb{O}_3^7 \cong \mathcal{I}(\mathbf{2} \times \mathbf{2})$ is equal to

$$1 + q + 2q^2 + 3q^3 + 3q^4 + 3q^5 + 3q^6 + 2q^7 + q^8 + q^9.$$

This is visualized in the next figure.

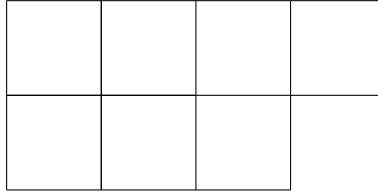
Figure 7.4: The poset 2×2 (bottom), its lattice of order ideals $\mathcal{I}(2 \times 2)$ (top left), and the rank function of $\mathbb{O}_3^7 \cong \mathcal{I}(2 \times 2)$ (top right)



7.3 The Embeddings $\mathbb{L}_w \hookrightarrow \mathbb{O}_j^n$

Recall that a *partition* of a positive number m is a weakly decreasing sequence $\lambda = (\lambda_1, \lambda_2, \dots, \lambda_l)$ such that $m = \lambda_1 + \lambda_2 + \dots + \lambda_l$. For example, $\lambda = (4, 3)$ is one partition of 7. A *Young diagram* is a way to visualize a partition as a left-justified collection of rows of boxes. For instance, to form the Young diagram associated to the partition $(4, 3)$ of 7, we draw an array of 7 boxes, consisting of a row of 4 boxes followed by a row of 3 boxes.

Figure 7.5: The Young diagram associated to the partition $(4, 3)$ of 7

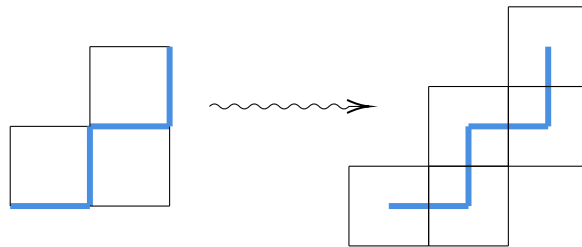


Definition 7.11. Let \mathcal{P} be a poset. Let $x, y \in \mathcal{P}$. The *closed interval* $[x, y]$ is the subset of \mathcal{P} defined by $z \in [x, y]$ if and only if $x \leq z \leq y$.

Young's lattice is the infinite poset whose nodes are Young diagrams of partitions, ordered by inclusion (see [34]). The minimal element is the empty set, and there is no maximal element. Each \mathbb{O}_j^n is isomorphic to a finite closed interval $[\emptyset, \lambda]$ in Young's lattice (see Theorem 7.13 for a proof), whose minimal element is the empty set and with maximal element a rectangular array of boxes λ (indeed, λ is the smallest rectangular array of boxes containing the minimal snake graph $G_{-}^{n,j}$).

Consider the dual cluster variable x_w^* on the snake graph G_w with $n \geq 1$ tiles. Let x_M be any Laurent monomial of x_w^* , represented by the lattice path L on G_w . We can naturally associate to L a word by labeling any E step in L by a , and any N step in L by b . Let G_M be the snake graph whose shape is determined by the assignment just described. Note that G_M has two more tiles than G_w .

Figure 7.6: Snake graphs from lattice paths



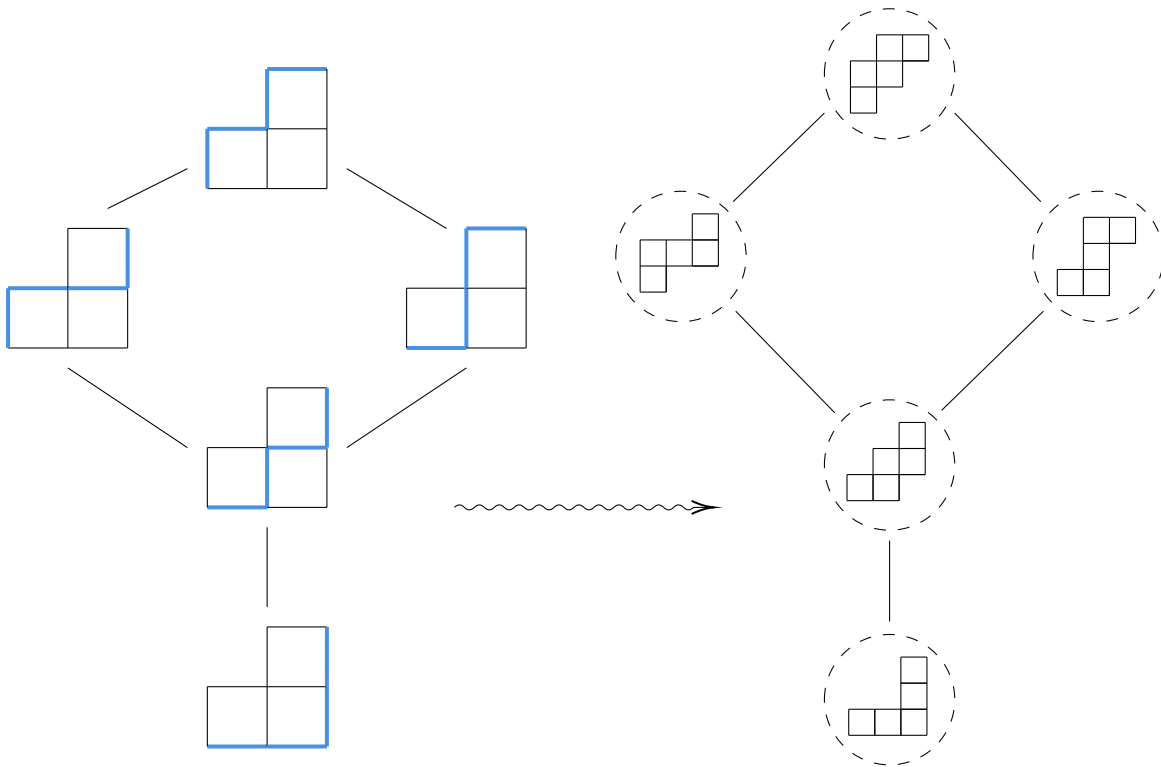
The above remarks give a map

$$\phi : \text{Supp}(x_w^*) \longrightarrow \mathcal{L}^{n+2}, x_M \mapsto G_M.$$

If we apply ϕ to the monomial weight of each node in \mathbb{L}_w we obtain an isomorphic poset $\mathbb{I}_w \cong \mathbb{L}_w$, where each node of \mathbb{I}_w is a snake graph in \mathcal{L}^{n+2} . The covering relation in \mathbb{I}_w is the one shown in Figure 7.2 above.

Example 7.12. Figure 7.7 shows the poset \mathbb{L}_{ab} on the left, and the isomorphic poset $\mathbb{I}_{ab} \cong \mathbb{L}_{ab}$ on the right.

Figure 7.7: The posets \mathbb{L}_{ab} and $\mathbb{I}_{ab} \cong \mathbb{L}_{ab}$



The above discussion leads to the next result, which states that each poset \mathbb{O}_j^{n+2} can be built from gluing together the lattice path posets corresponding to the snake graphs in some \mathbb{O}_k^n .

Theorem 7.13. *Suppose the words w, w_1 , and w_2 are each of length $n - 1$. Let \mathbb{L}_w be the poset of lattice paths on G_w . Let $\mathbb{L}_1 \doteq \mathbb{L}_{w_1}$ and $\mathbb{L}_2 \doteq \mathbb{L}_{w_2}$ be the posets of lattice paths on $G_1 \doteq G_{w_1}$ and $G_2 \doteq G_{w_2}$, respectively. Label their snake graph representations by $\mathbb{L}_1 \cong \mathbb{I}_1$ and $\mathbb{L}_2 \cong \mathbb{I}_2$.*

- (a) *Each poset \mathbb{O}_j^{n+2} is isomorphic to the poset of lattice paths in a rectangular grid.*
- (b) *The rank generating function of the graded poset \mathbb{O}_j^{n+2} is equal to a q -binomial coefficient.*
- (c) *Each poset \mathbb{O}_j^{n+2} is isomorphic to the closed interval $[\emptyset, \lambda]$ in Young's lattice.*
- (d) *Each lattice $\mathbb{L}_w \cong \mathbb{I}_w$ is isomorphic to a closed interval in one of the posets \mathbb{O}_j^{n+2} .*
- (e) *The two posets $\mathbb{L}_1 \cong \mathbb{I}_1$ and $\mathbb{L}_2 \cong \mathbb{I}_2$ are embedded as intervals into the same \mathbb{O}_j^{n+2} if and only if G_1 and G_2 are both elements of the same poset \mathbb{O}_i^n . Moreover, each \mathbb{O}_j^{n+2} is covered by the collection of such embeddings.*

Proof. (a) Suppose the minimal element of \mathbb{O}_j^{n+2} has word $a^{k_1}b^{k_2}$, where $k_1 + k_2 - 1 = n$.

Note that the covering relations in \mathbb{O}_j^{n+2} preserve the number of a 's and b 's in the shape of a snake graph. That is, the nodes of \mathbb{O}_j^{n+2} are precisely those snake graphs whose word has k_1 instances of the symbol a , and k_2 instances of the symbol b . This description makes clear the isomorphism between \mathbb{O}_j^{n+2} and the lattice paths in a $k_1 \times k_2$ grid.

- (b) As mentioned above, each poset of lattice paths in a rectangular grid is isomorphic to a closed interval $[\emptyset, \lambda]$ in Young's lattice. Now the claim follows from part (a).
- (c) As mentioned above, the rank generating function of lattice paths in a grid is equal to some q -binomial coefficient. The result now follows from (a).
- (d) Embed the underlying snake graph G_w into the minimal rectangular grid containing it. This realizes the poset \mathbb{L}_w as the interval $[L_-, L_+]$ inside the poset of lattice paths in this

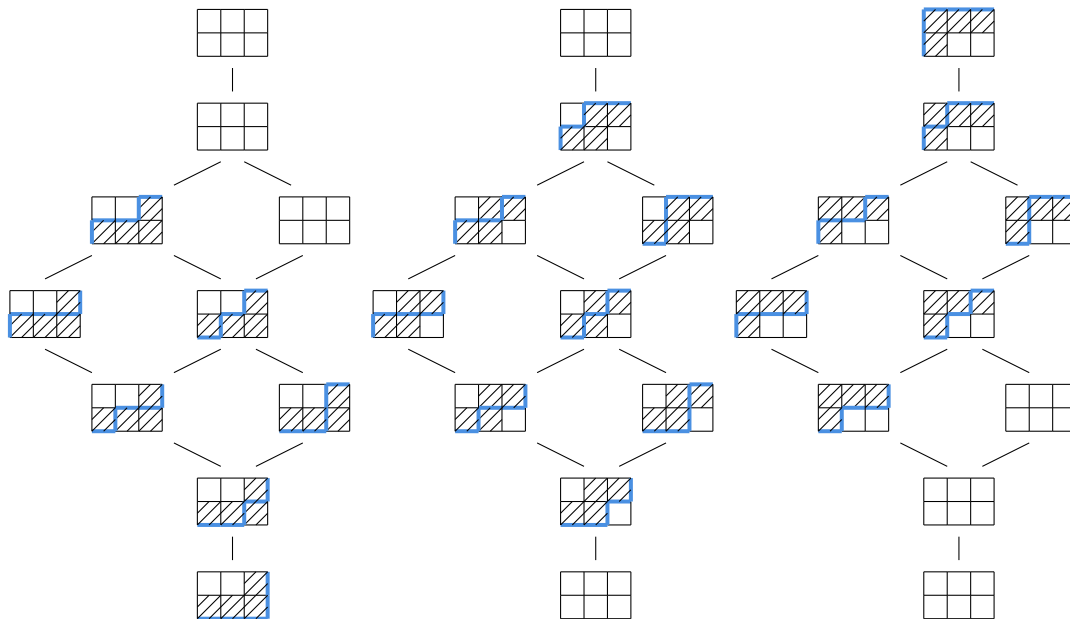
grid. As was indicated in part (a), the latter poset is isomorphic to \mathbb{O}_j^{n+2} for some j . Thus the claim holds.

- (e) The snake graphs G_1 and G_2 are nodes in the same poset if and only if both snake graphs are contained within the same minimal rectangular grid. This is true if and only if the lattice path posets \mathbb{L}_1 and \mathbb{L}_2 are embedded as intervals into the same poset of lattice paths in this minimal rectangular grid. By part (a), this is true if and only if \mathbb{L}_1 and \mathbb{L}_2 are embedded into the same \mathbb{O}_j^{n+2} . That \mathbb{O}_j^{n+2} is covered by the collection of these embeddings follows from the fact that any rectangular grid has a covering by snake graphs.

□

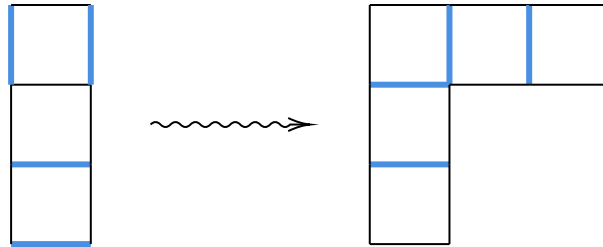
Example 7.14. Figure 7.8 shows three copies of the same poset, each of which is isomorphic to \mathbb{O}_2^6 . In each copy, we display one of the intervals (i.e., poset of lattice paths) in the cover from Theorem 7.13. Note that the three distinct snake graphs corresponding to each embedded interval shown are precisely the elements of \mathbb{O}_1^4 .

Figure 7.8: Three lattice path posets embedded into \mathbb{O}_2^6



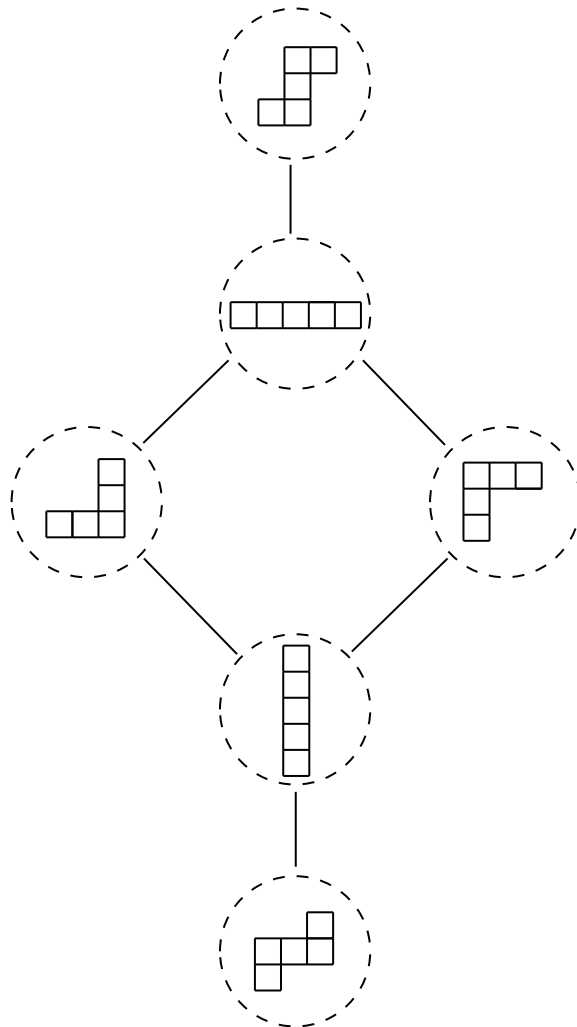
Remark 7.15. It is possible to dualize the above constructions (change the swap $ab \mapsto ba$ to $aa \mapsto bb$, reading off a snake graph from a perfect matching, etc.) to see explicitly that starting with perfect matchings on snake graphs gives analogous results.

Figure 7.9: Snake graphs from perfect matchings



Example 7.16. Below we show the “dual” of the poset \mathbb{O}_2^5 . This poset can be obtained by gluing together the two posets \mathbb{P}_{aa} and \mathbb{P}_{bb} , after realizing each perfect matching as a snake graph. Note that each node of this poset is dual (in the sense of snake graphs) to its respective node from Figure 7.3.

Figure 7.10: The poset dual to \mathbb{O}_2^5



Chapter 8

A Recursion and Two Rank Formulas

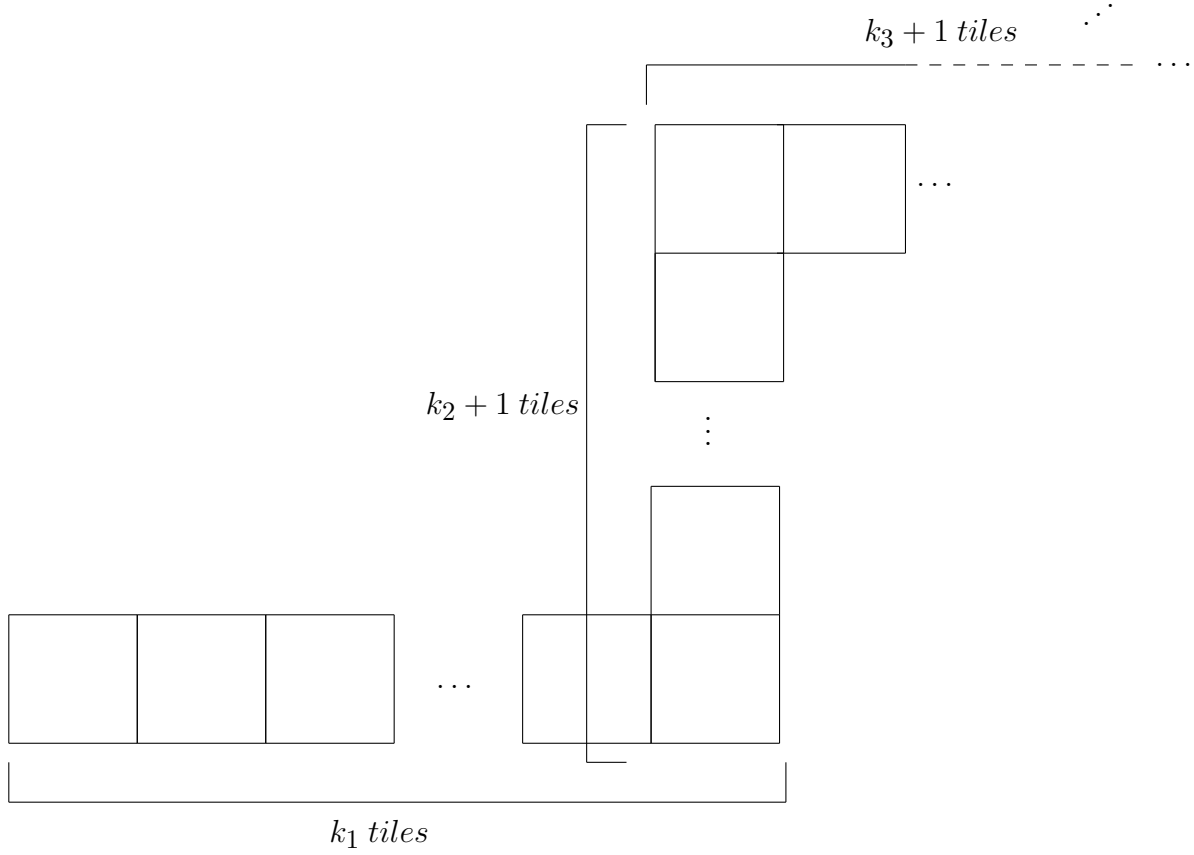
The first goal of this chapter is to give a recursive formula for the computation of $\mathbb{L}_w(q)$. Our second goal is to give a closed formula for $\mathbb{L}_w(q)$ in terms of products of *hooks*, snake graphs whose shape is either $a^{k_1}b^{k_2}$ or $a^{k_2}b^{k_1}$ for $k_1, k_2 \geq 2$. Thirdly, we combine this hook expansion with an interpretation of a snake graph as the central lattice path on a “stretched” zigzag snake graph to obtain a closed formula for $\mathbb{L}_w(q)$ in terms of the entries of the dual continued fraction $\text{CF}(w^*)$.

8.1 Lattice Path Recursion

A straight segment is *maximal* if it is not contained in any other straight segment. Decompose G_w into a union of d maximal overlapping straight segments as follows. Let k_1 be the number of tiles in the first row or column of G_w , k_d the number of tiles in the last row or column of G_w and $k_i + 1$ the number of tiles in the i^{th} row or column of G_w for $1 < i < d$.

Consider the dual continued fraction $\text{CF}(w^*) = [K_1, K_2, \dots, K_d]$, and assume $K_d \geq 2$ (this is no loss of generality, by the formula $[a_1, a_2, \dots, a_m, 1] = [a_1, a_2, \dots, a_m + 1]$). Form the continued fraction $\widehat{\text{CF}}(w^*) = [\widehat{K}_1, \widehat{K}_2, \dots, \widehat{K}_d]$ as follows:

Figure 8.1: The maximal straight segments of G_w



- (1) If $K_1 = 1$, then $\hat{d} = d - 1$. In this case, the first entry of $\widehat{\text{CF}}(w^*)$ is $\hat{K}_1 = K_1 + K_2 = 1 + K_2$. The last entry of $\widehat{\text{CF}}(w^*)$ is $\hat{K}_{\hat{d}-1} = K_d$. The rest of the entries are $\hat{K}_i = K_{i+1} + 1$ for $i \neq 1, d - 1$.
- (2) If $K_1 \neq 1$, then $\hat{d} = d$. In this case, the first entry of $\widehat{\text{CF}}(w^*)$ is $\hat{K}_1 = K_1$, and the last entry is $\hat{K}_d = K_d$. The rest of the entries are $\hat{K}_i = K_i + 1$.

The next lemma follows from the previous definition, duality, and the fact that the entries in $\text{CF}(w)$ give a decomposition of G_w into maximal zigzag segments.

Lemma 8.1. *With the notation above, we have $k_i = \hat{K}_i$ for each i .*

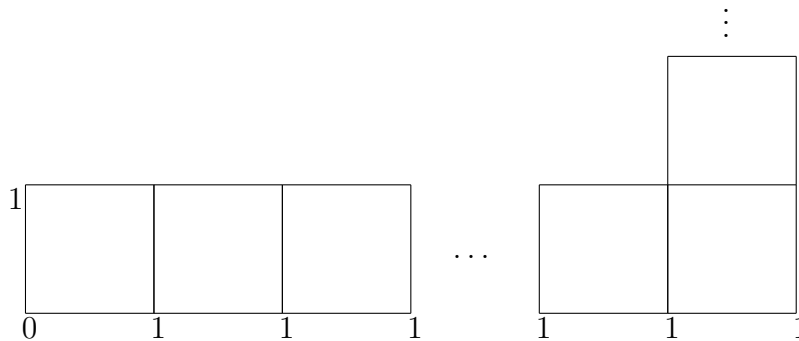
This result says that the entries in $\widehat{\text{CF}}(w^*)$ are the lengths of maximal straight segments in

the snake graph G_w .

We now recursively define a weight function ρ on the vertices of the snake graph G_w which assigns to each vertex of G_w a polynomial in q with positive integer coefficients. This weighting is such that if $G_{w'}$ is a connected subsnake graph with tiles T_1, T_2, \dots, T_j , then $\rho(x, y) = \mathbb{L}_{w'}(q)$, where (x, y) is the coordinate of the NE corner of the tile T_j . By Lemma 8.1, these weights are functions of the entries in $\text{CF}(w^*)$.

Suppose that G_w begins by going right. Initialize the recurrence with the conditions $\rho(0, 0) = 0$ and $\rho(0, 1) = \rho(x, 0) = 1$, for $x > 1$.

Figure 8.2: Initial step in the recurrence



The remaining vertices in the first maximal straight segment are determined by the condition

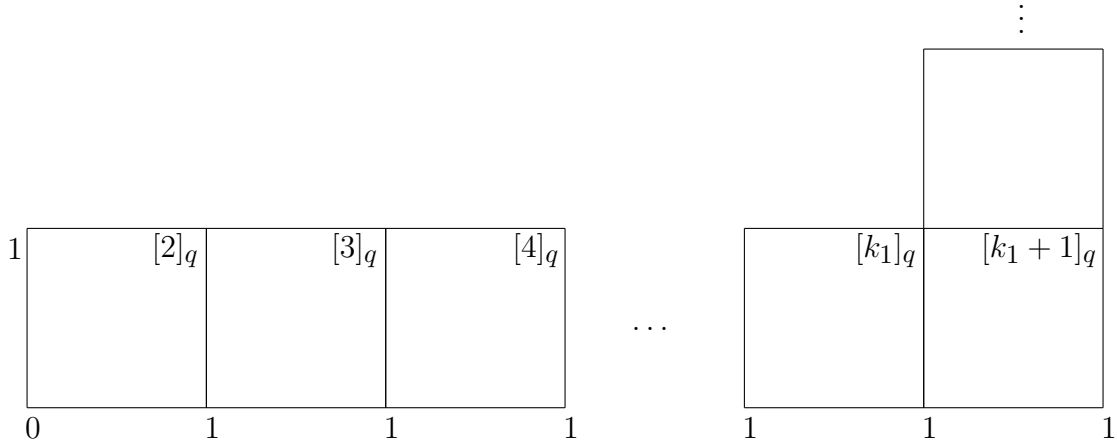
$$\rho(x, 1) = \rho(x, 0) + q\rho(x - 1, 1).$$

The outputs of ρ defined so far are displayed below in Figure 8.3. Recall that each $[m]_q = 1 + q + \dots + q^{m-1}$ is the q -analog of the integer m .

Next, $\rho(k_1 - 1, y) = \rho(k_1 - 1, 1) = [k_1]_q$, for each $y > 1$, and

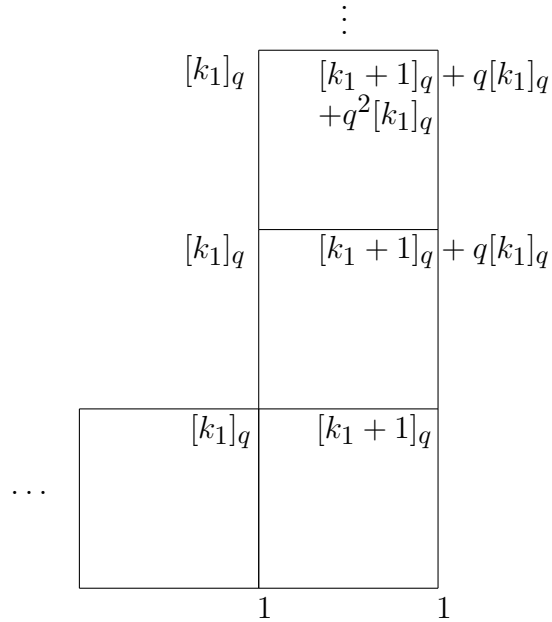
$$\rho(k_1, y) = \rho(k_1, y - 1) + q^y \rho(k_1 - 1, y)$$

Figure 8.3: The recurrence for the first maximal straight segment of G_w



for $y > 1$. The first few outputs $\rho(k_1 - 1, y) = [k_1]_q$ and $\rho(k_1, y)$ for $y > 1$ are shown in Figure 8.4.

Figure 8.4: The recurrence for the second maximal straight segment of G_w



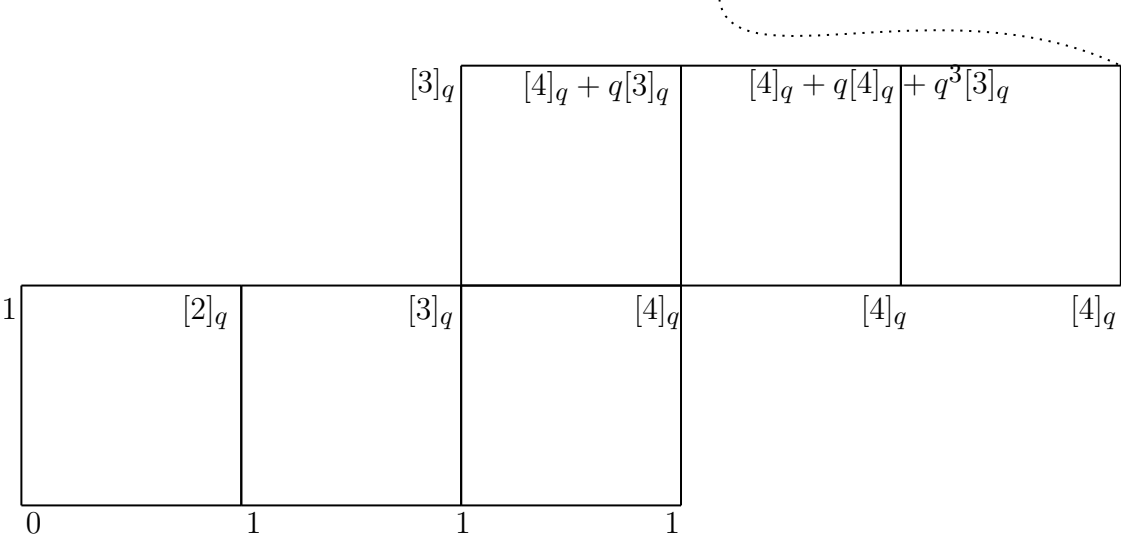
To compute the weights of the vertices in the third (horizontal) straight segment, we use the same recurrence relation that was used to compute the weights in the first straight segment, only the initial values are different. Similarly, the vertices in the fourth (vertical) straight segment are

computed using the second recurrence rule given above, except q^y is replaced with q^{y-k_2+1} . We continue along in this fashion until all outputs have been computed. A similar recurrence holds when G_w starts by going up.

Example 8.2. We use the recurrence just given to compute the lattice path rank function of the snake graph G_{w_3} from 7.1 above.

Figure 8.5: Recursive computation of the rank function $\mathbb{L}_{w_3}(q)$

$$\mathbb{L}_{w_3}(q) = [4]_q + q[4]_q + q^2[4]_q + q^3[3]_q = 1 + 2q + 3q^2 + 3q^3 + 3q^4 + 2q^5 + q^6$$



8.2 Hook Rank Formula

Now we provide a closed formula for any $\mathbb{L}_w(q)$. We continue to assume that G_w starts by going right.

Suppose G_w has d straight segments. Say tile T_i has an *exposed NW corner* if there is one tile glued to its S edge, and one tile glued to its E edge (these three tiles correspond to a subword ba in $\text{sh}(G_w)$). Similarly, we say tile T_i has an *exposed SE corner* if there is one tile glued to its N edge, and one tile glued to its W edge (corresponding to a subword ab in $\text{sh}(G_w)$). Let $\text{NW}(G_w)$

be the set of tiles of G_w with an exposed NW corner, and let $\text{SE}(G_w)$ be the set of tiles with an exposed SE corner.

If G_w starts by going right, then $u \doteq |\text{NW}(G_w)| = \left\lfloor \frac{d-1}{2} \right\rfloor$. For each $T_i \in \text{NW}(G_w)$, let T_i^{SE} and T_i^{NW} respectively denote the SE and NW corner of T_i .

For each i , any lattice path in \mathbb{L}_w must pass through either T_i^{SE} or T_i^{NW} (but not both). This allows us to partition \mathbb{L}_w into 2^u sets of lattice paths by specifying which corner in each $T_i \in \text{NW}(G_w)$ a path must pass through.

Consider the natural ordering on the tiles $\text{NW}(G_w)$ inherited from the ordering of the tiles of G_w . If t_i is one of the two corners of some $T_i \in \text{NW}(G_w)$, then the assignment $t_i \mapsto 0$ if $t_i = T_i^{\text{SE}}$ and $t_i \mapsto 1$ if $t_i = T_i^{\text{NW}}$ induces a poset isomorphism from u -tuples (t_1, t_2, \dots, t_u) to B_u , the Boolean lattice of rank u . Here, one element σ_2 in B_u covers another σ_1 if σ_2 can be obtained from σ_1 by switching one bit “0” in σ_1 to the bit “1”.

We now build another poset \mathcal{H} , and give an explicit isomorphism from it to a Boolean lattice. Introduce the following notation:

- $H_{i,i+1} = 1 + q[k_i]_q[k_{i+1}]_q$

- $H_i = [k_i]_q$,

- Define

$$H^{i,i+1} = \begin{cases} q^{k_i+k_{i+1}+1} & \text{if } i \neq 1 \text{ and } i+1 \neq l \\ q^{k_i+k_{i+1}} & \text{if } i = 1 \text{ or } i+1 = l. \end{cases}$$

Define a multiplication \circ on the symbols $H^{i,i+1}$. For $i < j$, define

$$H^{i,i+1} \circ H^{j,j+1} = \begin{cases} H^{i,i+1} H^{j,j+1} & \text{if } j \neq i+2 \\ q^{-1}(H^{i,i+1} H^{j,j+1}) & \text{if } j = i+2. \end{cases}$$

This new multiplication can be extended to products of more than two symbols.. If no confusion will result, we omit the comma appearing in the subscripts and superscripts of these symbols (e.g., we write H^{23} instead of $H^{2,3}$). We also omit the symbol “ \circ ” from the computations.

Starting with the minimal element $H_{12}H_{34} \dots H_{d-2,d-1}H_d$ if d is odd, or $H_{12}H_{34} \dots H_{d-3,d-2}H_{d-1,d}$ if d is even, and interpreting the local procedures

$$H_i H_{i+1} \mapsto H^i H^{i+1},$$

$$H_{i,i+1} H_{i+2} \mapsto H_i H^{i+1,i+2},$$

$$H_i H_{i+1,i+2} \mapsto H^{i,i+1} H_{i+2},$$

and

$$H_{i,i+1} H_{i+2,i+3} \mapsto H_i H^{i+1,i+2} H_{i+3}$$

as covering relations, gives a poset \mathcal{H} with additional node structure.

We now give an explicit isomorphism between the poset \mathcal{H} and the Boolean lattice B_u . Suppose for the moment that d is even, so that the minimal element of the poset above is $H_{12}H_{34} \dots H_{d-1,d}$. Send this element $H_{12}H_{34} \dots H_{d-1,d}$ to $(0, 0, \dots, 0) \in B_n$. Now sending $H_1 H^{23} H_4 H_{56} \dots \mapsto (1, 0, 0, \dots)$, $H_{12} H_3 H^{45} H_6 H_{78} \dots \mapsto (0, 1, 0, 0, \dots)$, etc. induces the aforementioned isomorphism. In other words, each weight in \mathcal{H} is given coordinates based on the symbols with upper

subscripts that it contains. The assignment is similar when i is odd.

Thus, the nodes H_σ of \mathcal{H} are indexed by $\sigma \in B_u$. The next result follows from the above constructions.

Theorem 8.3. *Fix the word w and consider the rank function $\mathbb{L}_w(q)$ of lattice paths on the snake graph G_w . Let B_u be the Boolean lattice of rank u . Recall the symbols H_σ , each parameterized by $\sigma \in B_u$ and representing a polynomial in q with positive integer coefficients. Then we have*

$$\mathbb{L}_w(q) = \sum_{\sigma \in B_u} H_\sigma.$$

Example 8.4. Consider the snake graph G_w and the lattice \mathbb{L}_w with its rank function $\mathbb{L}_w(q)$.

(1) If $\text{sh}(G_w) = a^{k_1-1}b^{k_2}a^{k_3-1}$, then

$$\mathbb{L}_w(q) = H_{12}H_3 + H_1H^{23}.$$

(2) If $\text{sh}(G_w) = a^{k_1-1}b^{k_2}a^{k_3}b^{k_4-1}$, then

$$\mathbb{L}_w(q) = H_{12}H_{34} + H_1H^{23}H_4.$$

(3) If $\text{sh}(G_w) = a^{k_1-1}b^{k_2}a^{k_3}b^{k_4}a^{k_5-1}$, then

$$\mathbb{L}_w(q) = H_{12}H_{34}H_5 + H_1H^{23}H_4H_5 + H_{12}H_3H^{45} + H_1H^{23}H^{45}.$$

(4) If $\text{sh}(G_w) = a^{k_1-1}b^{k_2}a^{k_3}b^{k_4}a^{k_5}b^{k_6-1}$, then

$$\mathbb{L}_w(q) = H_{12}H_{34}H_{56} + H_1H^{23}H_4H_{56} + H_{12}H_3H^{45}H_6 + H_1H^{23}H^{45}H_6.$$

Similar formulas can be derived for when G_w starts by going up, e.g., for G_w such that $\text{sh}(G_w) = b^{k_1-1}a^{k_2}b^{k_3-1}$, we have $\mathbb{L}_w(q) = H_1H_{23} + H^{12}H_3$.

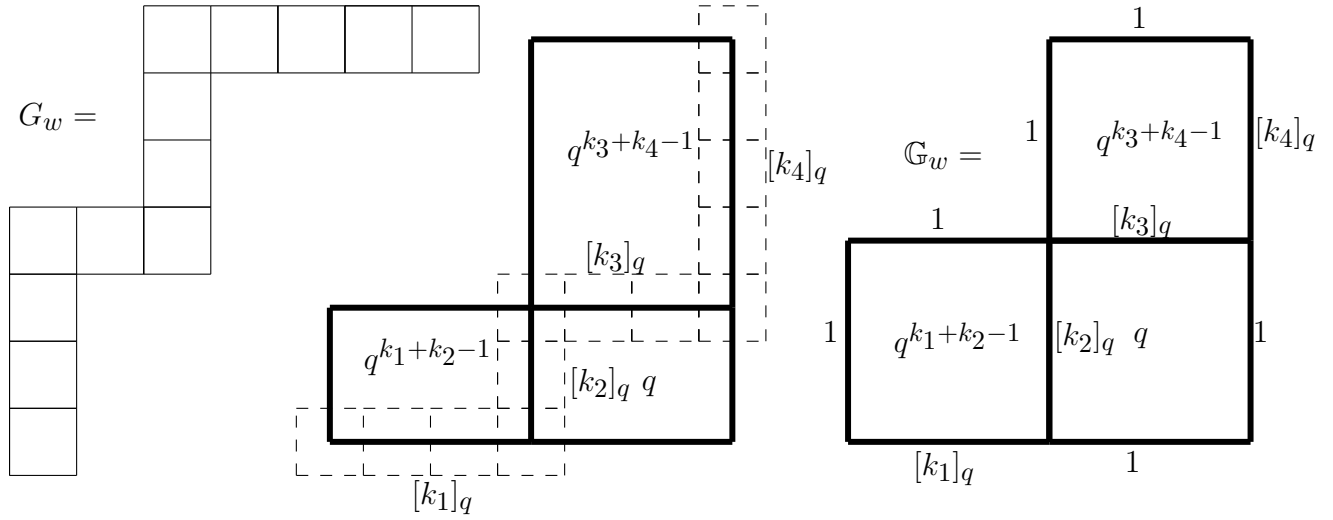
8.3 Fibonacci Rank Formula

The hook expansion formula from the previous section can be refined to an explicit closed formula for $\mathbb{L}_w(q)$, as a sum over “face-weighted” products of q -deformations of the entries k_i from $\text{CF}(w)^*$. Each term in this formula is the weight of a lattice path L on a zigzag snake graph \mathbb{G}_w with $d - 1$ tiles.

By the weight of L , we mean the product of the weights attached to the edges of L , multiplied by the product of face weights in the symmetric difference $L \ominus L_-$ (recall L_- is the minimal lattice path from Definition 6.6 above). Each edge weight is either equal to 1 or $[k_i]_q$ for some i , and each $[k_i]_q$ is used precisely once. Each face weight is either equal to q , or equal to a power of q with exponent equal to the number of tiles in some hook of G_w .

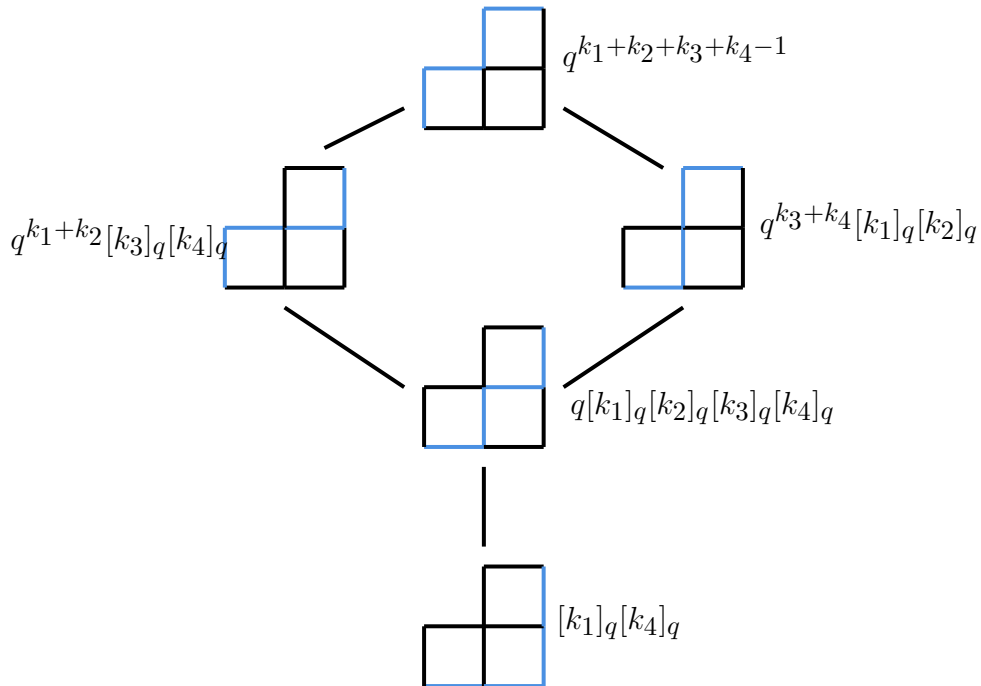
The snake graph \mathbb{G}_w is built from G_w by first reflecting G_w about the antidiagonal a_1 , and then treating G_w as the “middle” lattice path on \mathbb{G}_w . This construction in the case that G_w is built from four maximal straight segments is illustrated below.

Figure 8.6: The construction of \mathbb{G}_w from G_w



Summing over the weights of the paths on this zigzag snake graph gives a closed expression for the rank function $\mathbb{L}_w(q)$.

Figure 8.7: The poset \mathbb{G}_{ab} , its node weights, and the rank function $\mathbb{L}_w(q)$



$$\mathbb{L}_w(q) = [k_1]_q [k_4]_q + q [k_1]_q [k_2]_q [k_3]_q [k_4]_q + q^{k_1+k_2} [k_3]_q [k_4]_q + q^{k_3+k_4} [k_1]_q [k_2]_q + q^{k_1+k_2+k_3+k_4-1}$$

In particular, each such rank function expansion has a Fibonacci number of terms, which

are arranged into a Fibonacci cube. As mentioned above, the snake graph G_w is canonically associated to the node labeled by $000 \dots 0$ in this Fibonacci cube (see Example 3.45).

Let $\mathbb{L}(\mathbb{G}_w)$ denote the poset of lattice paths on \mathbb{G}_w . For any element $L \in \mathbb{L}(\mathbb{G}_w)$, let its weight as described above be denoted q_L .

Theorem 8.5. *Let w be any word. Suppose the snake graph G_w is built from d maximal straight segments. Then the rank function $\mathbb{L}_w(q)$ can be written as*

$$\mathbb{L}_w(q) = \sum_{L \in \mathbb{L}(\mathbb{G}_w)} q_L$$

where \mathbb{G}_w is the snake graph with $d - 1$ tiles defined above, and $\mathbb{L}(\mathbb{G}_w)$ is its poset of lattice paths.

Proof. This is essentially the hook expansion formula above, except we decompose the set of lattice paths using the corners in $\text{NW}(G_w) \cup \text{SW}(G_w)$ instead of just $\text{NW}(G_w)$.

□

Chapter 9

Unimodality and Symmetry

Recently, Morier-Genoud and Ovsienko gave a new notion of q -deformed continued fractions and rational numbers [26]. The q -deformation $[\frac{r}{s}]_q$ of a rational number $\frac{r}{s}$ is a rational function in q defined by a continued fraction formula. It turns out that $[\frac{r}{s}]_q$ is a rational function with positive integer coefficients.

The next result follows from Corollary B.4 in [26] and Theorem 6.22.

Theorem 9.1. *Recall the notation introduced directly before Theorem 4.5. Then for any w we have*

$$[CF(w)]_q = \frac{\mathbb{P}_w(q)}{\mathbb{P}_w^{a_1}(q)} = \frac{\mathbb{L}_{w^*}(q)}{\mathbb{L}_{w^*}^{a_1}(q)}$$

and

$$[CF(w^*)]_q = \frac{\mathbb{P}_{w^*}(q)}{\mathbb{P}_{w^*}^{b_1}(q)} = \frac{\mathbb{L}_w(q)}{\mathbb{L}_w^{b_1}(q)}.$$

In [26] it was conjectured that the numerator and denominator of any q -deformed rational is a unimodal polynomial (see Definition 7.4).

The unimodality of \mathbb{L}_w is known to be true in some special cases. For instance, \mathbb{L}_w is unimodal if

- (1) $\text{sh}(G_w)$ is straight (trivial), or
- (2) $\text{sh}(G_w)$ is zigzag (Fibonacci cubes are unimodal, see [27]), or

(3) C_{w^*} is an *up-down poset* (see [17], and [16] for a relation to Alexander polynomials of 2-bridge knots), a certain class of posets defined by the division algorithm.

Our first goal in this chapter is to prove that $\mathbb{L}_w(q)$ is unimodal in the case that G_w is built from at most four maximal straight segments (in fact, we prove something stronger than unimodality holds). Our second goal is to say when a poset \mathbb{P}_w or \mathbb{L}_w is symmetric, based on the shape of the underlying snake graph.

9.1 Rank Unimodality

We say the sequence (r_j) has a *plateau* if there exists $p \geq 1$ such that $r_{j_1} = r_{j_1+1} = \cdots = r_{j_1+p}$. A plateau is *small* if $p = 1$. The sequence (r_j) is *trapezoidal* if (r_j) is symmetric and

$$r_0 < r_1 < \cdots < r_j = \cdots = r_{n-j} > \cdots > r_n.$$

Say the sequence (r_j) is *weakly trapezoidal* if there exists some t such that

$$r_0 < r_1 < \cdots < r_j = \cdots = r_{j+t} > \cdots > r_n$$

such that if n is odd then at least one of the middle two terms $r_{\lfloor \frac{n}{2} \rfloor}$ or $r_{\lceil \frac{n}{2} \rceil}$ is maximal, and if instead n is even then at least the middle term $r_{\frac{n}{2}}$ is maximal. In particular, a weakly trapezoidal sequence is not assumed to be symmetric. A sequence is *almost weakly trapezoidal* if

$$r_0 \leq r_1 < r_2 < \cdots < r_j = \cdots = r_{j+t} > \cdots > r_{n-2} > r_{n-1} \geq r_n.$$

and the subsequence $(r_j)_{j=1}^{n-1}$ is weakly trapezoidal. Say the sequence (r_j) has *unimodal growth*

if the sequence $(|r_{j+1} - r_j|)$ is bimodal and nonconstant. The polynomial $\rho(q) = \sum_{i=0}^n r_i q^i$ is said to have a *plateau* if its sequence of coefficients does, etc.

Consider the hook snake graph G_w of shape $\text{sh}(G_w) = a^{k_1} b^{k_2}$. Let $k = \min\{k_1, k_2\}$, and let G_{w_0} be the subsnake graph of G_w of shape $\text{sh}(G_{w_0}) = a^{k-1} b^{k-1}$. Let $n_0 = 2k - 1$ be the (odd) number of tiles of G_{w_0} .

Proposition 9.2. *Consider the hook snake graph G_w of shape $\text{sh}(G_w) = a^{k_1-1} b^{k_2-1}$. Then for $k_1 \leq k_2$ we have*

$$\mathbb{L}_w(q) = 1 + q + 2q^2 + \cdots + k_1 q^{k_1} + \cdots + k_1 q^{k_2} + \cdots + 2q^{k_1+k_2-2} + q^{k_1+k_2-1}.$$

Proof. From the recursion given above we can compute $\mathbb{L}_w(q) = 1 + q[k_1]_q[k_2]_q$. Now the claim follows from Proposition 1.5 (1) in [7]. □

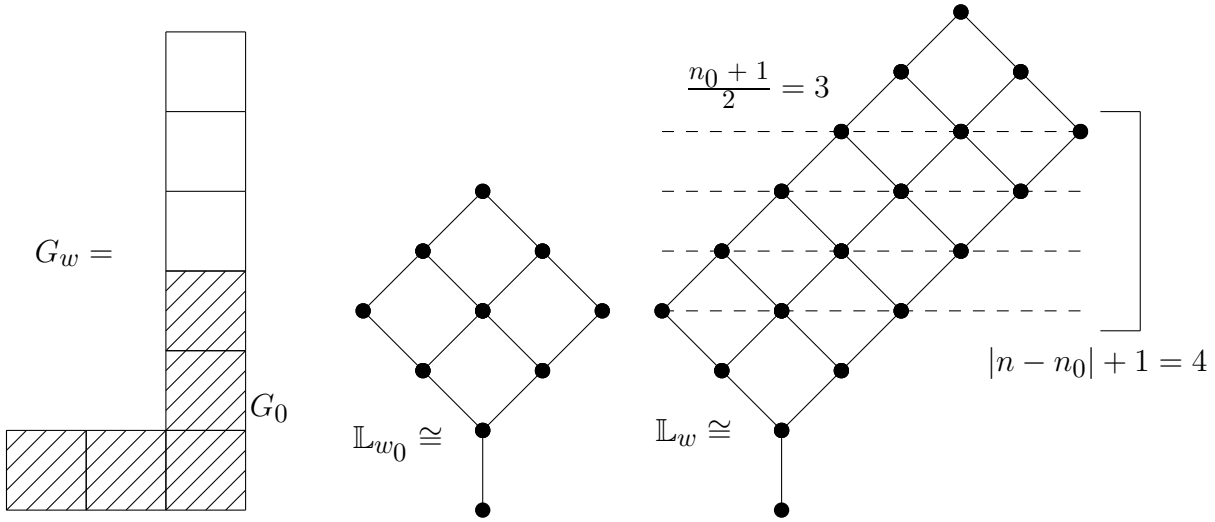
Corollary 9.3. *Consider the hook snake graph G_w of shape $\text{sh}(G_w) = a^{k_1-1} b^{k_2-1}$. Let $k = \min(k_1, k_2)$.*

- (a) *The first and last coefficients of $\mathbb{L}_w(q)$ are both equal to 1.*
- (b) *The maximum value of the coefficients of $\mathbb{L}_w(q)$ is equal to k .*
- (c) *The number of times the maximum value occurs is equal to $n - n_0 + 1 = n - 2k + 2$, in degrees $k, k + 1, \dots, n - k + 1$.*
- (d) *The polynomial $\mathbb{L}_w(q)$ has at least one small plateau, consisting of the first two coefficients. If $\mathbb{L}_w(q)$ has a second plateau, then each entry of this plateau is equal to the maximum value. There are no other plateaus.*
- (e) *The polynomial $\mathbb{L}_w(q)$ is almost weakly trapezoidal. In particular, $\mathbb{L}_w(q)$ is unimodal.*

Proof. All parts (a)-(e) follow directly from Proposition 9.2. □

Example 9.4. Consider G_w with $\text{sh}(G_w) = a^2b^5$, shown in the leftmost illustration in Figure below. The subsnake graph G_0 is shown shaded inside G . The middle figure is isomorphic to \mathbb{L}_{w_0} , and the rightmost lattice shown is isomorphic to \mathbb{L}_w . The maximal coefficient in the polynomial $\mathbb{L}_w(q)$ is equal to 3, and this maximal coefficient occurs 4 times. Here, $n = 8, n_0 = 5, k = k_1 = 3$, and $k_2 = 6$.

Figure 9.1: The snake graphs G_w and G_0 , and the associated posets \mathbb{L}_{w_0} and \mathbb{L}_w

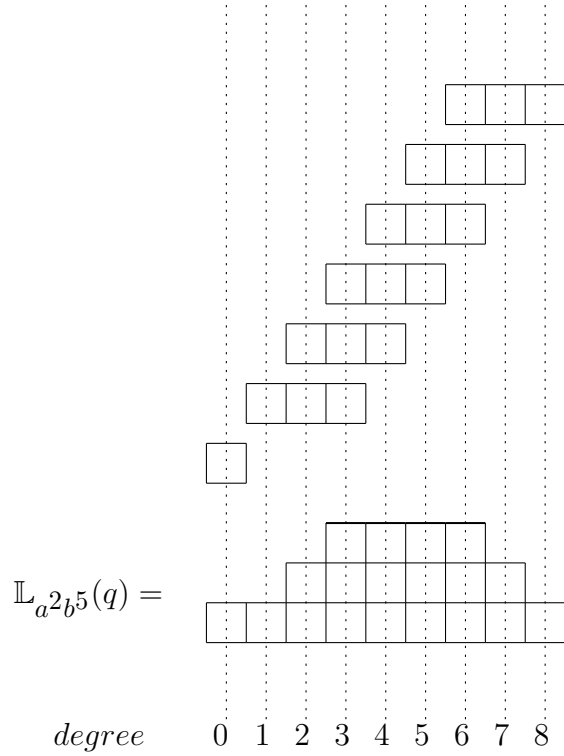


It is useful to visualize any rank function from a snake graph in terms of stacking square tiles. Each coefficient r_j of such a rank function is represented by r_j tiles stacked vertically. Figure 9.2 shows how the rank function $\mathbb{L}_{a^2b^5}(q)$ from the previous example is built, according to the expression $\mathbb{L}_{a^2b^5}(q) = 1 + q[3]_q + q^2[3]_q + \cdots + q^6[3]_q$.

Let $n, m \geq 1$, and suppose $n = k_1 + k_2 - 1$. Let $k = \min(k_1, k_2)$. Define the hook subsnake graphs $\mathcal{H} = \mathcal{H}_{k_1, k_2, m}$ of G_w to be of shape

$$\text{sh}(\mathcal{H}) = \begin{cases} a^{k_1-1}b^{\min(m-1, k_2-1)} & \text{if } k = k_1 \\ a^{\min(m-1, k_1-1)}b^{k_2-1} & \text{if } k = k_2 \end{cases}$$

Figure 9.2: The rank function $\mathbb{L}_{a^2b^5}(q)$ via block stacking



Let the coefficients of the rank function of lattice paths on $\mathcal{H}_{k_1, k_2, m}$ be called $\mathcal{H}_j(k_1, k_2, m)$. Note that when m is equal to or exceeds the length of the longer of the two straight segments that G_w is built from, then $\text{sh}(\mathcal{H}) = \text{sh}(G_w)$. In other words, writing $\mathbb{L}_w(q) = \sum_{j=0}^n r_j q^j$ we have that $\mathcal{H}_j(k_1, k_2, m) = r_j$ for m sufficiently large.

Define $\chi = \chi(k_1, k_2, m)$ by

$$\chi = \begin{cases} k + m - 1 & \text{if } m \leq n - 2k + 2 \\ \lfloor \frac{n+m}{2} \rfloor & \text{if } n - 2k + 2 < m < n \\ n & \text{if } n < m \end{cases}$$

and the coefficients

$$\tilde{\mathcal{H}}_j(k_1, k_2, m) = \begin{cases} 1, & \text{if } n - 2k + 2 < m < n \text{ and } 2 \mid (n + m) \text{ and } j = \frac{n+m}{2} \\ \mathcal{H}_j(k_1, k_2, m), & \text{else.} \end{cases}$$

Proposition 9.5. Consider the rank function $\mathbb{L}_w(q) = \sum_{j=0}^n r_j q^j$ of the hook snake graph G_w of shape $sh(G_w) = a^{k_1-1}b^{k_2-1}$ built from two maximal straight segments of length $k_1 \geq 2$ and $k_2 \geq 2$. Let the number of tiles of G_w be $n = k_1 + k_2 - 1$. Let $k = \min(k_1, k_2)$ and $m \geq 1$. Then we have

$$[m]_q \mathbb{L}_w(q) = [m]_q + \sum_{j=1}^{\chi} \tilde{\mathcal{H}}_j(k_1, k_2, m) [n + m - 2j + 1]_q q^j.$$

In any case, $[m]_q \mathbb{L}_w(q)$ is weakly trapezoidal, and has unimodal growth for $m \geq 2$.

Furthermore,

- (a) If $m < n - 2k + 2$, then $[m]_q \mathbb{L}_w(q)$ has a unique plateau consisting of maximal values, which is of length $(n - 2k + 1) - (m - 2)$ and is situated in degrees $k + (m - 1), k + m, \dots, n - k + 1$
- (b) If $m = n - 2k + 2$, then $[m]_q \mathbb{L}_w(q)$ has a maximum at degree $n - k + 1$, and no plateau.
- (c) If $n - 2k + 2 < m < n$ and $2 \nmid n + m$, then $[m]_q \mathbb{L}_w(q)$ has a unique (small) plateau, situated in degrees $\lfloor \frac{n+m}{2} \rfloor$ and $\lceil \frac{n+m}{2} \rceil$.
- (d) If $n - 2k + 2 < m < n$ and $2 \mid n + m$, then $[m]_q \mathbb{L}_w(q)$ has a maximum at degree $\frac{n+m}{2}$.
- (e) If $m = n$, then $[m]_q \mathbb{L}_w(q)$ has a unique (small) plateau, situated in degrees $n - 1$ and n .
- (f) If $m = n + 1$, then $[m]_q \mathbb{L}_w(q)$ has a maximum at degree n , and no plateau.
- (g) If $m > n + 1$, then $[m]_q \mathbb{L}_w(q)$ has a unique plateau, which is of length $m - n$ and situated in degrees $n, n + 1, \dots, m - 1$.

Proof. Write the rank function $\mathbb{L}_w(q)$ as

$$\mathbb{L}_w(q) = [1]_q + q[n]_q + q^2[n-2]_q + \cdots + q^k[n-2k+2]_q,$$

so that the product $[m]_q \mathbb{L}_w(q)$ is

$$[m]_q \mathbb{L}_w(q) = [m]_q + q[m]_q [n]_q + q^2 [m]_q [n-2]_q + \cdots + q^k [m]_q [n-2k+2]_q. \quad (9.1)$$

From [7] we have

$$[m]_q [n]_q = \sum_{j=1}^{\min(m,n)} [m+n-2j+1]_q q^{j-1}. \quad (9.2)$$

Explicitly,

- If $m < n$, then

$$[m]_q [n]_q = [n+(m-1)]_q + q[n+(m-3)]_q + \cdots + q^{m-1}[n-(m-1)]_q.$$

- If $m = n$, then

$$[m]_q [n]_q = [n]_q^2 = [2n-1]_q + q[2n-3]_q + \cdots + q^{n-1}[1]_q.$$

- If $m > n$, then

$$[m]_q [n]_q = [m+(n-1)]_q + q[m+(n-3)]_q + \cdots + q^{n-1}[m-(n-1)]_q.$$

We consider seven cases, based on the value of m relative $n - 2k + 2$ and n , and the parity of the sum $n + m$. In each case we use Equation 9.3 above to expand each product of q -numbers in Equation 9.1 and collect like terms to obtain the formula. This is shown explicitly in the first case only, as the rest are similar.

(a) $m < n - 2k + 2$: Here, the statement is

$$[m]_q \mathbb{L}_w(q) = [m]_q + \sum_{j=1}^{k+m-1} \mathcal{H}_j(k_1, k_2, m) [n + m - 2j + 1]_q q^j.$$

Using (2) to expand each term $q^j [m]_q [n - 2j]_q$ in (1) and collecting like terms gives the desired expression for $[m]_q \mathbb{L}_w(q)$:

$$\begin{aligned} [m]_q \mathbb{L}_w(q) &= [m]_q \left(1 + q \sum_{j=1}^k [(k_1 + k_2) - 2j + 1]_q q^{j-1} \right) \\ &= [m]_q \left(1 + \sum_{j=1}^k [(k_1 + k_2 - 1) - 2j + 2]_q q^j \right) \\ &= [m]_q \left(1 + \sum_{j=1}^k [n - 2j + 2]_q q^j \right) \\ &= [m]_q + \sum_{j=1}^k [m]_q [n - 2j + 2]_q q^j \\ &= [m]_q + \sum_{j=1}^k \sum_{i=1}^m [n - 2(i + j - 1) + 1]_q q^{i+j-1} \\ &= [m]_q + \sum_{j=1}^{k+m-1} \mathcal{H}_j(k_1, k_2, m) [n + m - 2j + 1]_q q^j \end{aligned} \tag{9.3}$$

Now let

$$\rho(q) \doteq \sum_{j=1}^{k+m-1} \mathcal{H}_j(k_1, k_2, m)[n+m-2j+1]_q q^j.$$

Note that when we increment j in this sum, the power of q goes up by one, while the term inside the bracket decreases by two. This fact, along with the fact that the coefficients $\mathcal{H}_j(k_1, k_2, m)$ form a weakly trapezoidal sequence, shows that $\rho(q)$ is weakly trapezoidal with unimodal growth.

In particular, the degrees of the terms whose coefficients make up the unique plateau of $\rho(q)$ are exactly the powers of q occurring in the last term $q^{k+m-1}[n-m-2k+3]$. Thus we read off that $\rho(q)$ has a plateau of maximal coefficients of length $(n-2k+1)-(m-2)$ situated in degrees $k+(m-1), k+m, \dots, n-k+1$.

Since $k > 1$ we have $m-1 < m < n-2k+2 < n-k+1$, so that adding the chain $[m]_q$ to $\rho(q)$ does not disturb the plateau of maximal coefficients of $\rho(q)$. In other words, $[m]_q + \rho(q)$ has the same plateau of maximal coefficients as $\rho(q)$. Since the coefficients $\mathcal{H}_j(k_1, k_2, m)$ form a weakly trapezoidal sequence, no other plateaus are created by adding the chain $[m]_q$ to $\rho(q)$. Hence $[m]_q \mathbb{L}_w(q)$ is weakly trapezoidal with unimodal growth, as claimed.

(b) $m = n - 2k + 2$:

In this case the formula can be computed to be

$$[m]_q \mathbb{L}_w(q) = [n-2k+2]_q + \sum_{j=1}^{n-k+1} \mathcal{H}_j(k_1, k_2, m)[2n-2k-2j+3]_q q^j,$$

and the last term in the sum $\rho(q) \doteq \sum_{j=1}^{n-k+1} \mathcal{H}_j(k_1, k_2, m)[2n-2k-2j+3]_q q^j$ is $[1]_q q^{n-k+1}$. Thus, $\rho(q)$ has a maximum at degree $n-k+1$. Just as before, adding the chain $[n-2k+2]_q$ to $\rho(q)$ does not disturb the unique plateau of maximal coefficients

of $\rho(q)$. Since the coefficients $\mathcal{H}_j(k_1, k_2, m)$ are weakly trapezoidal, no other plateaus are created by adding $[m]_q$ to $\rho(q)$. Thus the claim holds in this subcase as well.

- (c) $n - 2k + 2 < m < n$ and $2 \nmid n + m$: If n and m have opposite parity then there exists some c such that

$$n - 2c < m = n - 2c + 1 < n - 2c + 2.$$

Using Equation 9.3, we see that

$$[m]_q \mathbb{L}_w(q) = [m]_q + \sum_{j=1}^{n-c} \mathcal{H}_j(k_1, k_2, m) [n + m - 2j + 1]_q q^j.$$

This matches the form given in the statement, since $2 \nmid n + m$ implies $\lfloor \frac{n+m}{2} \rfloor = \frac{n+m-1}{2} = \frac{n+(n-2c+1)-1}{2} = n-c$. Again by using a degree argument we see that $[m]_q \mathbb{L}_w(q)$ is weakly trapezoidal with unimodal growth.

- (d) $n - 2k + 2 < m < n$ and $2 \mid n + m$: If $2 \mid m + n$ then there exists some c such that $m = n - 2c$. As in the previous case we use 9.3 to write

$$[m]_q \mathbb{L}_w(q) = [m]_q + \sum_{j=1}^{n-c} \mathcal{H}_j(k_1, k_2, m) [n + m - 2j + 1]_q q^j,$$

except that now $2 \mid n + m$ so that $\frac{n+m}{2} = n - c$. That the maximum of $\mathbb{L}_w(q)$ occurs in degree $\frac{n+m}{2}$ can be seen by computing the last term $[1]_q q^{\frac{n+m}{2}}$ in the sum.

- (e) $m = n$: Using Equation 9.3 gives

$$[m]_q \mathbb{L}_w(q) = [n]_q + \sum_{j=1}^n r_j [2n - 2j + 1]_q q^j.$$

The last term in the above sum $\sum_{j=1}^n r_j [2n - 2j + 1]_q q^j$ is $[1]_q q^n$, which shows that $\sum_{j=1}^n r_j [2n - 2j + 1]_q q^j$ has a maximum in degree n . That the last two terms are $[1]_q q^n$ and $2[3]_q q^{n-1}$ implies that whatever the maximum coefficient is, the previous coefficient is one less. Now adding $[n]_q = [n-1]_q + q^{n-1}$ to the sum $\sum_{j=1}^n r_j q^j [2n - 2j + 1]_q$ and again considering the term $[3]_q q^{n-1}$ shows that the small plateau in question exists, in degrees $n-1$ and n as claimed. That it is unique follows easily, as does the fact that the polynomial $[m]_q \mathbb{L}_w(q)$ is weakly trapezoidal with unimodal growth.

(f) $m = n + 1$: In this case we have

$$[m]_q \mathbb{L}_w(q) = [n+1]_q + \sum_{j=1}^n r_j [2n - 2j + 2]_q q^j.$$

To see that $[m]_q \mathbb{L}_w(q)$ has a unique maximum coefficient, consider the last term $q^n [2]_q$ from the sum $\rho(q) \doteq \sum_{j=1}^n r_j q^j [2n - 2j + 2]_q$. It follows that $\rho(q)$ has a unique maximal plateau in degrees n and $n+1$. Now adding the chain $[n+1]_q = [n]_q + q^n$ to $\rho(q)$ shows that $[n+1]_q \mathbb{L}_w(q)$ has a unique maximum coefficient, in degree n . That $[m]_q \mathbb{L}_w(q)$ is weakly trapezoidal with unimodal growth follows immediately.

(g) The formula here is

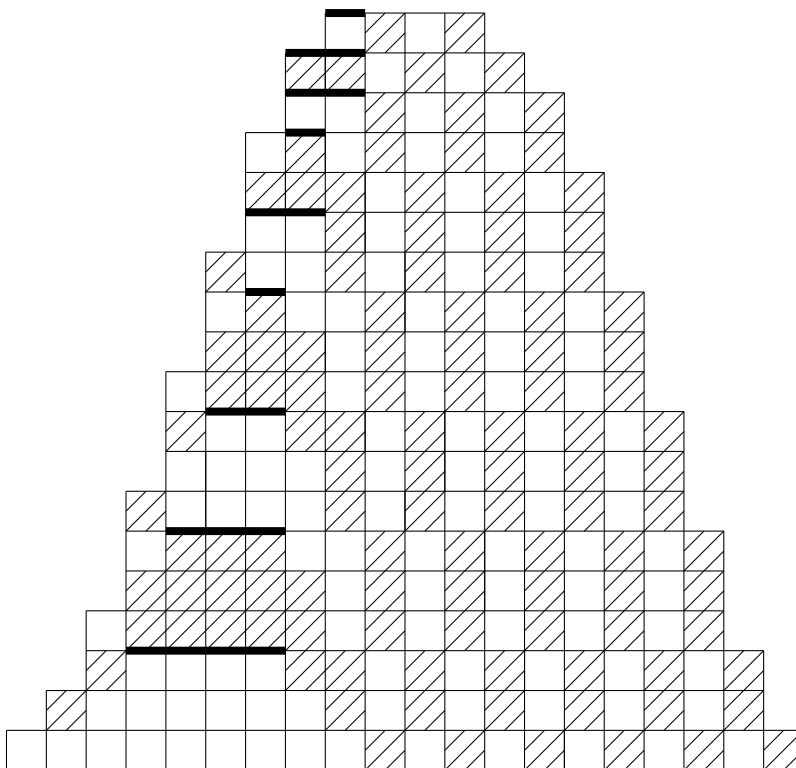
$$[m]_q \mathbb{L}_w(q) = [m]_q + \sum_{j=1}^n r_j [n + m - 2j + 1]_q q^j.$$

Again, the last coefficient $[m - n + 1]_q q^n$ tells us the behavior of the plateau of the sum above, and the claim follows.

□

Example 9.6. In Figure 9.3 below, we show the effect of multiplying the rank function $\mathbb{L}_{a^2b^5}(q)$ by $[m]_q$ for $1 \leq m \leq 12$. We have indicated each plateau of maximal coefficients of $[m]_q \mathbb{L}_{a^2b^5}(q)$ for $1 \leq m \leq 9 = n + 1$ with a bold line.

Figure 9.3: The rank function $[m]_q \mathbb{L}_{a^2b^5}(q)$ for $1 \leq m \leq 12$



Theorem 9.7. Consider the snake graph G_w and the rank generating function $\mathbb{L}_w(q)$.

- (a) Suppose the snake graph G_w with $n = k_1 + k_2 + k_3 - 1$ tiles has the shape $sh(G_w) = a^{k_1-1}b^{k_2}a^{k_3-1}$, where $k_1 \geq 2$, $k_2 \geq 1$, and $k_3 \geq 2$. Then the polynomial $\mathbb{L}_w(q)$ is weakly trapezoidal with unimodal growth. In particular, $\mathbb{L}_w(q)$ is unimodal.
- (b) Suppose the snake graph G_w with $n = k_1 + k_2 + k_3 + k_4 - 1$ tiles has the shape $sh(G_w) = a^{k_1-1}b^{k_2}a^{k_3}b^{k_4-1}$. Then the polynomial $\mathbb{L}_w(q) = \sum_{j=1}^n$ is weakly trapezoidal with unimodal growth. In particular, $\mathbb{L}_w(q)$ is unimodal.

Proof. (a) By Theorem 8.3 we can write

$$\mathbb{L}_w(q) = [k_3]_q \left(1 + q[k_1]_q [k_2]_q \right) + q^{k_2+k_3} [k_1]_q,$$

By Proposition 9.5 we have

$$\mathbb{L}_w(q) = \rho(q) + q^{k_2+k_3} [k_1]_q$$

where $\rho(q)$ is the weakly trapezoidal polynomial

$$\rho(q) \doteq [k_3]_q + \sum_{j=1}^{\chi} \tilde{\mathcal{H}}_j(k_1, k_2, k_3) [n - 2j + 1]_q q^j$$

with unimodal growth.

Note that the highest power occurring in $q^{k_2+k_3} [k_1]_q$ is $q^{k_1+k_2+k_3-1}$, which is one higher than the degree of $\rho(q)$. This remark, along with the fact that the coefficients $\mathcal{H}_j(k_1, k_2, k_3)$, have unimodal growth, implies that adding the chain $q^{k_2+k_3} [k_1]_q$ to $\rho(q)$ does not create any new plateaus. In particular, \mathbb{L}_w is unimodal.

- (b) Let $G_{w'}$ be the subsnake graph of G_w obtained by deleting the first k_1 tiles from G_w , and $G_{w''}$ the subsnake graph of $G_{w'}$ obtained by deleting the first $k_1 + k_2 - 1$ tiles from $G_{w'}$. Set $\rho'(q) = \mathbb{L}_{w'}(q)$ and $\rho''(q) = \mathbb{L}_{w''}(q)$. By the recurrence relation above we can write

$$\mathbb{L}_w(q) = \left([k_1]_q q \right) \rho'(q) + \rho''(q).$$

By part (a), $\rho'(q)$ is weakly trapezoidal with unimodal growth. It is clear that multiplying

$\rho'(q)$ by $q[k_1]_q$ preserves these properties.

Note that

$$\rho'(q) = [k_2]_q \left(1 + q[k_3]_q [k_4]_q \right) + q^{k_2+k_3} [k_4]_q.$$

In particular $\rho'(q)$ is built from $\rho''(q) = 1 + q[k_3]_q [k_4]_q$ by first multiplying by $[k_2]_q$ and then adding to the result the chain $q^{k_2+k_3} [k_4]_q$. Since $k_2 \geq 2$, the degree of the first entry of the plateau of $\rho'(q)$ is weakly larger than the degree of the first entry of the plateau of $\rho''(q)$. Multiplying $\rho'(q)$ by $[k_1]_q q$ can only shift the start of the plateau of $\rho'(q)$ further to the right, implying that the start of the plateau of $([k_1]_q q) \rho'(q)$ is to the right of the start of the plateau of $\rho''(q)$.

If the two plateaus in question overlap or are adjacent, then we are done. Otherwise, the lowest degree occurring in the plateau of $([k_1]_q q) \rho'(q)$ is strictly larger than $\max(k_3, k_4)$. In this case, the unimodal growth of the coefficients of $([k_1]_q q) \rho'(q)$ ensures that the addition of $\rho''(q)$ (whose consecutive coefficients are at most one apart) preserves the two properties in question. Hence, \mathbb{L}_w is unimodal in this case.

□

9.2 Rank Symmetry

Definition 9.8. Fix a word $w = w_1 w_2 \dots w_{n-1}$ of length $l(w) = n - 1$. Define the three words

$$w^T = w_1^* w_2^* \dots w_{n-1}^*,$$

$$w^\circ = w_{n-1} w_{n-2} \dots w_1,$$

and

$$\bar{w} = w_{n-1}^* w_{n-2}^* \cdots w_1^*.$$

We say that w is *symmetric* if $w^T = w$, and *self-conjugate* if $\bar{w} = w$. We say that G_w is *symmetric* if $\text{sh}(G_w)$ is symmetric, and *self-conjugate* if $\text{sh}(G_w)$ is self-conjugate.

Example 9.9. The word $w_1 = \text{sh}(G_{w_1})^* = aab$ from Example 7.5 is neither symmetric nor self-conjugate, while $w_2 = \text{sh}(G_{w_2})^* = aabb$ is self-conjugate and $w_3 = \text{sh}(G_{w_3})^* = baaab$ is symmetric. The word $\text{sh}(G_{w_1}) = w_1^* = baa$ is neither symmetric nor self-conjugate, while the words $\text{sh}(G_{w_2}) = w_2^* = baab$ and $\text{sh}(G_{w_3}) = w_3^* = aabaa$ are both symmetric.

Proposition 9.10. Fix the word w of length $l(w) = n - 1$. Recall the internal edges e_1, e_2, \dots, e_{n-1} of the snake graph G_w (see the discussion before Definition 3.25 above).

- (a) Suppose $l(w)$ is odd. Then the word $w = \text{sh}(G_w)^*$ is symmetric if and only if the word $w^* = \text{sh}(G_w)$ is symmetric.
- (b) If $l(w)$ is odd and w is symmetric, then G_w has 180° rotational symmetry about the midpoint of its middle internal edge, and the same is true for G_w^* .
- (c) Suppose $l(w)$ is even. Then the word $w = \text{sh}(G_w)^*$ is symmetric if and only if the word $w^* = \text{sh}(G_w)$ is self-conjugate, and $w = \text{sh}(G_w)^*$ is self-conjugate if and only if $w^* = \text{sh}(G_w)$ is symmetric.
- (d) If $l(w)$ is even and w is symmetric, then G_w is symmetric about the diagonal of its center tile $T_{\frac{n+1}{2}}$, and G_w^* has 180° rotational symmetry about the center of its middle tile $T_{\frac{n+1}{2}}$.
- (e) The snake graph G_w has 180° rotational symmetry if and only if C_{w^*} has 180° rotational symmetry. In this case, the graded poset \mathbb{L}_w is order-theoretically self-dual.

Proof. (a) If w is symmetric of odd length, then setting $m = \frac{l(w)+1}{2}$ we can write

$$w = w_1 w_2 \dots w_{m-1} w_m w_{m-1} \dots w_2 w_1.$$

If m is even, then taking the dual of w gives

$$w^* = w_1^* w_2 \dots w_{m-1}^* w_m w_{m-1}^* \dots w_2 w_1^*,$$

which is symmetric. Similarly, if m is odd then taking the dual gives

$$w^* = w_1^* w_2 \dots w_{m-1} w_m^* w_{m-1} \dots w_2 w_1^*,$$

which is also symmetric. Taking dual words now gives (a).

(b) Follows directly from (a).

(c) If $l(w)$ is even and symmetric, then for $m = \frac{l(w)}{2}$ we can write

$$w = w_1 w_2 \dots w_{m-1} w_m w_m w_{m-1} \dots w_2 w_1.$$

Suppose m is even. Then taking the dual gives

$$w^* = w_1^* w_2 \dots w_{m-1}^* w_m w_m^* w_{m-1} \dots w_2^* w_1,$$

which is self-conjugate. Similarly, if m is odd, then taking the dual of w gives

$$w_1^* w_2 \dots w_{m-1} w_m^* w_m w_{m-1}^* \dots w_2^* w_1,$$

which is again self-conjugate.

(d) Follows directly from (c).

(e) By construction, G_w has 180° symmetry if and only if C_w^* does. Let G_w° be G_w rotated by 180° . The result now follows from noting that the order-theoretic dual of \mathbb{L}_w is isomorphic to the poset of lattice paths on G_w° .

□

Corollary 9.11. *Consider the words w and w^* of length $n - 1$, the associated snake graphs G_w and G_w^* with n tiles, and the distributive lattices $D_w \cong \mathbb{P}_w \cong \mathbb{L}_{w^*}$ and $D_{w^*} \cong \mathbb{L}_w \cong \mathbb{P}_{w^*}$ of rank n .*

(a) *If $sh(G_w)$ is symmetric, then the poset \mathbb{L}_w is symmetric.*

(b) *If either $l(w)$ is odd and $sh(G_w)$ is symmetric, or $l(w)$ is even and $sh(G_w)$ is self-conjugate, then the poset \mathbb{P}_w is symmetric*

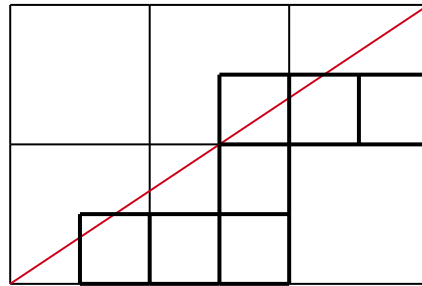
Proof. Follows directly from Proposition 9.10. □

Example 9.12. (a) The lattice path expansion on a zigzag snake graph with an even number of tiles is isomorphic to a Fibonacci cube of even order, and so is symmetric (this was shown in [27]). Trivially, the perfect matching expansion poset on this snake graph is symmetric, since it is a chain.

(b) Consider the snake graph G_w with the word $CF(w) = [a_1, a_2, \dots, a_k]$. Following [6], the *palindromification* of G_w is the snake graph G_{\leftrightarrow} with associated continued fraction $[a_n, a_{n-1}, \dots, a_2, a_1, a_2, \dots, a_{n-1}, a_n]$. Every palindromification G_{\leftrightarrow} has 180° symmetry about its center tile (see Theorem A in [6]). Let $\mathbb{L}_{\leftrightarrow}$ be the poset of lattice paths on G_{\leftrightarrow} . Then by Corollary 9.11, we know that $\mathbb{L}_{\leftrightarrow}$ are symmetric. Since $l(w)$ is even, the poset $\mathbb{P}_{\leftrightarrow}$ of perfect matchings on the palindromification is not symmetric.

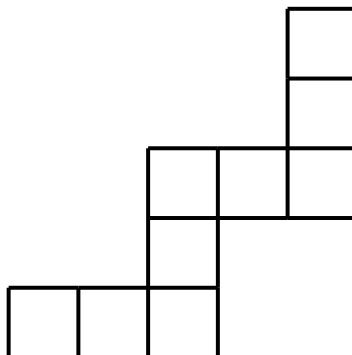
(c) A *Markov snake graph* is a snake graph which can be built from the Christoffel path in a p by q grid, where p and q are relatively prime positive integers (see [32], [6], and [33]). Figure 9.4 shows one example of a Markov snake graph. The number of perfect matchings on any Markov snake graph is equal to a Markov number. Every Markov snake graph is a palindromification (see [6]), so the conclusions in (b) hold here as well.

Figure 9.4: A Markov snake graph



(d) It is well-known that the infinite continued fraction expansion of $\sqrt{2}$ is equal to $[1, 2, 2, 2, \dots]$. Thus, we may write $1 + \sqrt{2} = [2, 2, 2, 2, \dots]$. The latter infinite fraction is called the *silver mean*. Consider any of the continued fractions obtained by truncating the continued fraction expansion of the silver mean after an odd number (larger than 1) of 2's. An example of a snake graph associated to such a continued fraction is shown below.

Figure 9.5: The snake graph with continued fraction $[2, 2, 2, 2, 2]$



By the Corollary 9.11, the perfect matching poset on the associated snake graph is symmetric, while the lattice path expansion poset on this snake graph is not symmetric.

Chapter 10

Expansion Posets as Groupoid Orbits

In this short chapter, we give an interpretation of the support of the cluster variable x_w as an orbit of a groupoid. This implies that the support of any two distinct cluster variables written with respect to the same initial seed are disjoint, so that in particular any x_w can be completely reconstructed from any one of its monomials.

Recall the definition of a groupoid, given as Definition 7.6 above. Consider the set of Laurent monomials from the extended cluster $(x_1, x_2, \dots, x_n, x_{n+1}, \dots, x_{2n+3})$. For each k with $1 \leq k \leq n$, define the element

$$\hat{y}_k = \frac{\prod_{i \rightarrow k} x_i}{\prod_{k \rightarrow j} x_j}. \quad (10.1)$$

(see [15]).

Define a groupoid \mathcal{F} whose objects are the Laurent monomials from the extended cluster above. There is a morphism $x_M \longrightarrow x_{M'}$ between two Laurent monomials x_M and $x_{M'}$ if $x_{M'} = \hat{y}x_M$ or $x_{M'} = \hat{y}^{-1}x_M$ for some \hat{y} , such that the reduced fraction $x_{M'}$ has the following properties:

- (1) No frozen variable appears in the denominator of $x_{M'}$.
- (2) No frozen variable which appears in the numerator of $x_{M'}$ is squared.

The rest of the morphisms in \mathcal{F} are compositions of such multiplications.

Theorem 10.1. *Consider the cluster variable x_w , and let $\text{Supp}(x_w)$ be the set of Laurent monomials in the Laurent expansion of x_w . Let $x_M \in \text{Supp}(x_w)$, and let $\mathcal{O}(x_M)$ be the connected component of \mathcal{F} containing x_M . Then*

$$\text{Supp}(x_w) = \mathcal{O}(x_M).$$

Proof. Let $x_{M'} \in \text{Supp}(x_w)$. If we represent both x_M and $x_{M'}$ as T -paths, then there is some sequence of T -path twists that takes x_M to $x_{M'}$. Notice that if two T -paths are related by a twist then there is a morphism between their respective weights. Indeed, T -path twists algebraically are multiplication by some \hat{y} as in (1), and furthermore a T -path has no red boundary edges nor does it use the same (blue) edge twice. Thus, there is a morphism $x_{M'} \rightarrow x_M$ and so $x_{M'} \in \text{Supp}(x_M)$. The reverse inclusion is similar. \square

Corollary 10.2. *Any cluster variable x_w is completely determined by any one of its monomials.*

Chapter 11

T -paths for Configurations of Flags

The work in this chapter is joint with Nicholas Ovenhouse.

In [9], a generalization of the decorated Teichmüller spaces was introduced, called higher Teichmüller spaces. These moduli spaces take as input in their construction a Lie group G and a marked surface S . It was shown in [9] that when $G = \mathrm{SL}_3$, the coordinate ring of this moduli spaces has a cluster structure.

Here we focus on the case when $G = \mathrm{SL}_3$ and S is a disc with marked points on the boundary. In this case, the moduli space reduces to the moduli space of configurations of affine flags.

In this final chapter, our first goal is to give a Laurent expansion formula which generalizes the T -path formula from Section 4.3, in the special case when the initial seed is constructed from a fan triangulation. Our second goal is to describe the poset structure of some of these Laurent expansions.

11.1 Decorated Teichmüller Spaces

Definition 11.1. Let Σ be a marked surface of genus g with b boundary components and m marked points located on boundary components, where each boundary component has at least one marked point. The *Teichmüller space* is the space of marked complete metrics on Σ having constant negative curvature -1 and a finite area, modulo the action of the connected component of the identity in the group of diffeomorphisms of Σ . Denote this space by $\mathcal{T}_{g,b}^m$.

Definition 11.2. Let Σ, g, b, m be as above. Let p be a marked point on the boundary of Σ . A *horocycle centered at p* is a circle orthogonal to any geodesic passing through p . Any horocycle centered at p can be parameterized by a positive real number called the *height* of the horocycle. The *decorated Teichmüller space* is denoted by $\widetilde{\mathcal{T}}_{g,b}^m$ and is defined as the total space of the trivial fiber bundle $\widetilde{\mathcal{T}}_{g,b}^m \rightarrow \mathcal{T}_{g,b}^m$ where the projection map is forgetting about horocycles. Each fiber is isomorphic to \mathbb{R}_+^m .

We now recall the construction of *Penner coordinates* on the decorated Teichmüller space. Let Δ be an ideal triangulation of Σ by geodesic arcs. Each edge e of the ideal triangulation has infinite hyperbolic length. However, we can define the *length* $l(e)$ of e to be the signed finite length of the segment between the two horocycles centered at the endpoints of e , where the sign of $l(e)$ is positive if the two horocycles don't intersect, and negative if they do.

Define $f(e) = \exp\left(\frac{l(e)}{2}\right)$. The functions $f(e)$ where e ranges over the edges in the triangulation Δ give a homeomorphism from the decorated Teichmüller space to $\mathbb{R}^{6g+3b+2m-6}$. The functions $f(e)$ are called *Penner coordinates*, or *lambda lengths*.

Any two Penner coordinates attached to the two arcs p and q involved in a flip of the underlying ideal triangulation are related by a *generalized Ptolemy relation*:

$$f(p)f(q) = f(a)f(c) + f(b)f(d),$$

where arcs a and c (respectively, b and d) are opposite one another in the unique quadrilateral with edges from Δ determined by the arcs p and q .

Definition 11.3. The *cluster algebra structure* on $\widetilde{\mathcal{T}}_{g,b}^m$, denoted $\mathcal{A}(\widetilde{\mathcal{T}}_{g,b}^m)$, is given by building a quiver, depending on Δ as before, but with nodes now labeled by Penner coordinates.

We have the following correspondences:

cluster variables in $\mathcal{A}(\widetilde{\mathcal{T}}_{g,b}^m) \longleftrightarrow$ Penner coordinates of arcs in Δ

seeds of $\mathcal{A}(\widetilde{\mathcal{T}}_{g,b}^m) \longleftrightarrow$ triangulations of Δ

seed mutations in $\mathcal{A}(\widetilde{\mathcal{T}}_{g,b}^m) \longleftrightarrow$ flips in Δ

11.2 Higher Teichmüller Spaces

We recall in this section a generalization of Teichmüller spaces introduced in [9].

Definition 11.4. Let G be a Lie group, and S a marked surface. The space of G -local systems on S is the character variety $\text{Hom}(\pi_1(S), G)/G$, where the quotient is by conjugation.

The moduli space \mathcal{M} defined in [9] parameterizes local systems on S with some additional structure, namely a choice of element in the quotient G/U for each marked point. Here, $U = [B, B]$ is the unipotent radical of a Borel subgroup $B \subset G$.

When $G = \text{SL}_n$, the quotient G/U parameterizes *affine flags*.

Definition 11.5. An *affine flag* in a vector space V is a saturated chain of subspaces

$$V_1 \subset V_2 \subset \cdots \subset V_{n-1} \subset V_n = \mathbb{R}^n,$$

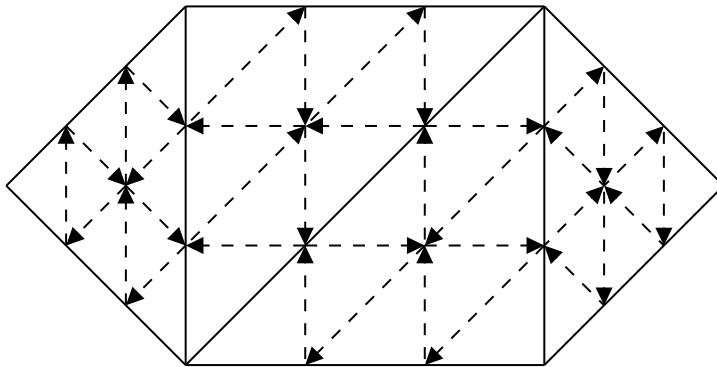
along with a choice of nonzero vector $v_i \in V_{i+1}/V_i$ in each successive quotient for $1 < i < n-1$.

When $G = \text{SL}_2$, the space \mathcal{M} parameterizes configurations of affine flags in \mathbb{R}^2 . Note that an affine flag in \mathbb{R}^2 is simply a choice of non-zero vector. The surface type cluster algebras we have considered in the previous chapters may be interpreted as rings of functions on \mathcal{M} .

Fix $G = \mathrm{SL}_3$ for the remainder of this chapter. In [9], it was shown that in this case the coordinate ring of \mathcal{M} has a cluster algebra structure. We now describe how to construct a seed for this cluster algebra.

As we have seen, when $G = \mathrm{SL}_2$ the nodes of the quiver associated to a triangulation are in one-to-one correspondence with the arcs (and boundary segments) of the triangulation, and the arrows of this quiver form clockwise 3-cycles inside the triangles of the triangulation. Instead, when $G = \mathrm{SL}_3$, each arc has two quiver nodes associated to it, and furthermore there is a vertex of the quiver for each triangle cut out by the triangulation. Now, each ideal triangle cut out by the triangulation has three 3-cycles contained within it, each having the internal face vertex in common. This quiver is called a *3-triangulation*.

Figure 11.1: A 3-triangulation



Flips of the triangulation are now governed not by a single quiver mutation, but by a sequence of four mutations. More precisely, to perform a flip of the triangulation at the diagonal δ_i , one must first mutate at both quiver vertices along the diagonal δ_i , and then subsequently mutate at the two vertices inside the triangles on either side of the diagonal δ_i .

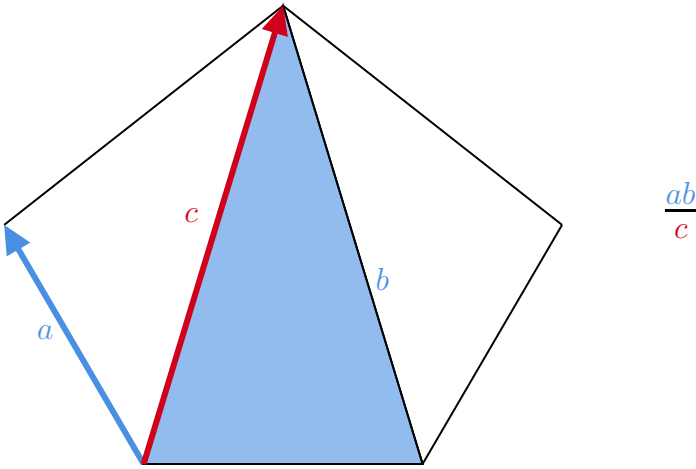
As for traditional surface cluster algebras, any cluster variable we are now considering may be expressed in terms of the initial cluster variables attached to this initial triangulation, via the flips and their governing mutation sequences just described.

11.3 Colored SL_3 Diagrams

Refer to the two initial cluster variables attached to any edge δ_i of the triangulation as *directed edges*, and call any cluster variable attached to the interior of a triangle a *face*. Each edge variable is visualized as a directed edge which is directed away from the endpoint of δ_i that it is closest to. Each face variable is visualized as a “filling” of the triangle containing it.

We visualize Laurent monomials in the initial cluster variables by representing each variable in such a monomial as just described, and superimposing each such representation onto the same diagram. Variables occurring in the numerator of a Laurent monomial will be pictured as blue, and those in the denominator will be pictured as red.

Figure 11.2: Visualization of a Laurent monomial



Any non-initial cluster variable may now be *resolved* with respect to the initial triangulation. That is, it can be expressed as a sum over products of directed edges and faces from the initial triangulation. Figure 11.3 shows the result of resolving a non-initial face in a triangulated square.

Figure 11.3: Face resolution

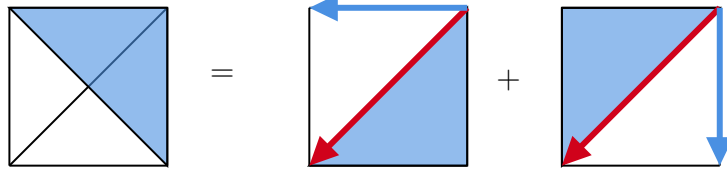
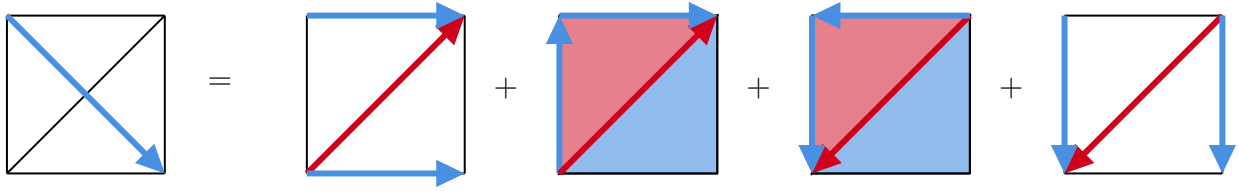


Figure 11.4 shows the result of resolving a non-initial directed edge in a triangulated square.

Figure 11.4: Edge resolution



Definition 11.6. Fix a triangulation Δ of the polygon Σ . A *colored SL_3 diagram* is a multiset of directed edges and triangular faces from Δ drawn superimposed on the same polygon, where each element is colored either blue or red.

By the above discussion, colored SL_3 diagrams are in bijection with the set of Laurent monomials built from the initial cluster variables attached to the triangulation Δ . The *weight* of the SL_3 diagram π is the associated Laurent monomial x_π .

11.4 Crossings in Colored SL_3 Diagrams

In this section, we say what it means for two colored SL_3 diagrams to be “crossing”. From now on, we restrict to fan triangulations Δ (see Definition 3.14).

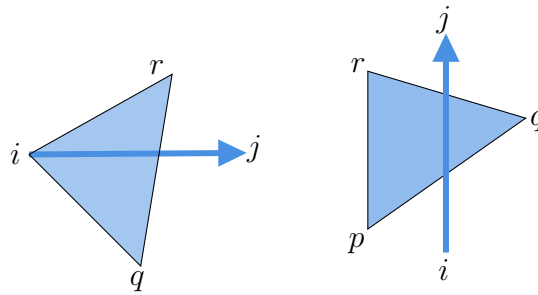
Definition 11.7. Two directed arcs $i \rightarrow j$ and $k \rightarrow l$ are said to be *crossing* if the underlying directed arcs are crossing in the usual sense.

Definition 11.8. A directed arc $i \rightarrow j$ and a face pqr are said to be *crossing* if:

- (1) $i = p$ and $q < j < r$ cyclically, i.e., $i \rightarrow j$ begins at one of the vertices of the triangle pqr , and has nontrivial intersection with the interior of pqr , or
- (2) $p < i < q < r$ cyclically, i.e., the arc $i \rightarrow j$ begins and ends outside pqr , and intersects two sides of pqr .

See the next figure for an illustration of (1) and (2) in Definition 11.8.

Figure 11.5: A directed edge and a face which cross



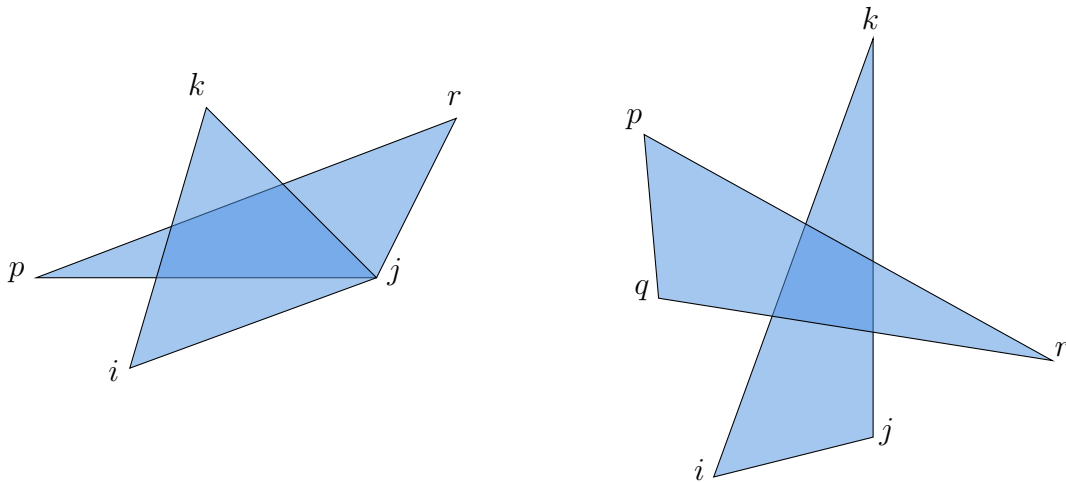
Remark 11.9. In (1) above, the directed arc $j \rightarrow i$ does *not* cross the face pqr . In (2), the orientation of the arc is irrelevant.

Definition 11.10. Two faces ijk and pqr are considered to be *crossing* if

- (1) $q = j$ and $i < j = q < r < k < p$ cyclically, or
- (2) $i < j < r < k < q < p$ cyclically.

See the next figure for an illustration of (1) and (2) in Definition 11.10.

Figure 11.6: Two crossing faces



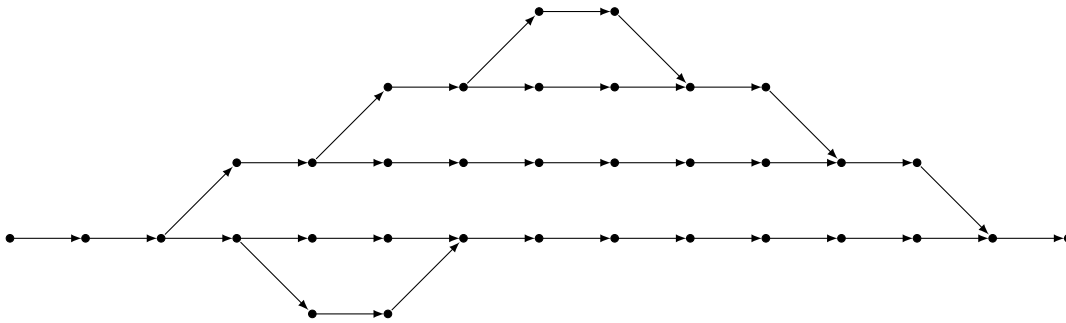
11.5 Fork-Join Networks

It is often convenient to model a simple process, algorithm, or computer program by a directed graph which encodes precedence. That is, the vertices are the states, and the edges are directed so that $i \rightarrow j$ means that i must happen before j . In this way, a directed path $i_1 \rightarrow i_2 \rightarrow \dots \rightarrow i_n$ models an algorithm which is totally sequential (the steps have a definite order).

In an algorithm which utilizes parallelism, such as multithreading, the main procedure may *fork*, creating a *child process*. After this, the main procedure and the child process may execute in parallel. It may be necessary for the parent and child to *join* at some point before continuing. This means that the parent and child must each finish their concurrent tasks before the main algorithm carries on in a sequential manner.

The next figure shows an example of a general fork-join network.

Figure 11.7: A fork-join network

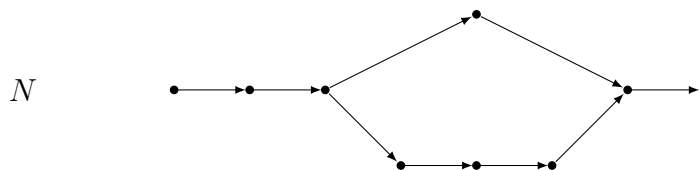


We will only consider processes with the following two properties:

- (A1) any fork must later be accompanied by a join, and
- (A2) there are no nested forks.

From now on, whenever we say “fork-join network” we will mean a network satisfying these two restrictions.

Figure 11.8: A fork-join network satisfying conditions (A1) and (A2)



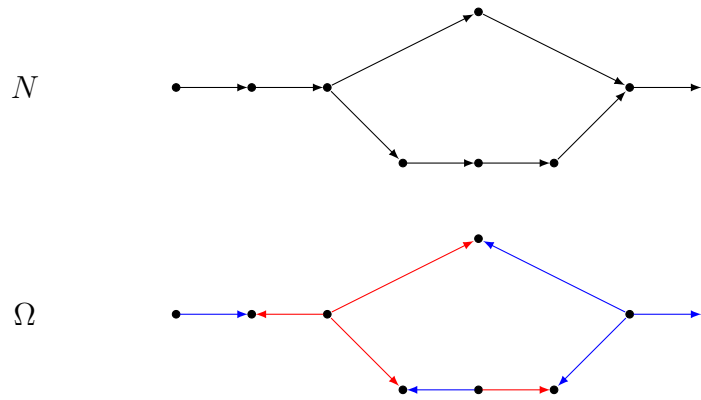
Definition 11.11. An *alternating fork-join network* is a directed graph Ω with the same underlying undirected graph as some fork-join network N such that

- (1) For any directed path through N from beginning to end, the odd-numbered edges of Ω are oriented the same as the corresponding edge in N , and the even-numbered edges are oriented opposite.
- (2) For any fork in N , the edge going into the fork must be inverted in Ω .
- (3) For any join in N , the edge leaving after the join must *not* be inverted in Ω .

We color each directed edge of an alternating fork-join network blue or red, according to the following rules.

- (1) The first arrow is colored blue.
- (2) Away from forks and joins, colors alternate along paths.
- (3) At a fork or join, the three edges incident that vertex are all colored the same color.

Figure 11.9: Construction of an alternating fork-join network Ω



Let Ω_1 and Ω_2 be two directed graphs. A *homomorphism of directed graphs* $g : \Omega_1 \rightarrow \Omega_2$ is a mapping of vertex sets such that if $i \rightarrow j$ in Ω_1 , then $g(i) \rightarrow g(j)$ is an edge of Ω_2 .

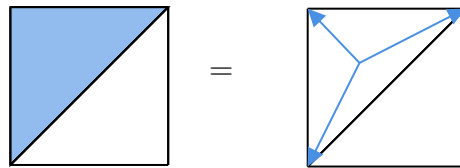
Definition 11.12. A homomorphism of directed graphs $g : \Omega_1 \rightarrow \Omega_2$ is called an *immersion* if for any vertex $v \in \Omega_1$, every vertex incident to v maps to a distinct vertex under g .

Definition 11.13. Let Ω_1 be an alternating fork-join network, and Ω_2 any directed graph. Suppose that $g : \Omega_1 \rightarrow \Omega_2$ is an immersion. The *image* of g is the associated multiset of edges in Ω_2 . That is, if $i \rightarrow j$ is an edge in Ω_1 , then $g(i) \rightarrow g(j)$ is an edge in Ω_2 , and if more than one edge from Ω_1 maps to $g(i) \rightarrow g(j)$, then we count the edge $g(i) \rightarrow g(j)$ with multiplicity equal to the cardinality of its preimage.

11.6 Generalized T -paths

We now generalize to our current setup the T -paths from Section 4.3. To this end, we picture each face variable as a *tripod*, as shown in the next figure. Each tripod resembles a web diagram from [10] and [11].

Figure 11.10: Faces as webs



Given the triangulation Δ , define the directed graph Ω_Δ as follows. There is one vertex of Ω_Δ for each vertex of Δ , and one vertex per triangle cut out by Δ . For each edge in Δ (including boundary segments) connecting vertices i and j , there is a pair of directed edges $i \rightarrow j$ and $j \rightarrow i$. For each triangle ijk cut out by Δ , there is a tripod consisting of three edges directed from the center vertex of the triangle to the three vertices i, j , and k .

Note that if $g : \Omega \rightarrow \Omega_\Delta$ is an immersion of a fork-join network, then the image is by definition a colored SL_3 diagram.

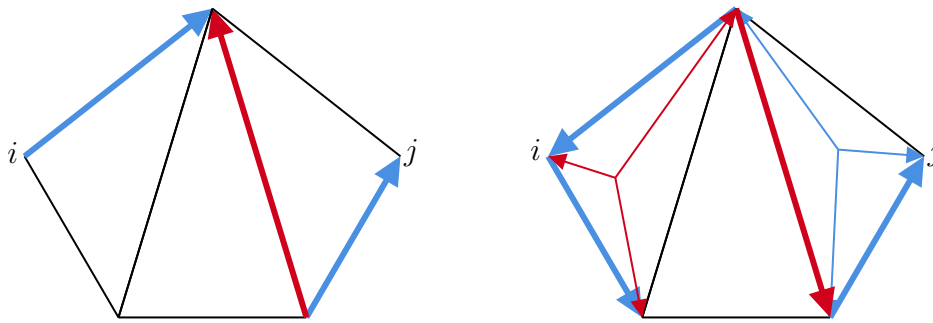
Definition 11.14. Suppose Ω is an alternating fork-join network, and $\Omega \rightarrow \Omega_\Delta$ is an immersion, which sends the source of Ω to i and the terminal vertex of Ω to j . We call the image of this immersion a T -path of edge type from i to j if:

- (T1) the image of any path through Ω does not use any edge of Ω_Δ more than once
- (T2) there are an odd number of elements in the diagram
- (T3) the red elements cross the directed arc $i \rightarrow j$
- (T4) once a path crosses an edge in Δ , it never returns to the original half of the polygon

The set of edge-type T -paths from i to j is denoted by \mathbb{T}_{ij} .

Figure 11.11 shows two edge-type T -paths. Note that the T -path pictured on the right is an immersion of the alternating fork-join network Ω pictured in Figure 11.9.

Figure 11.11: Two edge-type T -paths



Remark 11.15. For any T -path defined in Section 4.3, there is a corresponding SL_3 edge-type T -path obtained by orienting edges (for instance, see the diagram on the left in Figure 11.11).

Let γ be a face which is not a triangle from the triangulation Δ . Since we are assuming that Δ is a fan triangulation, there is at least one internal edge in Δ which terminates at one of the vertices of γ . We call any such edge a *splitting edge*. The vertex that is shared by a splitting edge and the face γ is called the *near vertex*, and the other endpoint of this splitting edge is called the *far vertex*.

We distinguish between two types of maximal (i.e., not contained in any subtriangulation) faces in a fan triangulation. There is the unique *fan face*, which has every internal diagonal as a splitting edge; and there are n *split faces*, which have precisely one splitting edge.

Definition 11.16. Consider the face ijk . A T -path of face type (with vertices i, j, k) is a triple of immersed alternating fork-join networks, terminating at i, j , and k , respectively, and with common source a tripod vertex within a triangle of Δ , such that

(F1) any of the three branches satisfies (T1), (T2), and (T4).

(F2) their red elements cross the triangle ijk .

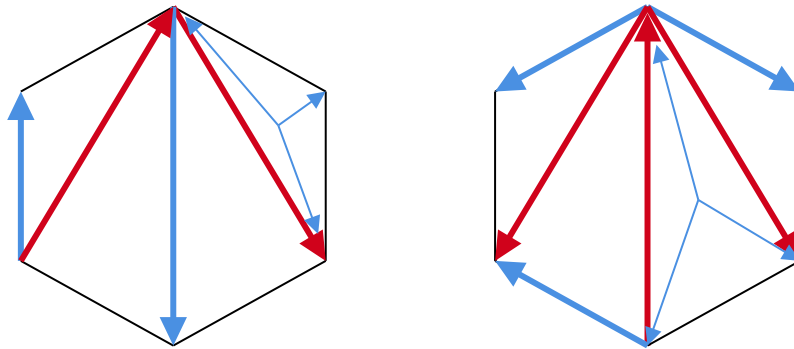
(F3) if one of the three paths arrives at i , j , or k using a forward blue edge, then that path must end

(F4) when a branch crosses any splitting edge, it must cross either at the far end after using a blue edge or at the near end after using a red edge.

The set of face-type T -paths with vertices i , j , and k is denoted by \mathbb{T}_{ijk} .

See the next figure for two examples of face-type T -paths.

Figure 11.12: Two face-type T -paths



11.7 The Recursion Lemmas

In this section, we prove two lemmas which allow us to write any set of T -paths with respect to a fan triangulation in terms of shorter T -paths. These lemmas moreover show that the two resolution rules given in Figure 11.3 and Figure 11.4 hold on the level of T -paths, as well. The first lemma concerns edge-type variables, and the second concerns face-type variables.

First, we show that the resolution of any cluster variable in a fan triangulation comes from immersing an alternating fork-join network, i.e., that (A1) and (A2) are satisfied for the preimage of any T -path in a fan triangulation.

Lemma 11.17. *Let γ be a directed edge or a face in a fan triangulation. If γ is a directed edge, then every term in the resolution of γ is the image of an alternating fork-join network. If γ is a face, then every term in the resolution of γ is the image of a triple of alternating fork-join networks.*

Proof. We proceed by induction on n , the number of internal diagonals in the triangulation. If $n = 1$ then examining the resolution rules in Figures 11.3 and 11.4 shows that the result is true in this case. So, suppose $n > 1$.

First consider the case when $\gamma = i \rightarrow j$ is the longest arc. Resolve γ with respect to the first edge from the triangulation that it crosses. This creates four diagrams, one of which having all its (directed edge) elements contained in the original triangulation. Of the remaining three diagrams, one will not contain any face variables. The first two colored edges of the latter diagram are contained within the triangulation, and the other edge is a blue edge contained in a subfan with one less triangle. If we resolve this blue edge, ignoring the first two edges, any child of this diagram will come from a fork-join network satisfying conditions (A1) and (A2). One can check that adding back to the leaves of this resolution the first two edges preserves the properties (A1) or (A2). The other two terms from the resolution each have five elements in their diagrams. In either case, the only element not in the original triangulation is a blue face; in fact, it is the same blue face in both diagrams. Now the result follows by an argument similar to the one used for the previous case.

Suppose γ is the fan face ijk , where i is the fan vertex. Resolve this face over the first diagonal that its non-boundary edge crosses, where we consider this edge oriented from k to j . Then the

only element in each child diagram which is not contained in the triangulation is a blue fan face, contained in a subfan with one less internal diagonal. Now the result follows much as before. Namely, we first resolve the diagram which only contains the non-initial face just mentioned. By induction, properties (A1) and (A2) are satisfied for every child of this diagram. Now one can check that adding back in the elements from the resolution that aren't this blue face gives a set of T -paths that satisfy (A1) and (A2).

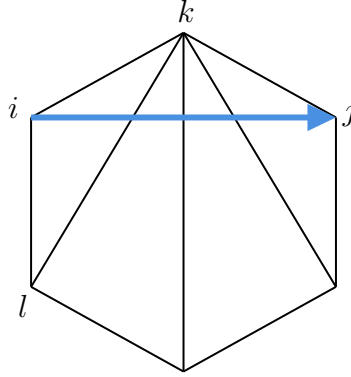
Suppose instead that γ is one of the n split faces ijk . Let i be the near vertex of the splitting edge, and let l be the other (fan) vertex. Then resolving with respect to the splitting edge gives two child diagrams whose non-initial elements are contained within some smaller fan triangulation. Each child diagram contains at most two elements which are not contained in the initial triangulation; one of these elements is the longest edge in a subfan (or, it is an edge in the triangulation), and the other is a fan face inside a subfan (or, it is a face of the triangulation). The result now follows by an argument similar to the one used in the previous two cases. \square

Remark 11.18. Each of the three remarks below can be seen by induction and the resolution rules in Figure 11.3 and Figure 11.4.

- (1) Any diagram obtained from resolving longest edge in a fan triangulation either contains no faces, or contains at most one pair of faces, one red and one blue.
- (2) Any diagram obtained from resolving the fan face in a fan triangulation contains precisely one blue face, which is where the T -path begins.
- (3) Any diagram obtained from resolving a split face in a fan triangulation contains either one blue face (the face where the T -path begins), or this blue face along with a pair of faces, one red and one blue.

Let $i \rightarrow j$ be the longest directed edge not in the triangulation Δ . Suppose the first edge that $i \rightarrow j$ crosses has endpoints labeled l and k , as shown in the next figure.

Figure 11.13: Set-up for Lemma 11.19



Lemma 11.19. Fix the fan triangulation Δ and consider the “longest” directed edge $\gamma = i \rightarrow j$ with l and k as in Figure 11.13.

- (a) There is a bijection between the set \mathbb{T}_{lj} and the subset of \mathbb{T}_{ij} consisting of the T -paths which begin with the edge ik and do not use the face ikl . In terms of monomials, this bijection is realized as multiplication by $\frac{x_{ik}}{x_{lk}}$.
- (b) There is a bijection between the set \mathbb{T}_{kj} and the subset of \mathbb{T}_{ij} consisting of the T -paths which begin with the edge il and do not use the face ikl . In terms of monomials, this bijection is realized as multiplication by $\frac{x_{il}}{x_{lk}}$.
- (c) There is a bijection between $\mathbb{T}_{jkl} \sqcup \mathbb{T}_{jkl}$ and the subset of \mathbb{T}_{ij} which includes the face ikl .

Proof. (a) Indeed, a path in \mathbb{T}_{lj} either begins with $l \rightarrow k$ or it does not. If it does not, then prepending with $i \rightarrow k$ and $(l \rightarrow k)^{-1}$ gives a T -path $i \rightarrow j$ which does not use the face ikl . If, on the other hand, it *does* begin with $l \rightarrow k$, then removing this first edge and replacing it with $i \rightarrow k$ gives a path $i \rightarrow j$.

The inverse of this map is described as follows. If a T -path from i to j begins with $i \rightarrow k$ and does not include the face ikl , then its second edge is either contained in the smaller polygon on the other side of edge kl , or its second edge is $(l \rightarrow k)^{-1}$ and its third edge is contained in the smaller polygon. In the first case, we replace the first edge $i \rightarrow k$ with $l \rightarrow k$ to obtain a T -path from k to j . In the second case, we remove the first two edges $(i \rightarrow k)(l \rightarrow k)^{-1}$, and what remains is a T -path from k to j .

(b) Similar to (a).

(c) If a T -path uses face ikl , then it begins either $(i \rightarrow k)(l \rightarrow k)^{-1}(l \rightarrow i)(ikl)^{-1}$, or $(i \rightarrow l)(k \rightarrow l)^{-1}(k \rightarrow i)(ikl)^{-1}$. The remainder of the T -path is a face-path in \mathbb{T}_{jkl} . Conversely, any face T -path between j , k , and l can be extended to two T -paths from i to j which use face ikl , corresponding to the two ways to go around the triangle. \square

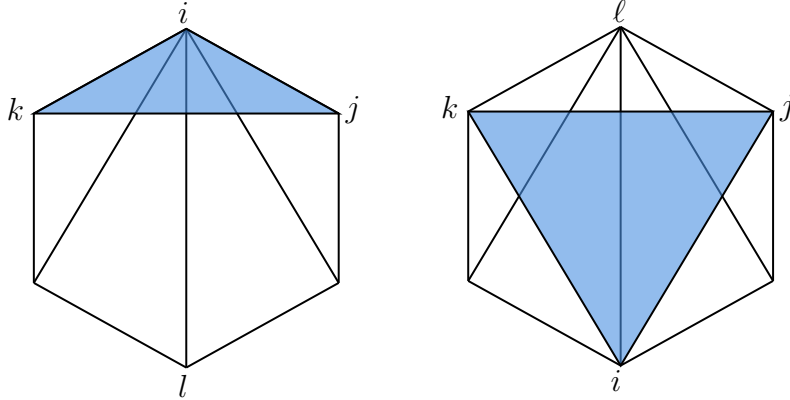
We now give the analogous lemma for face variables. Consider the face ijk which is not cut out by the triangulation Δ . Since we are only considering type A triangulations, there exists an internal diagonal from Δ which has as one of its endpoints one of the vertices i , j , or k . There are two cases; either ijk is the fan face, or one of the n split faces. We now fix notation in each case.

Suppose ijk is the fan face, where i is the fan vertex. In this case, every internal diagonal splits this face. Fix one of these splitting edges. This edge will have i as one of its endpoints; call the other endpoint l .

If instead ijk is split, then there is a unique splitting edge; call this internal diagonal il , where i is the near vertex and l is the far (fan) vertex.

The setup in either case is pictured in Figure 11.14 below.

Figure 11.14: Set-up for Lemma 11.20



Lemma 11.20. *Consider the face ijk , which is either the fan face or a split face. If ijk is the fan face, let i, j, k, l be as in the left of Figure 11.14; if ijk is a split face, let i, j, k, l be as in the right of Figure 11.14. Then there is a bijection*

$$\mathbb{T}_{ijk} \cong (\mathbb{T}_{ikl} \times \mathbb{T}_{ij}) \cup (\mathbb{T}_{ijl} \times \mathbb{T}_{ik})$$

In terms of monomials, this bijection is realized as multiplication by x_{il} .

Proof. Define a map $(\mathbb{T}_{ikl} \times \mathbb{T}_{ij}) \cup (\mathbb{T}_{ijl} \times \mathbb{T}_{ik}) \rightarrow \mathbb{T}_{ijk}$ by adding the red edge $i \rightarrow l$. More specifically, given a pair (φ, π) , where $\varphi \in \mathbb{T}_{ikl}$ and $\pi \in \mathbb{T}_{ij}$, adding the red edge $i \rightarrow l$ connects the branch of φ ending at l with π , creating a face-path in \mathbb{T}_{ijk} . Similarly, if we start with a pair (θ, κ) , with $\theta \in \mathbb{T}_{ijl}$ and $\kappa \in \mathbb{T}_{ik}$, then adding the red edge $i \rightarrow l$ will connect the branch of θ ending at l with κ , creating a face-path in \mathbb{T}_{ijk} .

We want to show that this map is a bijection. If this is true, then its inverse must be given by adding the blue edge $i \rightarrow l$. Starting with something in $(\mathbb{T}_{ikl} \times \mathbb{T}_{ij}) \cup (\mathbb{T}_{ijl} \times \mathbb{T}_{ik})$, adding the red edge $i \rightarrow l$ and then adding the blue edge $i \rightarrow l$ will cancel and the composition is the identity. All that needs to be checked is that for any face-path in \mathbb{T}_{ijk} , adding the blue edge $i \rightarrow l$

gives a colored diagram which can be interpreted as the superposition of a face path in \mathbb{T}_{ikl} with an edge-path in \mathbb{T}_{ij} (or a face in \mathbb{T}_{ijl} and an edge in \mathbb{T}_{ik}).

The edge il cuts the polygon in half, and any face-type T -path for triangle ijk must “begin” with a triangle of Δ on one of the two halves. Two of the three vertices ijk will already be on this half (either i, k or i, j), and the third will be on the other half. Let’s say we are in the first case, where the triangle is on the left half, containing k (the other case will be similar).

Since the three branches of the T -path start in the left half of the polygon, the two branches going to i and k will not leave the left half (by property (T4)). The third branch, which ends at j , must cross to the right half along the way. There are two cases we must consider: when this path crosses diagonal il and moves into the right half, it must do so either through vertex i or l .

ijk is the fan face: Part (b) of Remark 11.18 implies that the branch that we are considering now cannot cross over into the right half of the polygon through vertex l . Indeed, if this branch were to cross over at l , it would need to do so after using a blue edge by (F4) above. By the remark, the only possibility for the next edge used in the path is a red edge in the triangulation (since no red faces are produced in the resolution of a fan face). But, since we are in a fan triangulation, we are forced to next use the red edge $l \rightarrow i$. This is a contradiction, since we will now leave the left half of the polygon through the fan vertex i .

Therefore we must cross over to the right side through the fan vertex i . By (F4), the branch in question arrives at vertex i via a red edge.

There are two possibilities to consider; either the last edge of the path before it arrives at i is the red edge $i \rightarrow l$, or it is some other red edge which is not the splitting edge we have arbitrarily chosen. In the latter case, adding the blue edge $i \rightarrow l$ makes the beginning part (the part ending at l after the added blue edge) a face-type path in \mathbb{T}_{ikl} . The remainder of the path is an edge-path in \mathbb{T}_{ij} . Suppose instead that the last edge of the path before it arrives at i is the red edge $i \rightarrow l$

(which would again be immediately preceded by a blue edge ending at l). Then our suggested map, which adds the blue edge $i \rightarrow l$, will cancel this last edge. This beginning part of the path is a face-path in \mathbb{T}_{ikl} , and the part of the path after the cancelled edge is an edge-path in \mathbb{T}_{ij} . Thus, the map indeed gives an element of $\mathbb{T}_{ikl} \times \mathbb{T}_{ij}$. Thus, the claim holds in this case.

ijk is a split face: Consider the case where ijk is split, and when we leave the left half at vertex i . Condition (F4) above guarantees that this branch of the path must arrive at i with a red edge. It is easy to see using the resolution rule in Figure 11.3 and part (3) in Remark 11.18, that the red edge used to arrive at vertex i must be an edge in the triangulation (as opposed to an edge in a fork). Since we are in a fan triangulation, the only possibility is that the last edge of the path before it arrives at i is the red edge $i \rightarrow l$ (which would be immediately preceded by a blue edge ending at l). As in the case of the fan face, superimposing the blue edge $i \rightarrow j$ cancels this red edge, and the claim again follows much as before.

Now suppose that the path crosses into the right half at vertex l . In this case, the path cannot possibly use the red edge $i \rightarrow l$ (or else the path would cross over at i instead). So adding the blue edge $i \rightarrow l$ does not cancel anything, and the blue edge will remain. By (F4), the path arrives at l using a blue edge, and continues after l with a red edge. Thus, the first part of the path (ending at l) is a face-path in \mathbb{T}_{ikl} , and after adding the blue edge $i \rightarrow l$, the remaining part of the path becomes an edge-path in \mathbb{T}_{ij} . Hence the claim holds for split faces as well.

This completes the proof. □

11.8 Expansion Formulas in Fan Triangulations

In this section, we give an expansion formula valid for any arc or face variable in a fan triangulation.

Theorem 11.21. Consider the fan triangulation Δ .

- (a) Let $\gamma: i \rightarrow j$ be a directed edge not in the initial triangulation, with associated cluster variable x_γ . The Laurent expansion of x_γ in the initial cluster is

$$x_\gamma = \sum_{\pi \in \mathbb{T}_{ij}} x_\pi$$

- (b) Let ψ be a face (with vertices i, j, k) not in Δ , with variable x_ψ . The Laurent expansion of x_ψ is

$$x_\psi = \sum_{\varphi \in \mathbb{T}_{ijk}} x_\varphi$$

Proof. (a) We are in the situation pictured in Figure 11.13. Consider the quadrilateral with ij and kl as its two diagonals. By construction, triangle ikl is in Δ , but triangle jkl may not be. The sequence of 4 mutations which achieves a flip of the diagonal of this quadrilateral gives

$$x_\gamma = \frac{x_{ik}}{x_{lk}} x_{lj} + \frac{x_{ik} x_{li}}{x_{ikl} x_{lk}} x_{jkl} + \frac{x_{il}}{x_{kl}} x_{kj} + \frac{x_{il} x_{ki}}{x_{ikl} x_{kl}} x_{jkl}$$

The edges $l \rightarrow j$ and $k \rightarrow j$, and the triangle jkl , are within a smaller polygon, and so we may use induction:

$$x_\gamma = \frac{x_{ik}}{x_{lk}} \sum_{\pi \in \mathbb{T}_{lj}} x_\pi + \frac{x_{il}}{x_{kl}} \sum_{\pi \in \mathbb{T}_{kj}} x_\pi + \left(\frac{x_{il} x_{ki}}{x_{ikl} x_{kl}} + \frac{x_{ik} x_{li}}{x_{ikl} x_{lk}} \right) \sum_{\pi \in \mathbb{T}_{jkl}} x_\pi$$

The result now follows from Lemma 11.19.

- (b) The face $\psi = ijk$ is either the fan face shown on the left in Figure 11.14, or a split face, as shown on the right of Figure 11.14.

In either case, the flip mutation sequence gives

$$x_\psi = \frac{x_{ij}}{x_{il}}x_{ikl} + \frac{x_{ik}}{x_{il}}x_{ijl}$$

In the first term, triangle ikl and edge $i \rightarrow j$ are within smaller polygons. In the second term, triangle ijl and edge $i \rightarrow k$ are within smaller polygons. So we may use induction:

$$\begin{aligned} x_\psi &= \frac{1}{x_{il}} (x_{ij}x_{ikl} + x_{ik}x_{ijl}) \\ &= \frac{1}{x_{il}} \left(\sum_{\substack{\pi \in \mathbb{T}_{ij} \\ \varphi \in \mathbb{T}_{ikl}}} x_\pi x_\varphi + \sum_{\substack{\kappa \in \mathbb{T}_{ik} \\ \theta \in \mathbb{T}_{ijl}}} x_\kappa x_\theta \right) \end{aligned}$$

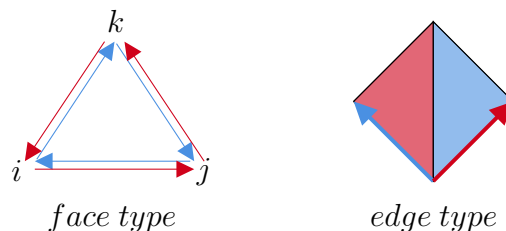
The result now follows from Lemma 11.20.

□

11.9 Some Expansion Posets

In this final section, we describe the poset structure on the Laurent monomials in the expansion of the fan face, and for the “longest” edge, in a fan triangulation. Covering relations are again multiplication by the \hat{y} variables defined in [15]. The corresponding colored SL_3 diagrams are shown below.

Figure 11.15: Covering relations



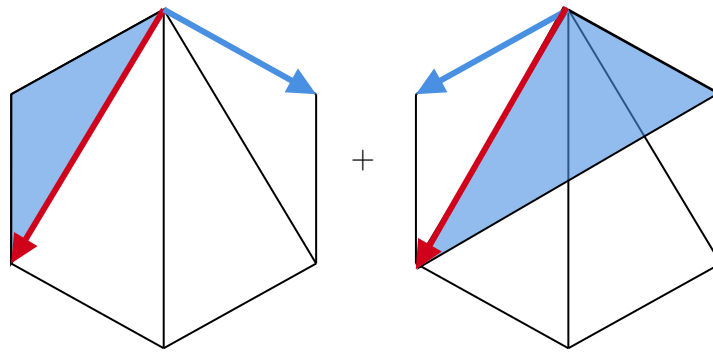
Suppose the triangulation Δ has n internal diagonals.

Proposition 11.22. *Consider the fan face γ . Then the poset \mathbb{T}_γ is isomorphic to a chain with $n + 1$ vertices.*

Proof. We induct on the number n of internal diagonals. By the resolution rule given in Figure 11.3 the result is true for $n = 1$. So suppose $n > 1$. Label the vertices of the face γ by i, j , and k , where k is the fan vertex of Δ . Let kl be the first internal diagonal of Δ that the directed edge $i \rightarrow j$ crosses.

Resolve γ with respect to the arc il to obtain two diagrams (see Figure 11.16 for an illustration of the two resulting diagrams for the fan face in a hexagon).

Figure 11.16: The first step in the resolution of the fan face in a hexagon

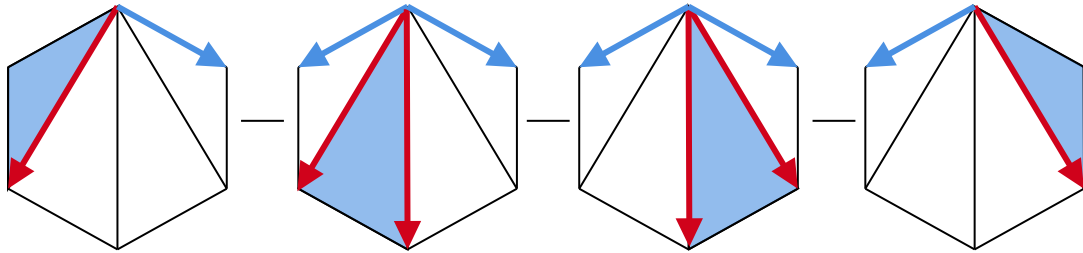


Note that one of these diagrams has all of its elements contained in the triangulation Δ . Call this diagram D . All of the elements in the other diagram are part of the fan triangulation, except one blue face, which is contained in a subfan triangulation with $n - 1$ internal diagonals.

Resolve the latter diagram with respect to the arc whose non-fan endpoint is “closest” to l . This produces two terms, with one of these terms having every element contained in the triangulation. This latter term is related to D by the first covering relation shown in Figure 11.15. Now the result follows by induction. □

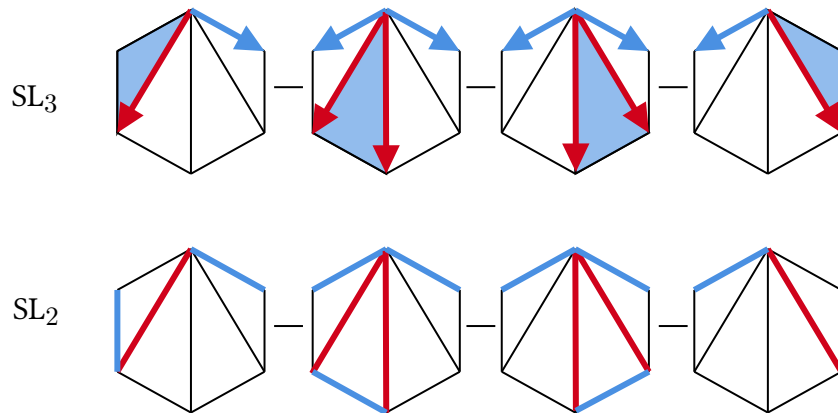
Example 11.23. Figure 11.17 shows the expansion poset of the fan face in a hexagon. The minimal element is the leftmost element shown, and the maximal element is the rightmost element shown.

Figure 11.17: Expansion poset of a fan face



Remark 11.24. There is a bijection between the terms in the expansion poset of a fan face, and the terms in the “ SL_2 ” T -path poset obtained from expanding the longest (undirected) edge in the same triangulation. Namely, given a term in the fan face poset, deleting the unique blue face and replacing it with the unique blue boundary edge boarding the deleted face, which is not adjacent to the fan vertex, gives the bijection. An example of this is indicated below.

Figure 11.18: The bijection between a fan face poset and the corresponding SL_2 T -path poset



Finally, we consider the longest edge in a fan triangulation Δ . Consider the lattice path L in \mathbb{Z}^2 which starts at the origin and has associated word $(ab^2)^n = ab^2ab^2 \dots$. Let L_γ be the set of points in \mathbb{Z}^2 that are on or below L and weakly above the horizontal axis of \mathbb{Z}^2 . Make L_γ

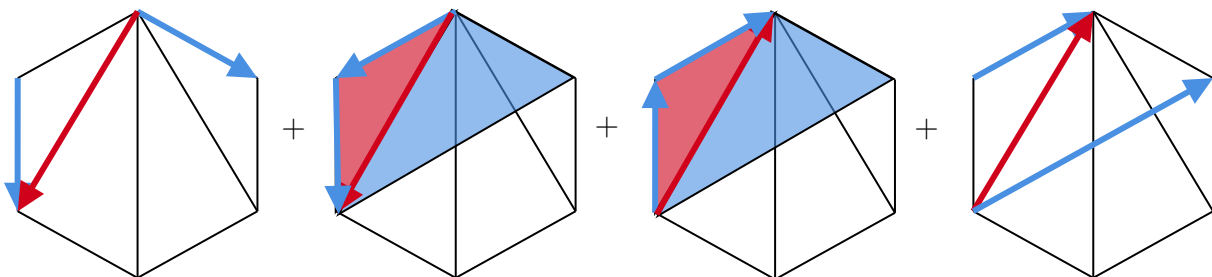
into (the Hasse diagram of) a poset by declaring a node (x_2, y_2) covers another (x_1, y_1) iff either $x_2 = x_1 + 1$ or $y_2 = y_1 + 1$ (but not both).

Proposition 11.25. *Let $\gamma = i \rightarrow j$ be the longest edge in a fan triangulation, and let x_γ be the associated cluster variable.*

- (a) *The Laurent expansion of x_γ contains $(n + 1)^2$ terms.*
- (b) *The minimal element is the T -path consisting of 3 edges; it first goes along the boundary away from the fan vertex, then goes along the diagonal closest to i , and then goes along the boundary to j .*
- (c) *The maximal element is the T -path consisting of 3 edges; it first goes to the fan vertex, then goes along the diagonal furthest from i , and then goes along the boundary edge to j .*
- (d) *The poset \mathbb{T}_γ is isomorphic to L_γ .*

Proof. We induct on n . Parts (a)-(d) are true for the base case by the resolution rule given in Figure 11.4, so suppose $n > 1$. Resolve the arc γ over the first diagonal it crosses to obtain four diagrams (these diagrams are shown below for the longest edge in a hexagon).

Figure 11.19: The first step in the resolution of the longest edge in a hexagon



One of these terms will consist of three directed edges that are contained within the triangulation; this is the minimal element. Call this minimal element M .

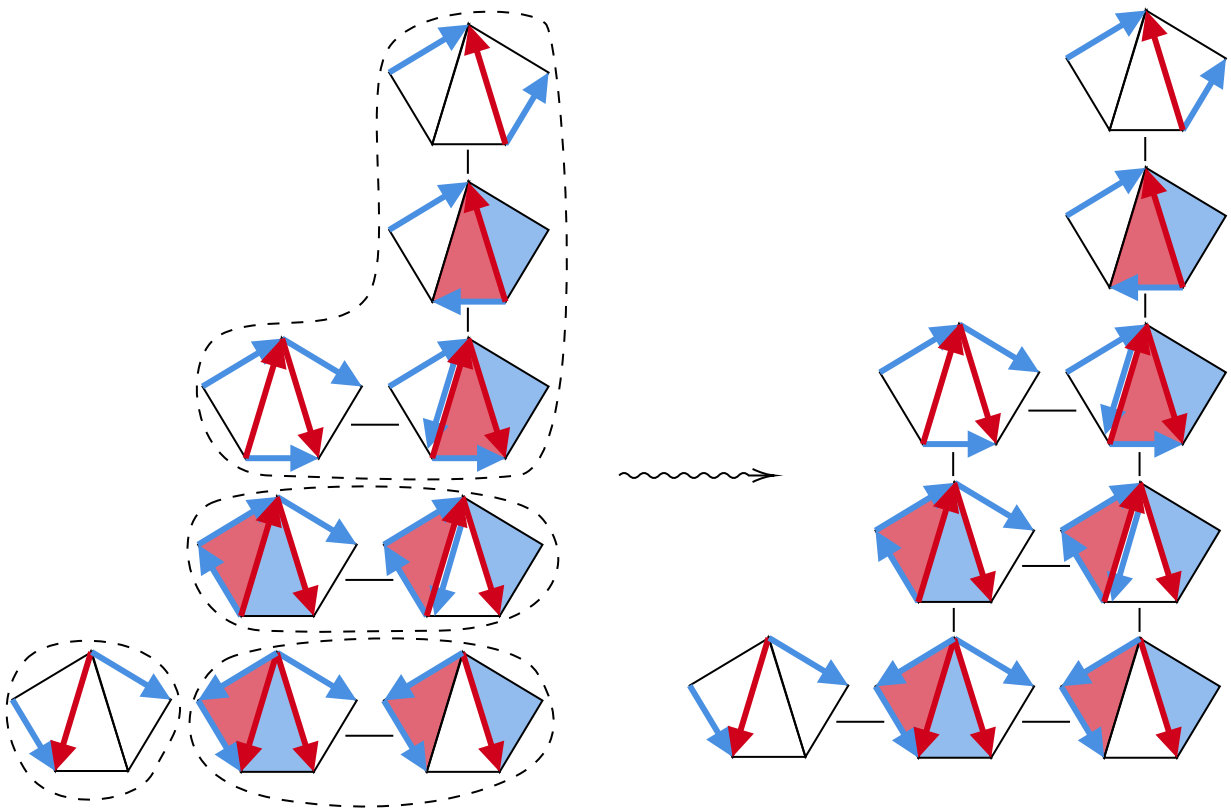
Two diagrams in the resolution consist of five terms. Both of these diagrams consist of a cycle around the first triangle, a red face inside the first triangle, and a blue face not contained in the triangulation. The only difference between these two diagrams is whether the initial 3-cycle around the first triangle goes clockwise or counterclockwise. Call the term with the counterclockwise cycle F_1 , and call the other F_2 .

As we have seen, each of these two diagrams expands into a chain poset with n terms. The terms from each of these posets are pairwise related by the face covering relation in the first triangle. Moreover, one can check that the minimal term in F_1 is connected to the minimal element M by the edge covering relation about the first internal diagonal. Gluing together M and the elements from F_1 and F_2 gives a poset. Call this poset P_1 . Embed this poset into the discrete plane by sending M to $(0, 0)$, and situating F_1 and F_2 in the first quadrant, along the lines $y = 0$ and $y = 1$, respectively.

The remaining diagram from the resolution of γ consists of three directed edges, two of which are elements in the triangulation. The remaining third element is the longest arc γ' in a subfan of Δ with $n - 1$ diagonals. By induction, this poset, which we call P_2 , is isomorphic to $L_{\gamma'}$. One can check that each of the n elements along the bottom row of P_2 is related to the corresponding element in F_2 by an edge covering relation about the first diagonal that γ crosses. Hence, (d) is true. Part (a) follows immediately from part (d). That (b) and (c) are true follow by induction. This completes the proof. □

Example 11.26. Figure 11.20 shows how the expansion poset of the longest edge in a pentagon is constructed via inductive gluing.

Figure 11.20: The gluing construction of the expansion poset of the longest edge in a pentagon



REFERENCES

REFERENCES

- [1] Rachel Bailey and Emily Gunawan. Cluster algebras and binary words.
- [2] Garrett Birkhoff et al. Rings of sets. *Duke Mathematical Journal*, 3(3):443–454, 1937.
- [3] Petter Brändén. Unimodality, log-concavity, real-rootedness and beyond. *Handbook of enumerative combinatorics*, 87:437, 2015.
- [4] Francesco Brenti. Log-concave and unimodal sequences in algebra, combinatorics, and geometry: an update, jerusalem combinatorics—93, 71–89. *Contemp. Math*, 178.
- [5] İlke Çanakçı and Ralf Schiffler. Cluster algebras and continued fractions. *Compositio mathematica*, 154(3):565–593, 2018.
- [6] İlke Çanakçı and Ralf Schiffler. Snake graphs and continued fractions. *European Journal of Combinatorics*, 86:103081, 2020.
- [7] Zhiyun Cheng, Sujoy Mukherjee, Jozef H Przytycki, Xiao Wang, and Seung Yeop Yang. Strict unimodality of q -polynomials of rooted trees. *arXiv preprint arXiv:1601.03465*, 2016.
- [8] Anna Felikson, Michael Shapiro, and Pavel Tumarkin. Cluster algebras and triangulated orbifolds. *Advances in Mathematics*, 231(5):2953–3002, 2012.
- [9] Vladimir Fock and Alexander Goncharov. Moduli spaces of local systems and higher teichmüller theory. *Publications Mathématiques de l’IHÉS*, 103:1–211, 2006.
- [10] Sergey Fomin and Pavlo Pylyavskyy. Tensor diagrams and cluster algebras. *arXiv preprint arXiv:1210.1888*, 2012.
- [11] Sergey Fomin and Pavlo Pylyavskyy. Webs on surfaces, rings of invariants, and clusters. *Proceedings of the National Academy of Sciences*, 111(27):9680–9687, 2014.
- [12] Sergey Fomin, Michael Shapiro, and Dylan Thurston. Cluster algebras and triangulated surfaces. part i: Cluster complexes. *arXiv preprint math/0608367*, 2006.
- [13] Sergey Fomin and Dylan Thurston. *Cluster algebras and triangulated surfaces part II: Lambda lengths*, volume 255. American Mathematical Society, 2018.
- [14] Sergey Fomin and Andrei Zelevinsky. Cluster algebras i: foundations. *Journal of the American Mathematical Society*, 15(2):497–529, 2002.

- [15] Sergey Fomin and Andrei Zelevinsky. Cluster algebras iv: coefficients. *Compositio Mathematica*, 143(1):112–164, 2007.
- [16] Rob Gaebler. Alexander polynomials of two-bridge knots and links. *Undergraduate Thesis*, 2004.
- [17] Emden R Gansner. On the lattice of order ideals of an up-down poset. *Discrete Mathematics*, 39(2):113–122, 1982.
- [18] Michael Gekhtman, Michael Shapiro, Alek Vainshtein, et al. Cluster algebras and weil-petersson forms. *Duke Mathematical Journal*, 127(2):291–311, 2005.
- [19] Michael Gekhtman, Michael Zalmanovich Shapiro, and Alek D Vainshtein. Cluster algebras and poisson geometry. *Moscow Mathematical Journal*, 3(3):899–934, 2003.
- [20] Emily Gunawan, Gregg Musiker, and Hannah Vogel. Cluster algebraic interpretation of infinite friezes. *European Journal of Combinatorics*, 81:22–57, 2019.
- [21] H Höft and M Höft. A fibonacci sequence of distributive lattices. *Fibonacci Quart*, 23(3):232–237, 1985.
- [22] W-J Hsu. Fibonacci cubes-a new interconnection topology. *IEEE Transactions on Parallel and Distributed Systems*, 4(1):3–12, 1993.
- [23] Sandi Klavžar. Structure of fibonacci cubes: a survey. *Journal of Combinatorial Optimization*, 25(4):505–522, 2013.
- [24] Kolja Knauer, Leonardo Martínez-Sandoval, and Jorge Luis Ramírez Alfonsín. On lattice path matroid polytopes: integer points and ehrhart polynomial. *Discrete & Computational Geometry*, 60(3):698–719, 2018.
- [25] Kyungyong Lee and Ralf Schiffler. Cluster algebras and jones polynomials. *Selecta Mathematica*, 25(4):58, 2019.
- [26] Sophie Morier-Genoud and Valentin Ovsienko. q -deformed rationals and q -continued fractions. *arXiv preprint arXiv:1812.00170*, 2018.
- [27] Emanuele Munarini and Norma Zagaglia Salvi. On the rank polynomial of the lattice of order ideals of fences and crowns. *Discrete mathematics*, 259(1-3):163–177, 2002.
- [28] Gregg Musiker and Ralf Schiffler. Cluster expansion formulas and perfect matchings. *Journal of Algebraic Combinatorics*, 32(2):187–209, 2010.
- [29] Gregg Musiker, Ralf Schiffler, and Lauren Williams. Positivity for cluster algebras from surfaces. *Advances in Mathematics*, 227(6):2241–2308, 2011.

- [30] Gregg Musiker, Ralf Schiffler, and Lauren Williams. Bases for cluster algebras from surfaces. *Compositio Mathematica*, 149(2):217–263, 2013.
- [31] Kathleen M O’Hara. Unimodality of gaussian coefficients: a constructive proof. *Journal of Combinatorial Theory, Series A*, 53(1):29–52, 1990.
- [32] James Propp. The combinatorics of frieze patterns and markoff numbers. *arXiv preprint math/0511633*, 2005.
- [33] Michelle Rabideau and Ralf Schiffler. Continued fractions and orderings on the markov numbers. *arXiv preprint arXiv:1801.07155*, 2018.
- [34] Bruce E Sagan. *The symmetric group: representations, combinatorial algorithms, and symmetric functions*, volume 203. Springer Science & Business Media, 2013.
- [35] Ralf Schiffler. A cluster expansion formula (a_n case). *the electronic journal of combinatorics*, 15(1):R64, 2008.
- [36] Ralf Schiffler. On cluster algebras arising from unpunctured surfaces ii. *Advances in Mathematics*, 223(6):1885–1923, 2010.
- [37] Ralf Schiffler and Hugh Thomas. On cluster algebras arising from unpunctured surfaces. *International Mathematics Research Notices*, 2009(17):3160–3189, 2009.
- [38] Richard P Stanley. Differential posets. *Journal of the American Mathematical Society*, 1(4):919–961, 1988.
- [39] Richard P Stanley. Log-concave and unimodal sequences in algebra, combinatorics, and geometry. *Ann. New York Acad. Sci*, 576(1):500–535, 1989.
- [40] A Muhammed Uludağ and Hakan Ayrar. Jimm, a fundamental involution. *arXiv preprint arXiv:1501.03787*, 2015.
- [41] Toshiya Yurikusa. Combinatorial cluster expansion formulas from triangulated surfaces. *arXiv preprint arXiv:1808.01567*, 2018.
- [42] Toshiya Yurikusa. Cluster expansion formulas in type a. *Algebras and Representation Theory*, 22(1):1–19, 2019.